UNIVERSIDADE ESTADUAL DE MARINGÁ
CENTRO DE CIÊNCIAS EXATAS
DEPARTAMENTO DE FÍSICA
PROGRAMA DE PÓS-GRADUAÇÃO EM FÍSICA

BRUNO ANGHINONI

ELECTROMAGNETIC FORCES INSIDE LINEAR DIELECTRIC MEDIA:
TOWARDS SOLVING THE ABRAHAM-MINKOWSKI CONTROVERSY

Maringá - PR
2022

BRUNO ANGHINONI

ELECTROMAGNETIC FORCES INSIDE LINEAR DIELECTRIC MEDIA

TOWARDS SOLVING THE ABRAHAM-MINKOWSKI CONTROVERSY

Tese apresentada à Universidade Estadual de Maringá, como requisito parcial para a obtenção do título de doutor em Física.

Orientador: Prof. Dr. Nelson G. C. Astrath
Coorientador: Prof. Dr. Luis C. Malacarne

Maringá - PR
2022

Dados Internacionais de Catalogação-na-Publicação (CIP)
(Biblioteca Central - UEM, Maringá - PR, Brasil)

Anghinoni, Bruno

A587e

Electromagnetic forces inside linear dielectric media : Towards solving the Abraham-Minkowski controversy / Bruno Anghinoni. -- Maringá, PR, 2022.
102 f.color., figs., tabs.

Orientador: Prof. Dr. Nelson G. C. Astrath.
Coorientador: Prof. Dr. Luis C. Malacarne.
Tese (Doutorado) - Universidade Estadual de Maringá, Centro de Ciências Exatas, Departamento de Física, Programa de Pós-Graduação em Física, 2022.

1. Física - Momento da luz. 2. Controvérsia Abraham-Minkowski. 3. Força ótica. 4. Eletromagnetismo. 5. Tensor de estresse-energia. I. G. C. Astrath, Nelson, orient. II. C. Malacarne, Luis, coorient. III. Universidade Estadual de Maringá. Centro de Ciências Exatas. Departamento de Física. Programa de Pós-Graduação em Física. IV. Título.

CDD 23.ed. 537

Jane Lessa Monção - CRB 9/1173

BRUNO ANGHINONI

ELECTROMAGNETIC FORCES INSIDE LINEAR DIELECTRIC MEDIA
TOWARDS SOLVING THE ABRAHAM-MINKOWSKI CONTROVERSY

Tese apresentada à Universidade Estadual de Maringá, como requisito parcial para a obtenção do título de doutor em Física.

Aprovado em: Maringá, 13 de outubro de 2022.

BANCA EXAMINADORA

Prof. Dr. Nelson G. C. Astrath (Orientador)
Universidade Estadual de Maringá – UEM

Prof. Dr. Marcos Paulo Belançon
Universidade Técnica Federal do Paraná – UTFPR

Prof. Dr. Pablo Lima Saldanha
Universidade Federal de Minas Gerais – UFMG

Prof. Dr. Rênio dos Santos Mendes
Universidade Estadual de Maringá – UEM

Prof. Dr. Breno F. de Oliveira
Universidade Estadual de Maringá – UEM

RESUMO

Esta tese aborda o antigo problema da determinação do momento linear de ondas eletromagnéticas dentro de materiais dielétricos, amplamente conhecido na literatura como controvérsia de Abraham-Minkowski. As principais formulações eletromagnéticas existentes relacionadas a esse problema são analisadas em detalhes, onde é mostrado que nenhuma delas fornece uma completa descrição da transferência de momento. Apresentamos então uma nova densidade de força eletromagnética baseada na aproximação dipolar para as fontes eletromagnéticas, que é verificada estar em concordância com a maioria dos experimentos relatados até o momento. Um procedimento numérico semi-analítico é posteriormente desenvolvido para obtenção dessa densidade de força numericamente sob configurações experimentais comuns para auxiliar novas investigações. Por fim, propomos uma maneira de adequadamente incorporar essa densidade de força a uma das formulações descritas [Phys. Rev. A **96**, 063834 (2017)], fornecendo uma potencial solução para a controvérsia de Abraham-Minkowski.

Palavras-chave: momento da luz, força ótica, controvérsia de Abraham-Minkowski, tensor de estresse-energia, Eletromagnetismo.

ABSTRACT

This thesis addresses the long-standing problem of determining the linear momentum of electromagnetic waves inside dielectric materials, widely known in the literature as the Abraham-Minkowski controversy. The main existing electromagnetic formulations related to this problem are analyzed in detail, where it is shown that none of them provides a complete description of momentum transfer. We then present a new electromagnetic force density based on the dipolar approximation for the electromagnetic sources, which is found to be in agreement with the majority of experiments reported up to date. A semi-analytical numerical procedure is subsequently developed to obtain such force density numerically under common experimental setups to support new investigations. At last, we propose a way to properly incorporate this force density into one of the described formulations [Phys. Rev. A **96**, 063834 (2017)], providing a potential resolution to the Abraham-Minkowski controversy.

Keywords: momentum of light, optical force, Abraham-Minkowski controversy, stress-energy tensor, Electromagnetism.

List of Figures

3.1 Convention for permittivities in radiation pressure equation 35
3.2 Radiation pressure for oblique incidence 38

4.1 Optical propagator behavior 49
4.2 Abbe-sine and energy conservation conditions 52
4.3 Coordinate systems for beam refraction at lens 53
4.4 Laser beam focused on a planar dielectric interface 57
4.5 Geometry of the simulated problem 65
4.6 Beam intensity 66
4.7 Beam waist inside the dielectric medium 66
4.8 Time-averaged radial electromagnetic force densities 67
4.9 Time-averaged longitudinal electromagnetic force densities 68
4.10 Time-averaged radiation pressure at the air-water interface 68
4.11 Gaussian time modulation for pulsed excitation 69
4.12 Peak Abraham force and instantaneous radial force density 69

List of Tables

3.1 Comparison between electromagnetic force densities 33

List of Abbreviations

ASR Angular Spectrum Representation

MA Microscopic Ampère

MDW mass density wave

MP mass-polariton

QED Quantum Electrodynamics

Contents

1 Introduction **1**

1.1 Literature survey ... 2

1.2 Overview ... 5

2 Electromagnetic formalisms **6**

2.1 Electromagnetic stress-energy tensor general properties ... 7

2.2 Hidden momentum ... 10

2.3 Electromagnetic stress-energy tensor formulations ... 11

2.3.1 Minkowski formulation ... 12

2.3.2 Abraham formulation ... 13

2.3.3 Ampère formulation ... 14

2.3.4 Einstein-Laub formulation ... 16

2.3.5 Chu formulation ... 18

2.3.6 Mass-polariton formulation ... 19

2.4 Electro- and magnetostriction effects ... 21

3 Microscopic Ampère formulation **23**

3.1 Dipolar sources ... 24

3.1.1 Time-dependent dipoles ... 26

3.2 Electromagnetic force density ... 28

3.2.1 Radiation pressure ... 34

3.3 Comparison to experiments ... 36

3.3.1 Radiation pressure experiments ... 37

3.3.2 Photon momentum experiments ... 38

3.3.3 Bulk force experiments ... 39

3.3.4 Total force experiments ... 40

3.4 Stress-energy tensor ... 41

3.4.1 Relation to MP formulation ... 42

4 Numerical calculation of the electromagnetic force density **46**

4.1 Angular Spectrum Representation ... 47

4.1.1 Far field regime ... 50
4.2 Focused laser beams ... 51
4.2.1 Focused gaussian beam ... 54
4.2.2 Gaussian beams focused on planar dielectric interfaces ... 57
4.3 Pulsed gaussian beam and momentum density ... 59
4.4 Force densities ... 62
4.5 Simulations ... 64
4.5.1 Continuous excitation ... 65
4.5.2 Pulsed excitation ... 68
4.5.3 Fluid dynamics with electromagnetic forces ... 70

5 Conclusions **71**

References **73**

Appendix A Covariant electrodynamics in flat space-time **84**

Appendix B Fresnel equations **87**

Appendix C Radiation pressure at oblique incidence **88**

Appendix D The paraxial approximation of electromagnetic fields **89**

Appendix E Magnetic field expressions for x-polarization **91**

CHAPTER 1

Introduction

The concept of light in Physics has certainly a very rich history, which is inevitably tied to the history of Physics itself. For example, light has been the definitive connection between Electricity and Magnetism when both areas were unified by Maxwell by the end of the XIX century. Light has also played an important role in the birth and development of Quantum Mechanics in the beginning of the XX century, where it was first described as a discrete entity by Planck and Einstein. The dual nature of light as wave and particle has also inspired theoretical Physics, where the fundamental concept of waves of matter was postulated and later confirmed in the middle of the XX century.

Even though our knowledge of the behavior of light grew immensely in the last century, we still can not say it is completely understood. In particular, there is no consensus yet on how light exchanges momentum when propagating inside matter. In fact, this seemingly simple problem has been around for more than a hundred years. It was originally known as Abraham-Minkowski controversy, and started in 1908 when Minkowski [1] used the wave description of light to predict the momentum magnitude of a photon propagating inside a dielectric media of refractive index n as

$$p_{\mathrm{M}} = np_0, \tag{1.1}$$

i.e., a linear increase of the vacuum momentum p_0 with n. One year later, Abraham [2] adopted the particle description of light and obtained the momentum magnitude of the same photon as

$$p_{\mathrm{A}} = p_0/n, \tag{1.2}$$

showing now an inverse dependence of p_0 with n. The Abraham-Minkowski controversy originates from these conflicting results and has not been decisively clarified to this date. Indeed, this problem is recognized nowadays to be not exclusive to dielectrics – it is also present in waveguides [3], plasmas [4, 5], metals [6, 7] and metamaterials [8].

Although the Abraham-Minkowski controversy is originally a fundamental Physics problem, it is closely related to many applications. In fact, the search for the definitive knowledge of electromagnetic momentum transfer and optical forces in matter has drawn much attention over the last few decades. Historically, this occurred mainly due to the development of a technique called single-beam optical gradient trap, which is widely known nowadays as optical tweezers. This optical tool was first devised by Ashkin in 1978 [9] and successfully applied by Ashkin *et al.* in 1986 [10], where they reported the optical trapping of dielectric particles of sizes from 10 μm to approximately 25 nm by employing focused laser beams illumination. Since then, the application of optical manipulation techniques has become more flexible and has grown in numbers significantly [11–17], being found especially in biological systems [18] and atomic physics [19]. Additionally, controlling optomechanical effects are of great interest for the development of photonic devices [20–23] and for optofluidic technology [24–26].

1.1 Literature survey

Being a century-old problem, the Abraham-Minkowski controversy is widely covered within the specialized literature. Here, we will mention separately and in chronological order the most important works from both experimental and theoretical sides, focusing on the former.

The first experimental investigation known dates back to 1901, when Lebedev examined the pressure exerted by light when reflecting off metal surfaces [27]. The topic was revisited only five decades later, in 1954, when Jones and Richards [28] found that the force exerted by light on opaque objects was proportional to the refractive index of the medium in which the objects were immersed. This experiment was repeated in 1978 by Jones and Leslie [29] with increased accuracy and showed the same results. In 1973, Ashkin and Dziedzic [30] measured the deformation of a free surface of transparent dielectric liquid generated by a focused light pulse, obtaining a result compatible with momentum as given by Minkowski formulation. In 1975, Walker and Lahoz [31] used a driven torsional pendulum under low frequencies to measure a torque that agreed with Abraham's formulation. Gibson *et al.* [32] measured in 1980 the photon drag effect in germanium and silicon and the results were correctly described by Minkowski's momentum. In 2001, Casner and Delville [33] reported surface deformations at the interface of phase-separated liquid mixtures that were compatible with Minkowski's formulation. The photon recoil momentum due to the index of refraction in a dilute gas of atoms was measured by Campbell *et al.* [34] in 2005 and was observed to be proportional to the gas' index of refraction. She *et al.* [35] reported in 2008 a direct observation of a force generated by outgoing light at the end of a nanometer silicon filament, which they concluded to be supported by Abraham's momentum; nevertheless, the work was criticized by Brevik [36] and Mansuripur [37], who claimed such conclusion was incorrect. The interpretation of She's *et al.* [35] results has also been discussed in a more recent work [38]. In 2011, O. Emile and J. Emile [39] reported an Abraham-like deformation of an air-water interface by applying a low-power laser beam under total internal reflection. This work was criticized theoretically by Brasselet [40] and experimentally by Verma *et al.* [41], who claimed the deformation observed was not due to the radiation pressure acting at the interface. Still in 2011, Rikken and Tiggelen [42] observed a momentum transfer of Abraham-type in a gas at low frequency excitations. The same authors reported, in the following year, measurements of forces in accordance with Abraham formulation on a high permittivity non-magnetic dielectric [43]. In 2014, Astrath *et al.* [44] performed an experiment similar to that of Ashkin and Dziedzic by measuring the deformation of a free interface of water/air generated by focused light, obtaining similar quantitative results on the water surface displacement. One year later, Zhang *et al.* [45] performed yet another similar experiment, but obtained a surface deformation in agreement with Abraham's momentum. Zhang *et al.*'s work was supported by a theoretical argument by Leonhardt [46], who solved approximate coupled electromagnetic-fluid dynamics equations to show that both Abraham's and Minkowski's momentum can arise in this situation, depending on some experimental parameters. Capeloto *et al.* [47] tried in 2015 to reproduce the results by Zhang *et al.*, but consistently found only Minkowski-type deformations for water under the same conditions – and also for some other different dielectric fluids. Also in 2015 Verma and Singh [48] reported a Minkowski-type deformation of an air-water interface under different incidence angles near the critical angle for total internal reflection. In 2017, Choi *et al.* [49] used an optical fiber waveguide to measure the deformation of an air/liquid interface, and the results were in accordance with Abraham's formulation. In the same year, Verma *et al.* [50] systematically scanned a wide range of experimental parameters while measuring the dynamics of a water surface excited by laser beams and found agreement with Minkowski's theory under all tested conditions. Still in 2017, Kundu *et al.* [51] reported an Abraham-like deformation in graphene oxide surface due to radiation pressure. However, in the following year, the work was criticized by Brevik [52], who claimed the deformation observed was due to the material's electric conductivity, and not radiation pressure itself. It has also been pointed out that the deformation of the medium in the experiment by Kundu *et al.* is irreversible when it is a result of the breaking of chemical bonds in the material, which is not described by the conventional optical force concepts [53]. In 2019, measurements of the photon drag effect in thin metal films agreed with Minkowski's momentum [54], except under some specific conditions, where the momentum transfer was observed to be of opposite sign – a result that still lacks theoretical explanation. Also in 2019 Schaberle *et al.* [55] studied the photon momentum transfer at air-water interfaces under total internal reflection and the results agreed with Minkowski's momentum. Still in 2019, Chaudhary and Singh [56] reported radiation pressure effects close to pico-Newton resolution in water using low power laser beams – again, the results agreed with Minkowski's momentum. Most recently, in 2021, Xi *et al.* measured the angular dependence of the opto-mechanical force acting on dielectric optical fibers [57], and the observed asymmetry could not be readily related to any known formulation.

The literature is also vast regarding theoretical investigations. As already stated, we will only mention some of the most important contributions. In 1953, Balazs [58] developed a thought experiment on momentum conservation and concluded that Abraham's claim was the correct one. In 1973, Gordon [59] demonstrated that for non-dispersive dielectric media the momentum of electromagnetic fields should be of Abraham's form, but Minkowski's form can also be used under some circumstances to calculate the radiation pressure on objects embedded in such dielectric media. In 1991, Nelson [60] proposed a theoretical solution to the Abraham-Minkowski controversy, calculating the momentum of the electromagnetic wave in a dielectric medium and a corresponding pseudomomentum of the medium alone. In 2006, Leonhardt [61] showed that, for a Bose-Einstein condensate, Minkowski's momentum is related to the phase of the condensate, while Abraham's momentum describes the flow of the dielectric. In 2007, Pfeifer *et al.* [62] suggested a subtle solution for the controversy: the division of the total energy-momentum tensor into electromagnetic and material components should be arbitrary – so, both Minkowski's and Abraham's formulations have a material counterpart, and the sum of these components yield the same total energy and momentum. Padgett [63] showed in 2008 that the diffraction phenomenon within a dielectric is supported by Minkowski's momentum. In a celebrated work in 2010, Barnett [64] identified Abraham's momentum as the kinetic momentum and Minkowski's momentum as the canonical momentum, claiming to have resolved the controversy. This interpretation was endorsed by Kemp [65] in a review in the following year. Also in 2011, Brevik and Elligsen [66] solved analytically some static fields configurations and stated that describing the conserved quantities of the system is not sufficient to support one formulation over another – instead, one must look into the experimental observations. Later, in 2017, Kemp and Sheppard [67] showed that neither Minkowski nor Abraham formulations are universally correct, for their failure to describe energy and momentum fluxes in some metamaterials. Also in 2017 Brevik employed a field-theoretical procedure, obtaining Minkowski's momentum from the canonical formalism [68]. One year later, Brevik showed that, contrary to the claims, most of the reported experiments are actually unable to distinguish between Abraham's and Minkowski's momentum [69].

1.2 Overview

This thesis is organized as follows. In Chapter 2, we review the main properties required by any valid electromagnetic stress-energy tensor candidate and describe each considered formulation in detail, showing none of them is universally correct. In Chapter 3, we propose a new formulation based on microscopic dipolar sources for dielectric media. This formulation is then compared to the literature both theoretically and experimentally. In Chapter 4 we present a numerical method to calculate the electromagnetic forces generated in dielectric media by focused gaussian beams and some related simulations. At last, in Chapter 5 the central results of the work are summarized and some future work perspectives are suggested.

CHAPTER 2

Electromagnetic formalisms

For a system with arbitrary electromagnetic sources ρ and $\mathbf{J}$, Maxwell's equations for an inertial reference frame at rest are given in standard units by

$$\varepsilon_0 \boldsymbol{\nabla} \cdot \mathbf{E} = \rho, \tag{2.1}$$

$$\boldsymbol{\nabla} \cdot \mathbf{B} = 0, \tag{2.2}$$

$$\frac{1}{\mu_0} \boldsymbol{\nabla} \times \mathbf{B} - \varepsilon_0 \frac{\partial \mathbf{E}}{\partial t} = \mathbf{J}, \tag{2.3}$$

$$\boldsymbol{\nabla} \times \mathbf{E} + \frac{\partial \mathbf{B}}{\partial t} = 0, \tag{2.4}$$

where ρ is the electric charge density, $\mathbf{J}$ is the electric current density, $\mathbf{E}$ is the electric field and $\mathbf{B}$ is the magnetic induction field. These equations are known, respectively, as Gauss' law, Gauss' law for magnetism, Ampère-Maxwell's law and Faraday's law. This set is the most general form of Maxwell's equations for a system at rest – however, this form is often also unpractical, because the true microscopic sources ρ and $\mathbf{J}$ for continuous distributions, such as ordinary matter, are impossible to be completely known. Thus, for dielectric media, Maxwell's equations are usually given as

$$\boldsymbol{\nabla} \cdot \mathbf{D} = \rho_{\mathrm{f}}, \tag{2.5}$$

$$\boldsymbol{\nabla} \cdot \mathbf{B} = 0, \tag{2.6}$$

$$\boldsymbol{\nabla} \times \mathbf{H} - \frac{\partial \mathbf{D}}{\partial t} = \mathbf{J}_{\mathrm{f}}, \tag{2.7}$$

$$\boldsymbol{\nabla} \times \mathbf{E} + \frac{\partial \mathbf{B}}{\partial t} = 0, \tag{2.8}$$

where $\mathbf{D}$ is the electric displacement field and $\mathbf{H}$ is the magnetic field. The medium response in this form is given in terms of a polarization field $\mathbf{P}$ and a magnetization field

$\mathbf{M}$, with $\mathbf{D} = \varepsilon_0 \mathbf{E} + \mathbf{P}$ and $\mathbf{B} = \mu_0 (\mathbf{H} + \mathbf{M})$. The subscript “f” is used to denote the free electric charge density ρ_f and free electric current density $\mathbf{J}_\mathrm{f}$. Any bound (as opposed to free) charge and current densities are effectively described in terms of $\mathbf{P}$ and $\mathbf{M}$ in bulk as

$$\rho_\mathrm{b} = -\boldsymbol{\nabla} \cdot \mathbf{P} \tag{2.9}$$

and

$$\mathbf{J}_\mathrm{b} = \boldsymbol{\nabla} \times \mathbf{M} + \frac{\partial \mathbf{P}}{\partial t}. \tag{2.10}$$

The fields obtained from Maxwell’s equations in this last presented form are known as macroscopic fields, because the microscopic responses of the medium are taken as smoothed spatial averages, resulting in $\mathbf{P}$ and $\mathbf{M}$. This averaging procedure is expected to produce loss of information about the system, becoming especially significant when dissipative processes are relevant [70]. Indeed, as shown in Ref. [71], descriptions using effective bound charges and bound currents are unable to correctly describe the microscopical distribution of force because the internal surface terms are always being neglected.

2.1 Electromagnetic stress-energy tensor general properties

The principles of conservation of energy and momentum for the electromagnetic fields can be described by the standard continuity equations. Assuming no external mechanical sources, these equations are [72]

$$\mathbf{f} = -\overleftrightarrow{\boldsymbol{\nabla}} \cdot \overleftrightarrow{\mathbf{T}} - \frac{\partial \mathbf{g}}{\partial t}, \tag{2.11}$$

$$\phi = -\boldsymbol{\nabla} \cdot \mathbf{S} - \frac{\partial W}{\partial t}, \tag{2.12}$$

where $\overleftrightarrow{\mathbf{T}}$ is the electromagnetic stress tensor, $\mathbf{g}$ is the electromagnetic momentum density, $\mathbf{f}$ is the force density generated by the fields, ϕ is the power density delivered by the fields, $\mathbf{S}$ is the electromagnetic energy flux and W is the electromagnetic energy density. Notice that Eqs. (2.11) and (2.12) – and, in fact, any supplementary equation for electromagnetic force/momentum/energy – are of course not Maxwell’s equations themselves, but must always be consistent with them. Specifically, the force density is given by

$$\mathbf{f} = \rho \mathbf{E} + \mathbf{J} \times \mathbf{B}, \tag{2.13}$$

which is known as Lorentz force law. This equation is both experimentally verified and covariant (see Appendix A) – there is currently no doubt about its validity within classical Electromagnetism. Consequently, it is expected that at least one problematic aspect of the Abraham-Minkowski controversy is related to how the sources ρ and $\mathbf{J}$ are modeled in each formulation. This will be discussed later in this chapter and in the next chapter.

In vacuum, we have $\mathbf{f} = 0$ and $\phi = 0$ in Eqs. (2.11) and (2.12), and their terms are given unambiguously by

$$\overleftrightarrow{\mathbf{T}}_{\text{vac}} = \frac{1}{2}\left(\varepsilon_0|\mathbf{E}|^2 + \mu_0^{-1}|\mathbf{B}|^2\right)\overleftrightarrow{\mathbf{I}} - \varepsilon_0\mathbf{E}\otimes\mathbf{E} - \mu_0^{-1}\mathbf{B}\otimes\mathbf{B}, \tag{2.14}$$

$$\mathbf{g}_{\text{vac}} = \varepsilon_0\mathbf{E}\times\mathbf{B}, \tag{2.15}$$

$$\mathbf{S}_{\text{vac}} = \mu_0^{-1}\mathbf{E}\times\mathbf{B}, \tag{2.16}$$

$$W_{\text{vac}} = \frac{1}{2}\left(\varepsilon_0|\mathbf{E}|^2 + \mu_0^{-1}|\mathbf{B}|^2\right), \tag{2.17}$$

where $\overleftrightarrow{\mathbf{I}}$ is the unit dyadic and ε_0 and μ_0 are the vacuum permittivity and permeability, respectively. The tensor given in Eq. (2.14) is known as Maxwell stress tensor [73] (see Appendix A for its covariant form). To derive it, we start from the Lorentz force law, Eq. (2.13), substituting ρ and $\mathbf{J}$ according to Eqs. (2.1) and (2.3), obtaining

$$\mathbf{f} = (\boldsymbol{\nabla}\cdot\mathbf{E})\,\mathbf{E} + \left(\frac{1}{\mu_0}\boldsymbol{\nabla}\times\mathbf{B} - \varepsilon_0\frac{\partial\mathbf{E}}{\partial t}\right)\times\mathbf{B}. \tag{2.18}$$

Next, with the aid of Faraday's law, the time derivative term is rewritten as

$$\varepsilon_0\frac{\partial\mathbf{E}}{\partial t}\times\mathbf{B} = \varepsilon_0\frac{\partial}{\partial t}(\mathbf{E}\times\mathbf{B}) + \varepsilon_0\mathbf{E}\times(\boldsymbol{\nabla}\times\mathbf{E}). \tag{2.19}$$

Inserting this result in Eq. (2.18) and rearranging, we have

$$\mathbf{f} = \varepsilon_0[(\boldsymbol{\nabla}\cdot\mathbf{E})\,\mathbf{E} - \mathbf{E}\times(\boldsymbol{\nabla}\times\mathbf{E})] - \frac{1}{\mu_0}[\mathbf{B}\times(\boldsymbol{\nabla}\times\mathbf{B})] - \varepsilon_0\frac{\partial}{\partial t}(\mathbf{E}\times\mathbf{B}). \tag{2.20}$$

Now, recalling that $\boldsymbol{\nabla}\cdot\mathbf{B} = 0$ and using the vector calculus identity $\mathbf{A}\times(\boldsymbol{\nabla}\times\mathbf{A}) = (\mathbf{A}\cdot\boldsymbol{\nabla})\mathbf{A} - \boldsymbol{\nabla}|\mathbf{A}|^2/2$, we obtain

$$\begin{aligned}\mathbf{f} = {}& \varepsilon_0[(\boldsymbol{\nabla}\cdot\mathbf{E})\,\mathbf{E} + (\mathbf{E}\cdot\boldsymbol{\nabla})\mathbf{E}] + \frac{1}{\mu_0}[(\boldsymbol{\nabla}\cdot\mathbf{B})\,\mathbf{B} + (\mathbf{B}\cdot\boldsymbol{\nabla})\mathbf{B}] \\ & -\frac{1}{2}\boldsymbol{\nabla}\left(\varepsilon_0|\mathbf{E}|^2 + \frac{1}{\mu_0}|\mathbf{B}|^2\right) - \varepsilon_0\frac{\partial}{\partial t}(\mathbf{E}\times\mathbf{B}).\end{aligned} \tag{2.21}$$

This is a continuity equation as Eq. (2.11) with $\overleftrightarrow{\mathbf{T}}$ and $\mathbf{g}$ given by Eqs. (2.14) and

(2.15), respectively. The continuity equation for energy is obtained by first dot-multiplying Ampère-Maxwell's law by $\mathbf{E}$, then dot-multiplying Faraday's law by $\mathbf{B}$ and taking the difference between these two equations, yielding

$$-\frac{1}{\mu_0}\boldsymbol{\nabla}\cdot(\mathbf{E}\times\mathbf{B})-\frac{1}{2}\frac{\partial}{\partial t}\left(\varepsilon_0|\mathbf{E}|^2+\frac{1}{\mu_0}|\mathbf{B}|^2\right)=0, \tag{2.22}$$

from where $\mathbf{S}$ and W in Eqs. (2.16) and (2.17) are readily identified.

In the context of special relativity, it is convenient to rewrite Eqs. (2.11) and (2.12) as a single continuity equation for an appropriate four-vector. Considering a flat space-time (also known as Minkowski space) and using Einstein summation convention for repeated indices, the four-dimensional continuity equation reads

$$\eta^{\mu\sigma}f_\sigma=f^\mu=-\partial_\nu\mathcal{T}^{\mu\nu}, \tag{2.23}$$

where $\mu,\nu=0,1,2,3$. The metric convention adopted is

$$\eta_{\mu\nu}=\begin{pmatrix}-1&0&0&0\\0&1&0&0\\0&0&1&0\\0&0&0&0\end{pmatrix}, \tag{2.24}$$

while

$$x^\nu=(ct,x,y,z)\,, \tag{2.25}$$

$$\partial_\nu=\frac{\partial}{\partial x^\nu}=\left(\frac{1}{c}\frac{\partial}{\partial t},\frac{\partial}{\partial x},\frac{\partial}{\partial y},\frac{\partial}{\partial z}\right), \tag{2.26}$$

$$f^\nu=(\phi/c,f_x,f_y,f_z)\,, \tag{2.27}$$

and

$$\mathcal{T}^{\mu\nu}=\begin{pmatrix}W&S_x/c&S_y/c&S_z/c\\cg_x&T_{xx}&T_{xy}&T_{xz}\\cg_y&T_{yx}&T_{yy}&T_{yz}\\cg_z&T_{zx}&T_{zy}&T_{zz}\end{pmatrix}, \tag{2.28}$$

with $c=(\varepsilon_0\mu_0)^{-1/2}$ being the speed of light in vacuum.

Eq. (2.28) represents a four-dimensional tensor, which in our context is known as electromagnetic stress-energy tensor. To satisfy the conservation of angular momentum, it is known from Field Theory that the total stress-energy tensor from a closed system must be symmetric [72]. Therefore, if $\mathcal{T}$ describes a pure electromagnetic system, we must have $\mathbf{S}=c^2\mathbf{g}$ and $T_{ij}=T_{ji}$, for $i,j=x,y,z$ and $i\neq j$. Besides, to secure the equivalence of physical laws in different arbitrary inertial systems, any appropriate tensor candidate must also be form-invariant under Lorentz transformations.

Lastly, we emphasize that only the total stress-energy tensor of the system of field and matter must be symmetric and invariant [74]. Thus, it is always possible to choose a matter counterpart for the total tensor that will make it mathematically correct; nevertheless, the physical significance of this choice depends on the specific description of the matter-field interaction adopted.

2.2 Hidden momentum

In 1967, Shockley and James identified [75] a previously unrecognized source of linear momentum that should arise when a magnetic dipole moment $\mathbf{m}$ interacts with an electric field – even if both did not vary in time. This source became known as hidden momentum, and is given as

$$\mathbf{p}_{\mathrm{h}} = \frac{1}{c^2}(\mathbf{m} \times \mathbf{E}). \tag{2.29}$$

Since then, many works tried to properly interpret this puzzling term, which is inevitably tied to the Abraham-Minkowski controversy. Some authors claimed that it occurs as a relativistic effect in systems that are macroscopically at rest, but contain internally moving parts, such as a common electric circuit [74, 76–78] (see also Ref. [79] and references therein). It was also shown that hidden momentum is necessary to keep the correct relativistic properties of energy, momentum and rest mass of a charge and current carrying body [80]. Indeed, it was recently suggested the hidden momentum is a general relativistic concept, not exclusive to electromagnetic systems [81].

Apart from these historical conceptual issues, it was formally shown [82] that starting from the conventional Quantum Electrodynamics (QED) Lagrangian for a point, spinless charged particle in relativistic motion and properly applying the center of mass-energy theorem there must be an extra momentum given by Eq. (2.29). Classically, the correct interpretation of hidden momentum is actually quite simple: a moving electric dipole develops a magnetic dipole. More specifically, this occurs when the electric dipole moment $\mathbf{p}$ of a particle moving with velocity $\mathbf{u}$, both measured in the laboratory frame, is Lorentz-transformed to the particle's rest frame [83]. To first order in $|\mathbf{u}|/c$, the new electric dipole moment is [84] $\mathbf{p}' = \mathbf{p} - \mathbf{u} \times \mathbf{m}'/c^2$, where $\mathbf{p}'$ and $\mathbf{m}'$ are the particle's electric and magnetic dipole moments, respectively, in its rest frame. The hidden momentum contribution then comes exactly from this last term.

In 1984 Aharonov and Casher showed in a seminal work [85] that the hidden momentum arises as a topological quantum effect when describing the interaction between a charged particle and a magnetic moment, where they obtained Eq. (2.29) as a non-relativistic limit of the Dirac equation – in this context, the hidden momentum is also known in the literature as Aharonov-Casher interaction. In analogy with the Aharonov-Bohm effect [86], this interaction does not necessarily generate a force, but introduces a phase shift in the wave function of the system, which has already been observed – see Refs. [87, 88] for example.

Notice that the symmetry inherent to Maxwell's equations requires the existence of an effect analogous to hidden momentum for magnetic dipoles, i.e., an effect due to moving magnetic dipoles generating electric dipoles. This indeed takes place and is known in the literature as Röntgen interaction. Its momentum is given by $\mathbf{p}_\mathrm{R} = -\mathbf{p} \times \mathbf{B}$, and can also be rigorously obtained from the QED framework [82, 89, 90]. This interaction can also generate a topological phase [91], but, to our knowledge, such effect has not been observed yet.

Although hidden momentum has certainly been subject of more intense discussions in the literature, both interactions presented here are of equal importance, and they are expected to take essential part in the eventual resolution of the Abraham-Minkowski problem. They are known to arise when the center of mass-energy of the system is regarded as a dynamic variable – however, the Röntgen term appears naturally even in non-relativistic derivations (see Refs. [90, 92] for example), while the hidden momentum necessarily requires a relativistic treatment, as shown in Ref. [82]. More specifically, the Röntgen interaction and hidden momentum contribute to the electromagnetic force density as, respectively, $\mathbf{f}_\mathrm{R} = \,\mathrm{d}(\mathbf{P} \times \mathbf{B})/\,\mathrm{d}t$ and $\mathbf{f}_\mathrm{h} = -\,\mathrm{d}(\mathbf{M} \times \mathbf{E}/c^2)/\,\mathrm{d}t$, where the minus signs added to both equations stem from the fact that the force densities are generated due to the fields losing their momentum. The latter contribution is important even in systems with non-relativistic velocities [80], and so it must be properly added *ad hoc* in the results from non-relativistic derivations.

2.3 Electromagnetic stress-energy tensor formulations

In this section, we will present and discuss the main electromagnetic formulations existing in the literature. Besides the two formulations that name the Abraham-Minkowski controversy, there are other historically important formulations which will also be addressed in this work. Specifically, we will consider the Ampère formulation, the Einstein-Laub formulation [93], the Chu formulation [94], and the recent mass-polariton formulation [95–100].

2.3.1 Minkowski formulation

In 1908, Minkowski [1] built his stress tensor for linear dielectric media by employing the Lorentz force density; however, he erroneously associated all the charge densities to $\mathbf{D}$, as he used $\boldsymbol{\nabla}\cdot\mathbf{D}=\rho$ instead of $\boldsymbol{\nabla}\cdot\mathbf{D}=\rho_{\mathrm{f}}$ in his derivation [101]. Minkowski's tensor is given by

$$\overleftrightarrow{\mathbf{T}}_{\mathrm{M}}=\frac{1}{2}\left(\mathbf{D}\cdot\mathbf{E}+\mathbf{B}\cdot\mathbf{H}\right)\overleftrightarrow{\mathbf{I}}-\mathbf{D}\otimes\mathbf{E}-\mathbf{B}\otimes\mathbf{H}, \tag{2.30}$$

while the momentum density is $\mathbf{g}_{\mathrm{M}}=\mathbf{D}\times\mathbf{B}$. Note that for a non-magnetic, isotropic and linear dielectric, the magnitude of $\mathbf{g}_{\mathrm{M}}$ is proportional to n^3E^2 if the electromagnetic wave is taken to be plane. We know the electric field amplitude falls as $1/n$ when entering such dielectric media from vacuum – thus, when compared to vacuum, the magnitude of $\mathbf{g}_{\mathrm{M}}$ increases by n, in accordance with Eq. (1.1).

To find the associated electromagnetic force density, the divergence operator is applied to $\overleftrightarrow{\mathbf{T}}_{\mathrm{M}}$, yielding

$$\begin{aligned}-\overleftrightarrow{\boldsymbol{\nabla}}\cdot\overleftrightarrow{\mathbf{T}}_{\mathrm{M}}=&\,\varepsilon\left(\boldsymbol{\nabla}\cdot\mathbf{E}\right)\mathbf{E}+\varepsilon\left(\mathbf{E}\cdot\boldsymbol{\nabla}\right)\mathbf{E}-\tfrac{1}{2}|\mathbf{E}|^2\boldsymbol{\nabla}\varepsilon+\left(\mathbf{E}\otimes\mathbf{E}\right)\cdot\boldsymbol{\nabla}\varepsilon-\tfrac{1}{2}\varepsilon\boldsymbol{\nabla}\left(|\mathbf{E}|^2\right)\\&+\mu(\boldsymbol{\nabla}\cdot\mathbf{H})\,\mathbf{H}+\mu\left(\mathbf{H}\cdot\boldsymbol{\nabla}\right)\mathbf{H}+(\mathbf{H}\otimes\mathbf{H})\cdot\boldsymbol{\nabla}\mu-\tfrac{1}{2}\mu\boldsymbol{\nabla}(|\mathbf{H}|^2)-\tfrac{1}{2}|\mathbf{H}|^2\boldsymbol{\nabla}\mu.\end{aligned} \tag{2.31}$$

By using the the vector calculus property $\frac{1}{2}\boldsymbol{\nabla}\left(\mathbf{A}\cdot\mathbf{A}\right)=\left(\mathbf{A}\cdot\boldsymbol{\nabla}\right)\mathbf{A}-\left(\boldsymbol{\nabla}\times\mathbf{A}\right)\times\mathbf{A}$ and Maxwell's equations, the electromagnetic force density reduces to

$$\mathbf{f}_{\mathrm{M}}=-\frac{1}{2}|\mathbf{E}|^2\boldsymbol{\nabla}\varepsilon-\frac{1}{2}|\mathbf{H}|^2\boldsymbol{\nabla}\mu, \tag{2.32}$$

where it is assumed that the refractive index is not time dependent.

The energy continuity equation is obtained by first dot multiplying Eq. (2.7) by $\mathbf{E}$ and Eq. (2.8) by $\mathbf{H}$ and then subtracting them, yielding

$$\left(\boldsymbol{\nabla}\times\mathbf{H}\right)\cdot\mathbf{E}-\left(\boldsymbol{\nabla}\times\mathbf{E}\right)\cdot\mathbf{H}=\mathbf{E}\cdot\mathbf{J}_{\mathrm{f}}+\mathbf{E}\cdot\frac{\partial\mathbf{D}}{\partial t}+\mathbf{H}\cdot\frac{\partial\mathbf{B}}{\partial t}. \tag{2.33}$$

Using the vector property $\boldsymbol{\nabla}\cdot(\mathbf{U}\times\mathbf{W})=(\boldsymbol{\nabla}\times\mathbf{U})\cdot\mathbf{W}-\mathbf{U}\cdot(\boldsymbol{\nabla}\times\mathbf{W})$ and considering linear isotropic media, the last equation can be rewritten as

$$-\boldsymbol{\nabla}\cdot\left(\mathbf{E}\times\mathbf{H}\right)-\frac{1}{2}\frac{\partial}{\partial t}\left(\mathbf{D}\cdot\mathbf{E}+\mathbf{B}\cdot\mathbf{H}\right)=\mathbf{E}\cdot\mathbf{J}_{\mathrm{f}}, \tag{2.34}$$

from where it can be identified

$$\mathbf{S}_{\mathrm{M}}=\mathbf{E}\times\mathbf{H}, \tag{2.35}$$

$$W_{\mathrm{M}}=\frac{1}{2}\left(\mathbf{D}\cdot\mathbf{E}+\mathbf{B}\cdot\mathbf{H}\right) \tag{2.36}$$

and

$$\phi_{\mathrm{M}} = \mathbf{E} \cdot \mathbf{J}_{\mathrm{f}}. \tag{2.37}$$

Minkowski's stress-energy tensor is relativistically invariant [67], but clearly not symmetric, because $\mathbf{S}_{\mathrm{M}} \neq c^2 \mathbf{g}_{\mathrm{M}}$. It predicts a momentum transfer which is linear with the refractive index n, and seems to agree with most of the experiments so far. It has been suggested that this tensor actually corresponds to the canonical momentum of the electromagnetic wave in dielectric media [64].

2.3.2 Abraham formulation

In 1909, Abraham built a tensor equal to Minkowski's, but altered the momentum density to make the tensor symmetric [2],

$$\mathbf{g}_{\mathrm{Ab}} = \frac{1}{c^2} \mathbf{E} \times \mathbf{H}, \tag{2.38}$$

while keeping the remaining terms unchanged. For plane waves propagating inside non-magnetic, isotropic and linear dielectrics, the magnitude of $\mathbf{g}_{\mathrm{Ab}}$ is proportional to nE^2. Again, as we know the electric field amplitude falls as $1/n$ when entering dielectric media from vacuum, the magnitude of $\mathbf{g}_{\mathrm{Ab}}$ relative to vacuum also falls as $1/n$, justifying Eq. (1.2).

It can be verified that the force density is given by

$$\mathbf{f}_{\mathrm{Ab}} = \mathbf{f}_{\mathrm{M}} + \frac{\partial}{\partial t} \left(\mathbf{g}_{\mathrm{M}} - \mathbf{g}_{\mathrm{Ab}} \right), \tag{2.39}$$

where the time derivative term is known in the literature as Abraham force[1]. Explicitly, for linear, isotropic media, we have

$$\mathbf{f}_{\mathrm{Ab}} = -\frac{1}{2} |\mathbf{E}|^2 \boldsymbol{\nabla} \varepsilon - \frac{1}{2} |\mathbf{H}|^2 \boldsymbol{\nabla} \mu + \frac{n^2 - 1}{c^2} \frac{\partial}{\partial t} \left(\mathbf{E} \times \mathbf{H} \right), \tag{2.40}$$

where $n = \sqrt{\varepsilon_{\mathrm{r}} \mu_{\mathrm{r}}}$ is the medium refractive index, with $\varepsilon_{\mathrm{r}} = \varepsilon / \varepsilon_0$ and $\mu_{\mathrm{r}} = \mu / \mu_0$ being the relative permittivity and permeability, respectively. The continuity equation for energy is the same as Minkowski's, i.e., $\phi_{\mathrm{Ab}} = \phi_{\mathrm{M}}$, $W_{\mathrm{Ab}} = W_{\mathrm{M}}$ and $\mathbf{S}_{\mathrm{Ab}} = \mathbf{S}_{\mathrm{M}}$.

Abraham's change made the stress-energy tensor symmetric, while its invariance was believed to have been removed [67] – however, a recent work showed that it is possible to write this tensor in an invariant form [100]. There is a suggestion that Abraham's

[1] This is, of course, a force density term, but we follow the literature and call it "Abraham force". We refer to "Abraham force density" as the full force density equation from Abraham's formulation, i.e., Eq. (2.40).

momentum transfer, which is proportional to $1/n$, is actually the kinetic momentum of the electromagnetic field part of the system [64].

2.3.3 Ampère formulation

Ampère formulation, also known as Ampère-Lorentz formulation, is the one appearing in every modern electromagnetic theory textbook. It treats the microscopic response of dielectric media classically in terms of electric charges alone. Microscopic electric dipoles generate the polarization, while the magnetization is generated by tiny closed loops of electric current (usually referred to as Ampèrian loops), which represent the motion of the bound electrons. Classically, it is known that such closed current loops act like effective magnetic dipoles – i.e., in this formulation, the magnetization will be caused by bound electric currents. The use of this microscopic model can be justified by the agreement with measurements of the intrinsic magnetic dipole of neutrons [102]. Following Section 2, Maxwell's equations are then written for **E** and **B** with bound sources as:

$$\varepsilon_0 \boldsymbol{\nabla} \cdot \mathbf{E} = \rho_{\mathrm{f}} - \boldsymbol{\nabla} \cdot \mathbf{P}, \tag{2.41}$$

$$\boldsymbol{\nabla} \cdot \mathbf{B} = 0, \tag{2.42}$$

$$\frac{1}{\mu_0} \boldsymbol{\nabla} \times \mathbf{B} - \varepsilon_0 \frac{\partial \mathbf{E}}{\partial t} = \mathbf{J}_{\mathrm{f}} + \frac{\partial \mathbf{P}}{\partial t} + \boldsymbol{\nabla} \times \mathbf{M}, \tag{2.43}$$

$$\boldsymbol{\nabla} \times \mathbf{E} + \frac{\partial \mathbf{B}}{\partial t} = 0. \tag{2.44}$$

The force density is given by Lorentz force, Eq. (2.13), with charge density

$$\rho = \rho_{\mathrm{f}} - \boldsymbol{\nabla} \cdot \mathbf{P} \tag{2.45}$$

and current density

$$\mathbf{J} = \mathbf{J}_{\mathrm{f}} + \frac{\partial \mathbf{P}}{\partial t} + \boldsymbol{\nabla} \times \mathbf{M}, \tag{2.46}$$

which yields

$$\mathbf{f}_{\mathrm{A}} = \left(\rho_{\mathrm{f}} - \boldsymbol{\nabla} \cdot \mathbf{P}\right) \mathbf{E} + \left(\mathbf{J}_{\mathrm{f}} + \frac{\partial \mathbf{P}}{\partial t} + \boldsymbol{\nabla} \times \mathbf{M}\right) \times \mathbf{B}. \tag{2.47}$$

Last equation can be rewritten as

$$\mathbf{f}_{\mathrm{A}} = \varepsilon_0 \left(\boldsymbol{\nabla} \cdot \mathbf{E}\right) \mathbf{E} + \left(\frac{1}{\mu_0} \boldsymbol{\nabla} \times \mathbf{B} - \varepsilon_0 \frac{\partial \mathbf{E}}{\partial t}\right) \times \mathbf{B}, \tag{2.48}$$

where Gauss' law and Ampère's law have been used. Writing now the time derivative term as the derivative of a product and using the two remaining Maxwell's equations, the force can be written as

$$\begin{aligned}\mathbf{f}_{\mathrm{A}} &= \varepsilon_0\left[(\boldsymbol{\nabla}\cdot\mathbf{E})\,\mathbf{E}-\frac{1}{2}\boldsymbol{\nabla}\,(\mathbf{E}\cdot\mathbf{E})+(\mathbf{E}\cdot\boldsymbol{\nabla})\,\mathbf{E}\right]\\ &+ \frac{1}{\mu_0}\left[(\boldsymbol{\nabla}\cdot\mathbf{B})\,\mathbf{B}-\frac{1}{2}\boldsymbol{\nabla}\,(\mathbf{B}\cdot\mathbf{B})+(\mathbf{B}\cdot\boldsymbol{\nabla})\,\mathbf{B}\right]-\varepsilon_0\frac{\partial\,(\mathbf{E}\times\mathbf{B})}{\partial t}.\end{aligned} \tag{2.49}$$

The last equation can, finally, be written in a compact way using the tensor notation as

$$\mathbf{f}_{\mathrm{A}} = -\overleftrightarrow{\boldsymbol{\nabla}}\cdot\overleftrightarrow{\mathbf{T}}_{\mathrm{A}}-\frac{\partial\mathbf{g}_{\mathrm{A}}}{\partial t} \tag{2.50}$$

where

$$\overleftrightarrow{\mathbf{T}}_{\mathrm{A}} = \frac{1}{2}\left(\varepsilon_0|\mathbf{E}|^2+\frac{1}{\mu_0}|\mathbf{B}|^2\right)\overleftrightarrow{\mathbf{I}}-\varepsilon_0\mathbf{E}\otimes\mathbf{E}-\frac{1}{\mu_0}\mathbf{B}\otimes\mathbf{B}, \tag{2.51}$$

is the Ampère stress tensor and

$$\mathbf{g}_{\mathrm{A}} = \varepsilon_0\mathbf{E}\times\mathbf{B} \tag{2.52}$$

is the Ampère momentum density.

The continuity equation for energy is obtained by first dot multiplying Eq. (2.43) by $\mathbf{E}$ and Eq. (2.44) by $\mathbf{H}$ and subtracting the resulting equations as

$$\begin{aligned}&-\frac{1}{\mu_0}\boldsymbol{\nabla}\cdot(\mathbf{E}\times\mathbf{B})-\frac{1}{2}\frac{\partial}{\partial t}\left(\varepsilon_0|\mathbf{E}|^2+\frac{1}{\mu_0}|\mathbf{B}|^2\right)=\\ &\mathbf{E}\cdot\mathbf{J}_{\mathrm{f}}+\mathbf{E}\cdot\frac{\partial\mathbf{P}}{\partial t}+\mathbf{E}\cdot(\boldsymbol{\nabla}\times\mathbf{M})\,,\end{aligned} \tag{2.53}$$

from where it can be identified

$$\mathbf{S}_{\mathrm{A}} = \frac{1}{\mu_0}\,(\mathbf{E}\times\mathbf{B})\,, \tag{2.54}$$

$$W_{\mathrm{A}} = \frac{1}{2}\left(\varepsilon_0|\mathbf{E}|^2+\frac{1}{\mu_0}|\mathbf{B}|^2\right), \tag{2.55}$$

and

$$\phi_{\mathrm{A}} = \mathbf{E}\cdot\mathbf{J}_{\mathrm{f}}+\mathbf{E}\cdot\frac{\partial\mathbf{P}}{\partial t}+\mathbf{E}\cdot(\boldsymbol{\nabla}\times\mathbf{M})\,. \tag{2.56}$$

As it can be seen, $\mathbf{S}_{\mathrm{A}} = c^2\mathbf{g}_{\mathrm{A}}$, so Ampère stress-energy tensor is indeed symmetric, being thus able to correctly describe angular momentum conservation. Besides, it is also relativistically invariant [67].

Lastly, the hidden momentum contribution must be added to Ampère's formulation, as discussed in Section 2.2. It generates an extra force density

$$\mathbf{f}_{\mathrm{h}} = \frac{1}{c^2}\frac{\partial}{\partial t}\,(\mathbf{M}\times\mathbf{E})\,, \tag{2.57}$$

accompanied by a hidden energy flux

$$\mathbf{S}_{\mathrm{h}} = \mathbf{M} \times \mathbf{E}. \tag{2.58}$$

This last term guarantees that there is no divergence in the continuity equation for energy, Eq. (2.12), when considering magnetic interfaces. This can be readily seen, since the total energy flux is then given by $\mathbf{S}_{\mathrm{total}} = \mathbf{S}_{\mathrm{A}} + \mathbf{S}_{\mathrm{h}} = \mathbf{E} \times \mathbf{H}$, which is well behaved at interfaces when the divergent operator is applied.

2.3.4 Einstein-Laub formulation

In the Einstein-Laub formulation, the polarization and magnetization are thought, respectively, as "consisting of spatial displacements of electric and magnetic mass particles of dipoles that are bound to equilibrium positions" [93]. The electric and magnetic fields are treated as equivalents, and so are the electric and magnetic dipoles. This means that both dipole types are modeled as two monopoles close together with opposite charge of the corresponding type. First, the force on the free electric charges plus electric dipoles is given as

$$\mathbf{f}_1 = \rho_{\mathrm{f}} \mathbf{E} + (\mathbf{P} \cdot \boldsymbol{\nabla})\, \mathbf{E}, \tag{2.59}$$

and, analogously for the magnetic dipoles, as

$$\mathbf{f}_2 = \mu_0 \,(\mathbf{M} \cdot \boldsymbol{\nabla})\, \mathbf{H}. \tag{2.60}$$

Next, an argument is developed to show that the force generated on an electric current-carrying element is proportional to $\mathbf{H}$, generating the force density term

$$\mathbf{f}_3 = \left(\mathbf{J}_{\mathrm{f}} + \frac{\partial \mathbf{P}}{\partial t} \right) \times \mu_0 \mathbf{H}, \tag{2.61}$$

and the analogous term for the electric field

$$\mathbf{f}_4 = -\frac{1}{c^2} \frac{\partial \mathbf{M}}{\partial t} \times \mathbf{E}. \tag{2.62}$$

The Einstein-Laub force density is then given by the sum of these four terms. Using Maxwell's macroscopic equations, the force density can be written as

$$\begin{aligned} \mathbf{f}_{\mathrm{EL}} &= (\boldsymbol{\nabla} \cdot \mathbf{D})\, \mathbf{E} + (\mathbf{P} \cdot \boldsymbol{\nabla})\, \mathbf{E} + \mu_0 \,(\mathbf{M} \cdot \boldsymbol{\nabla})\, \mathbf{H} + \left(\boldsymbol{\nabla} \times \mathbf{H} - \varepsilon_0 \frac{\partial \mathbf{E}}{\partial t} \right) \times \mu_0 \mathbf{H} \\ &+ \left(\boldsymbol{\nabla} \times \mathbf{E} + \mu_0 \frac{\partial \mathbf{H}}{\partial t} \right) \times \varepsilon_0 \mathbf{E}. \end{aligned} \tag{2.63}$$

Grouping the time derivatives and using $\boldsymbol{\nabla} \cdot \mathbf{B} = 0$, we have

$$\begin{aligned} \mathbf{f}_{\mathrm{EL}} &= (\boldsymbol{\nabla} \cdot \mathbf{D})\, \mathbf{E} + (\mathbf{P} \cdot \boldsymbol{\nabla})\, \mathbf{E} + \mu_0\, (\mathbf{M} \cdot \boldsymbol{\nabla})\, \mathbf{H} + (\boldsymbol{\nabla} \cdot \mathbf{B})\, \mathbf{H} - \frac{\varepsilon_0}{2} \boldsymbol{\nabla}\, (\mathbf{E} \cdot \mathbf{E}) \\ &+ \varepsilon_0\, (\mathbf{E} \cdot \boldsymbol{\nabla})\, \mathbf{E} - \frac{\mu_0}{2} \boldsymbol{\nabla}\, (\mathbf{H} \cdot \mathbf{H}) + \mu_0\, (\mathbf{H} \cdot \boldsymbol{\nabla})\, \mathbf{H} - \frac{1}{c^2} \frac{\partial}{\partial t}\, (\mathbf{E} \times \mathbf{H})\, . \end{aligned} \tag{2.64}$$

This can be conveniently written in tensor notation as

$$\mathbf{f}_{\mathrm{EL}} = -\overleftrightarrow{\boldsymbol{\nabla}} \cdot \overleftrightarrow{\mathbf{T}}_{\mathrm{EL}} - \frac{\partial \mathbf{g}_{\mathrm{EL}}}{\partial t}, \tag{2.65}$$

where

$$\overleftrightarrow{\mathbf{T}}_{\mathrm{EL}} = \frac{1}{2} \left(\varepsilon_0 |\mathbf{E}|^2 + \mu_0 |\mathbf{H}|^2 \right) \overleftrightarrow{\mathbf{I}} - \mathbf{D} \otimes \mathbf{E} - \mathbf{B} \otimes \mathbf{H} \tag{2.66}$$

is the Einstein-Laub stress tensor and $\mathbf{g}_{\mathrm{EL}}$ is the Einstein-Laub momentum density, which is equal to Abraham's, i.e., $\mathbf{g}_{\mathrm{EL}} = \mathbf{g}_{\mathrm{Ab}}$.

The energy continuity equation is obtained similarly to the previous formulations, and is given by

$$-\boldsymbol{\nabla} \cdot (\mathbf{E} \times \mathbf{H}) - \frac{1}{2} \frac{\partial}{\partial t} \left(\varepsilon_0 |\mathbf{E}|^2 + \mu_0 |\mathbf{H}|^2 \right) = \mathbf{E} \cdot \mathbf{J}_{\mathrm{f}} + \mathbf{E} \cdot \frac{\partial \mathbf{P}}{\partial t} + \mu_0 \mathbf{H} \cdot \frac{\partial \mathbf{M}}{\partial t}, \tag{2.67}$$

from where we identify

$$\mathbf{S}_{\mathrm{EL}} = \mathbf{E} \times \mathbf{H}, \tag{2.68}$$

$$W_{\mathrm{EL}} = \frac{1}{2} \left(\varepsilon_0 |\mathbf{E}|^2 + \mu_0 |\mathbf{H}|^2 \right), \tag{2.69}$$

and

$$\phi_{\mathrm{EL}} = \mathbf{E} \cdot \mathbf{J}_{\mathrm{f}} + \mathbf{E} \cdot \frac{\partial \mathbf{P}}{\partial t} + \mu_0 \mathbf{H} \cdot \frac{\partial \mathbf{M}}{\partial t}. \tag{2.70}$$

We can see that Einstein-Laub's stress-energy tensor is symmetric only for linear and isotropic media, and it is known to be not invariant under Lorentz transformations [67]. It does not need the inclusion of the hidden momentum contribution; however, it is strongly criticized for having a non-zero self-force [103]. Besides, the force generated on electric charges is experimentally verified to be proportional to $\mathbf{B}$ [104], not $\mathbf{H}$, as Eq. (2.60) considers, and the magnetic dipole force in this model also should be proportional to $\mathbf{B}$ instead of $\mathbf{H}$, as Eq. (2.62) describes [105]. Einstein-Laub's formulation generates the same total force as Ampère's formulation if the hidden momentum contribution can be neglected in the latter [106]; however, their spatial distributions can be significantly different [107].

At last, there is a very subtle problem in the derivation of the stress tensor for this formulation, which does not seem to have been yet recognized. The force densities are initially written for microscopic dipoles – but later, in Eq. (2.63), the source terms are substituted by their corresponding fields according to the macroscopic Maxwell's equations. This procedure is, of course, not expected to work. In other words, Eq. (2.65) is most generally not true, as it does not represent the sum of Eqs. (2.59) to (2.62) for arbitrary sources.

2.3.5 Chu formulation

Chu's formulation was developed to treat the forces on moving fluids [94]. It uses the so-called E-H representation, where the presence of matter is added as source terms in Maxwell's equation. For a reference frame at rest, the E-H equations are

$$\boldsymbol{\nabla} \cdot \mathbf{E} = \frac{\rho_{\mathrm{f}}}{\varepsilon_0} - \frac{1}{\varepsilon_0} \boldsymbol{\nabla} \cdot \mathbf{P}, \tag{2.71}$$

$$\boldsymbol{\nabla} \cdot \mathbf{H} = -\boldsymbol{\nabla} \cdot \mathbf{M}, \tag{2.72}$$

$$\boldsymbol{\nabla} \times \mathbf{H} - \varepsilon_0 \frac{\partial \mathbf{E}}{\partial t} = \mathbf{J}_{\mathrm{f}} + \frac{\partial \mathbf{P}}{\partial t}, \tag{2.73}$$

$$\boldsymbol{\nabla} \times \mathbf{E} + \mu_0 \frac{\partial \mathbf{H}}{\partial t} = -\mu_0 \frac{\partial \mathbf{M}}{\partial t}. \tag{2.74}$$

In this formulation, there is a separation of the electromagnetic part and a matter-field interaction part. The electromagnetic part is identical to the well-known Maxwell stress energy tensor,

$$\overleftrightarrow{\mathbf{T}}_{\mathrm{C}} = \frac{1}{2} \left(\varepsilon_0 |\mathbf{E}|^2 + \mu_0 |\mathbf{H}|^2 \right) \overleftrightarrow{\mathbf{I}} - \varepsilon_0 \mathbf{E} \otimes \mathbf{E} - \mu_0 \mathbf{H} \otimes \mathbf{H}, \tag{2.75}$$

with momentum density $\mathbf{g}_{\mathrm{C}} = \mathbf{g}_{\mathrm{Ab}}$. We recall the crucial detail that the fields in this formulation must be calculated according to the E-H equations shown in the presence of matter. In this situation, $\overleftrightarrow{\mathbf{T}}_{\mathrm{C}}$ is known as the Chu stress tensor – which is symmetric and invariant [67].

The interaction part is described by the tensor

$$\overleftrightarrow{\mathbf{T}}_{\mathrm{int}} = -\mathbf{P} \otimes \mathbf{E} - \mu_0 \mathbf{M} \otimes \mathbf{H} \tag{2.76}$$

and the momentum density $\mathbf{g}_{\mathrm{int}} = 0$. Chu's microscopic interpretation is identical to Einstein-Laub's: electric and magnetic dipoles are the sources of polarization and magnetization and the electromagnetic fields are treated in a dual way. In fact, the sum of the tensors $\overleftrightarrow{\mathbf{T}}_{\mathrm{C}}$ and $\overleftrightarrow{\mathbf{T}}_{\mathrm{int}}$ produces, mathematically, the Einstein-Laub tensor – which is expected, since both formulations use the same microscopic model for matter. Considering a system at rest, Chu's force density is then the same as Einstein-Laub's, with their total stress-energy tensors sharing the same properties.

2.3.6 Mass-polariton formulation

The mass-polariton (MP) formulation [95–100] is motivated by noticing that none of the previous formulations is able to satisfy the covariance principle from special relativity when applying the center of mass-energy theorem to the so-called Einstein's box thought experiment. In this experiment, we have initially a photon in vacuum with energy $\hbar\omega$ and velocity c and a dielectric medium block of mass M and refractive index n at rest. The photon then strikes the medium, propagating through it with velocity $v = c/n$, while the medium acquires a velocity V. According to the center of mass-energy theorem, we must have

$$V_{\mathrm{cme}} = \frac{\hbar\omega c}{\hbar\omega + Mc^2} = \frac{\hbar\omega v + Mc^2 V}{\hbar\omega + Mc^2}, \tag{2.77}$$

where V_{cme} is the velocity of the center of mass-energy of the system. Equating the numerators, we have $\hbar\omega/c = \hbar\omega/(nc) + MV$, which suggests the photon has an Abraham-type momentum. However, we can see that if the photon has energy $E = \hbar\omega$ and momentum $p = \hbar\omega/(nc)$, the covariant energy-momentum relation $E^2 = (pc)^2 + (m_0c^2)^2$ can not be satisfied if we set the rest mass of the photon as zero. The same problem occurs if we choose a Minkowski-type momentum, i.e., if we take $p = n\hbar\omega/c$. This simple result suggests the possibility that the photon inside the medium actually couples to the atoms, creating a bound state of field and matter with a non-zero rest mass. This is exactly the proposal of the MP formulation.

In the MP formulation, there is a coupled state of the electromagnetic field and matter with a small but non-zero rest mass – the mass-polariton itself –, which is related to an atomic mass density wave (MDW) driven forward by the optical forces acting on the medium as the applied electromagnetic wave propagates through it [95]. This atomic MDW is composed of the rest energy associated with local variations in the atomic density resulting from the displacement of atoms by the optical force density. Besides, there is a very small energy transfer from the field to the kinetic energy of the medium due to the movement of the atoms.

By employing Lorentz transformations, it can be shown [95] that for linear, isotropic and dispersionless media the mass-polariton momentum is $p_{\mathrm{MP}} = n\hbar\omega/c$, while the small mass transferred by the MDW is given by $\delta m = (n^2 - 1)\hbar\omega/c^2$. These results are indeed able to satisfy the center of mass-energy condition, Eq. (2.77), as well as the energy covariance condition. Additionally, it can also be shown that in this formulation the field momentum is $p_{\mathrm{field}} = \hbar\omega/(nc)$, while the MDW momentum is the difference of the MP and field momentum, i.e., $p_{\mathrm{MDW}} = (n - 1/n)\hbar\omega/c$. However, notice that due to the coupling of field and matter only p_{MP} and δm are directly measurable. Also notice that this form of momentum, explicitly separated into field and matter parts as Abraham-type and Minkowski-type respectively, can also be found in Ref. [101] – although no further discussion in terms of the small mass transfer and covariance condition is presented there.

According to the interpretation just discussed, the total stress-energy tensor of the mass-polariton state of light is composed of a field part and a material part as [95, 98–100]

$$\mathcal{T}_{\mathrm{MP}} = \mathcal{T}_{\mathrm{field}} + \mathcal{T}_{\mathrm{MDW}}. \tag{2.78}$$

It is assumed that the Abraham force density, Eq. (2.40), is the correct optical force density in the laboratory frame for a linear medium with no dispersion, no losses and in mechanical equilibrium. Therefore, the field part of the MP formulation is, in the laboratory frame, equal to the Abraham stress energy tensor [95, 98, 99, 108]

$$\mathcal{T}_{\mathrm{field}} = \mathcal{T}_{\mathrm{Ab}}. \tag{2.79}$$

The matter part of MP stress-energy tensor is related to the MDW and is given by the difference of the stress-energy tensors of the medium in the presence and absence of light as [95, 98–100]

$$\begin{aligned}\mathcal{T}_{\mathrm{MDW}} &= \begin{pmatrix} \rho_{\mathrm{a}} c^2 & \rho_{\mathrm{a}} \mathbf{v}_{\mathrm{a}}^{\mathrm{T}} c \\ \rho_{\mathrm{a}} \mathbf{v}_{\mathrm{a}} c & \rho_{\mathrm{a}} \mathbf{v}_{\mathrm{a}} \otimes \mathbf{v}_{\mathrm{a}} \end{pmatrix} - \begin{pmatrix} \rho_{\mathrm{a0}} c^2 & \mathbf{0} \\ \mathbf{0} & \mathbf{0} \end{pmatrix} \\ &= \begin{pmatrix} \rho_{\mathrm{MDW}} c^2 & \rho_{\mathrm{MDW}} \mathbf{v}_{\mathrm{MDW}}^{\mathrm{T}} c \\ \rho_{\mathrm{MDW}} \mathbf{v}_{\mathrm{MDW}} c & \rho_{\mathrm{MDW}} \mathbf{v}_{\mathrm{a}} \otimes \mathbf{v}_{\mathrm{MDW}} \end{pmatrix}.\end{aligned} \tag{2.80}$$

Here, $\rho_{\mathrm{a}} = m_0 n_{\mathrm{a}}$ is the atomic mass density, $\rho_{\mathrm{a0}} = m_0 n_{\mathrm{a0}}$ is the atomic mass density in the absence of light with the corresponding number density n_{a0} and $\mathbf{v}_{\mathrm{MDW}} = \rho_{\mathrm{a}} \mathbf{v}_{\mathrm{a}}/\rho_{\mathrm{MDW}}$ is the local velocity of light in the medium. The mass density of the atomic MDW is defined as $\rho_{\mathrm{MDW}} = \rho_{\mathrm{a}} - \rho_{\mathrm{a0}} = m_0(n_{\mathrm{a}} - n_{\mathrm{a0}})$. The MDW energy density $\rho_{\mathrm{MDW}} c^2$ is the rest energy originating from the atomic number density difference $n_{\mathrm{a}} - n_{\mathrm{a0}}$ generated by the Abraham force driving the atoms forward. Therefore, being a result from the compression of atoms closer to each other by the optical force density of a light pulse (and not from the increase of kinetic energy), the rest energy density $\rho_{\mathrm{MDW}} c^2$ does not vanish in the assumed non-relativistic limit. On its turn, the kinetic energy of atoms, which is transferred from the field to the medium, is extremely small due to its quadratic dependence on the small atomic velocity [100].

The stress-energy tensor $\mathcal{T}_{\mathrm{MP}}$ was shown to satisfy all conservation and symmetry requirements [98, 100] and also agreed with computer simulations of the continuum dynamics of elastic media in the presence of optical forces [96] and angular momentum transfer (from both orbital and spin origins) [97].

2.4 Electro- and magnetostriction effects

When electromagnetic fields are applied to a dielectric medium, it is observed there are electromagnetic forces acting towards the regions of higher field intensity. For polarizable media, this phenomenon is known as electrostriction, while its magnetic analogue is known as magnetostriction. They are transient effects: the medium responds by increasing its local pressure (for fluids) or local strain (for solids) until the associated electromagnetic forces are completely counterbalanced. This happens approximately in a time scale given by the time taken for pressure waves to propagate a distance equal to the characteristic spatial scale of the region affected by the fields [109]. After this time, the material reaches equilibrium and striction forces have no significant extra effect over the material.

Another important feature is that the striction effects always produce a zero total force when integrated over the volume of the material. Since the striction forces are written as gradients (as we will shortly see), their volumetric integrals can always be transformed into exterior surface integrals. The surface of integration must be closed and lie outside the material – but is otherwise arbitrary. Thus, we use the same argument as Ref. [67]: we choose this surface to be contained within an artificial vacuum layer of infinitesimal thickness surrounding the material. In this case, striction forces are always zero, and the physical situation is recovered as the thickness tends to zero. Therefore, striction forces do not generate any effect on the material's center of mass – they are important only in local force considerations.

The properties just described lead to electro- and magnetostriction being usually ignored in the analysis of experiments related to the Abraham-Minkowski controversy; they must, however, inevitably be present in a definitive description of the light-matter interaction. For example, striction effects are often directly related to the stability of fluids exposed to electromagnetic fields [110–113] and also provide a nonlinear coupling able to generate stimulated Brillouin scattering [114, 115]. In any case, these effects are not very well understood theoretically. From all the formulations presented, striction forces are, in some way, contemplated only by the Einstein-Laub formulation [116] and, consequently, by Chu formulation, as they share the same force density. For static fields, there is a phenomenological force density description given by Landau and Lifshitz [117] as

$$\mathbf{f} = -\frac{1}{2}|\mathbf{E}|^2\boldsymbol{\nabla}\varepsilon - \frac{1}{2}|\mathbf{H}|^2\boldsymbol{\nabla}\mu + \frac{1}{2}\boldsymbol{\nabla}\left[|\mathbf{E}|^2\rho_{\mathrm{m}}\left(\frac{\partial\varepsilon}{\partial\rho_{\mathrm{m}}}\right)_T\right] + \frac{1}{2}\boldsymbol{\nabla}\left[|\mathbf{H}|^2\rho_{\mathrm{m}}\left(\frac{\partial\mu}{\partial\rho_{\mathrm{m}}}\right)_T\right], \tag{2.81}$$

where ρ_{m} is the mass density. Here, the first and second terms are the same present in Abraham and Minkowski formulations, which act on inhomogeneous regions – usually the interface between media. The third and fourth terms are the electro- and magnetostriction force densities, respectively. The partial derivatives are calculated at constant temperature T because the medium's polarization and magnetization usually depend on T. Eq. (2.81) is also known as Helmholtz force density [116, 118, 119].

For non-polar and non-magnetic media, we can use the Clausius-Mossotti relation [120] for the microscopic field correction, providing $\rho_{\mathrm{m}}(\partial\varepsilon/\partial\rho_{\mathrm{m}})_T = (\varepsilon - \varepsilon_0)(\varepsilon + 2\varepsilon_0)/3$. This procedure has successfully been applied, for example, in Refs. [121, 122]. Notice, however, that Eq. (2.81) valid only for systems in thermodynamical equilibrium. If the excitation is time-dependent, the derivatives in Eq. (2.81) must be calculated at constant entropy for the hypersonic components (see chapter 9 of Ref. [114]). This was employed for below-optical frequencies, for example, in Ref. [123]. For optical frequencies, however, measurements of the striction effects are very difficult to perform, since thermal effects typically dominates over them [124].

In the context discussed, we will present a new formulation – the Microscopic Ampère formulation –, which is the main result of this work and will be discussed in detail in next chapter. This formulation will be able to contemplate the striction effects and will have a clear microscopic interpretation, with no need for phenomenological approaches.

CHAPTER 3

Microscopic Ampère formulation

As we have seen in Chapter 2, every known formulation for the electromagnetic stress-energy tensor presents its own problems [125]. Generally, every formulation except Einstein-Laub's and Chu's do not account naturally for electro- and magnetostriction effects. The main problems of each formulation shall be individually discussed next.

First, Minkowski's formulation totally neglects the bound charges inside the material [101]. In fact, had he used the correct charge density, he would have obtained Ampère's conventional formulation without the hidden momentum, i.e., Eqs. (2.51) and (2.52). As Abraham's formulation only differs from Minkowski's in the momentum density, it should share this same problem. Besides, both formulations have not shown any connection to known models of electromagnetic sources.

Ampère's formulation does adopt the appropriate classical microscopic model, i.e., the electric sources are given as ideal dipoles and the magnetic sources as tiny current loops [102]. This formulation works properly if we are interested only in the movement of the center of mass of rigid bodies – indeed, it can be written in covariant form, as shown in Appendix A; however, as only the macroscopic effects of polarizations and magnetizations are considered, Ampère's formulation is not expected to correctly describe the microscopic force distribution inside materials [71].

The Einstein-Laub formulation, on its turn, has been built considering the usual dipolar approximation for the electromagnetic fields inside matter, but adopts an incorrect model for the microscopic magnetization mechanism, as it assumes the existence of magnetic monopoles, which have never been observed [102]. For non-magnetic materials, its related force density should be correct; however, there would still remain strong theoretical issues, like the absence of Lorentz invariance of the electromagnetic stress-energy tensor. Although attributing different contributions to light and matter, Chu's formulation follows the same microscopic model of Einstein and Laub.

Lastly, the MP formulation is very promising as it theoretically contemplates many aspects of the problem, being particularly consistent with a formal covariant theory of light in dispersive media [126]. However, it is essentially an extension of Abraham's formulation, and so lacks a clear microscopic description of the electromagnetic sources as well.

In the context just presented, it seems then natural to consider a formulation that arises from the charge and current distributions related to microscopic electric and magnetic dipoles. Such formulation will be developed here, and will be shown to present many of the characteristics necessary to explain the existing experiments.

3.1 Dipolar sources

In this section and in the following one, we will derive the electromagnetic forces on a neutral, ideal classical dipole composed of two point charges of opposite value $\pm q$ separated by a distance $|\mathbf{d}|$. The chosen inertial reference frame is the rest frame of the dipole – consequently, the velocity of the dipole's center of mass is taken as zero. Under these circumstances, the static electric potential associated to this charge distribution at a point $\mathbf{r}$ is given by

$$\varphi(\mathbf{r}) = \frac{1}{4\pi\varepsilon_0}\left[\frac{q}{|\mathbf{r}+\mathbf{d}/2|} - \frac{q}{|\mathbf{r}-\mathbf{d}/2|}\right], \tag{3.1}$$

where ε_0 the free space permittivity. The origin of the coordinate system is placed in the mid point between the charges, with the charge $+q$ being at $+\mathbf{d}/2$ and the charge $-q$ being at $-\mathbf{d}/2$. We assumed, for simplicity, that the charges are located in vacuum, as the final result will not depend on this choice. In addition, for a neutral dipole as we consider here, the choice of the origin of the coordinate system does not affect the dipole's moment – so, also for simplicity, we choose here the origin as the dipole's unperturbed center of mass.

If the observation point $\mathbf{r}$ is relatively far from $\mathbf{d}$, i.e., $|\mathbf{r}| \gg |\mathbf{d}|$, to order $|\mathbf{d}|^2/|\mathbf{r}|^2$ we have [120, 127]

$$\varphi(\mathbf{r}) = \frac{1}{4\pi\varepsilon_0}\frac{\mathbf{p}\cdot\hat{\mathbf{r}}}{r^2}, \tag{3.2}$$

with $\mathbf{p} = q\mathbf{d}$ being the electric dipole moment and the unit vector $\hat{\mathbf{r}} = \mathbf{r}/|\mathbf{r}|$. Notice that $|\mathbf{d}|$ is typically smaller than 1 nm. Under the optical regime we have $|\mathbf{r}| \sim \lambda \sim 0.1$ μm, resulting in a relative error in Eq. (3.2) of order 10^{-4}, which should provide a good approximation for optical excitations.

Notice that Eq. (3.2) can also be written as

$$\varphi(\mathbf{r}) = -\frac{\mathbf{p}}{4\pi\varepsilon_0}\cdot\boldsymbol{\nabla}\left(\frac{1}{r}\right), \tag{3.3}$$

which can be conveniently inserted into Poisson's equation for the electric potential, $\nabla^2\varphi = -\rho/\varepsilon_0$, allowing us to obtain the electric charge density associated to the dipole as

$$\rho(\mathbf{r}) = \frac{\mathbf{p}}{4\pi} \cdot \boldsymbol{\nabla} \left[\nabla^2 \left(\frac{1}{r}\right)\right] = -(\mathbf{p} \cdot \boldsymbol{\nabla})\delta^3(\mathbf{r}), \tag{3.4}$$

where $\delta^3(\mathbf{r})$ is the three-dimensional Dirac delta function, i.e., $\delta^3(\mathbf{r}) = \delta(x)\delta(y)\delta(z)$.

An analogous procedure must be carried out for the magnetic dipole moment. The vector potential of a static point magnetic dipole at rest located at the origin is given by [120, 127]

$$\mathbf{A}(\mathbf{r}) = \frac{\mu_0}{4\pi} \frac{\mathbf{m} \times \hat{\mathbf{r}}}{r^2}, \tag{3.5}$$

where $\mathbf{m} = (1/2) \int \mathbf{r} \times \mathbf{J}(\mathbf{r})\, \mathrm{d}^3\mathbf{r}$ is the magnetic dipole moment. The magnetic induction $\mathbf{B}$ generated by this magnetic dipole is then

$$\mathbf{B}(\mathbf{r}) = \boldsymbol{\nabla} \times \mathbf{A} = \mu_0 \mathbf{m}\delta^3(\mathbf{r}) - \frac{\mu_0}{4\pi} \mathbf{m} \cdot \boldsymbol{\nabla} \left(\frac{\hat{\mathbf{r}}}{r^2}\right). \tag{3.6}$$

The electric current density $\mathbf{J}$ is given in this case by Ampère-Maxwell's law as $\mathbf{J} = \mu_0^{-1}\boldsymbol{\nabla} \times \mathbf{B}$. Using $\mathbf{B}$ given in Eq. (3.6), we can see that

$$\mathbf{J}(\mathbf{r}) = \boldsymbol{\nabla} \times \big(\mathbf{m}\delta^3(\mathbf{r})\big) = -\mathbf{m} \times \boldsymbol{\nabla}\delta^3(\mathbf{r}), \tag{3.7}$$

where the vector property $\boldsymbol{\nabla} \times (a\mathbf{v}) = a\boldsymbol{\nabla} \times \mathbf{v} - \mathbf{v} \times \boldsymbol{\nabla} a$ was used, with a being an arbitrary scalar function.

At last, a time dependent electric field can cause the electric dipole separation $\mathbf{d}$ to vary in time – even if the dipole's center of mass remains at rest. This will naturally generate a local, microscopic electric current, which will interact with the magnetic induction, providing the time-dependent extra term $\dot{\mathbf{p}}\delta^3(\mathbf{r})$ to the current density $\mathbf{J}$. Mathematically, this can be shown through the continuity equation:

$$\boldsymbol{\nabla} \cdot \mathbf{J} = -\frac{\partial \rho}{\partial t} = -(\dot{\mathbf{p}} \cdot \boldsymbol{\nabla})\delta^3(\mathbf{r}), \tag{3.8}$$

where we used Eq. (3.4). The last term can be rewritten as $\boldsymbol{\nabla} \cdot (\dot{\mathbf{p}} \cdot \delta^3(\mathbf{r}))$, which readily provides $\mathbf{J} = \dot{\mathbf{p}}\delta^3(\mathbf{r})$, as the divergence of Eq. (3.7) is always zero. An alternative derivation can be found in Ref. [127].

Notice that we have obtained here the time dependence of the microscopic electromagnetic sources in the ideal dipolar approximation through a somewhat simple argument: the application of the continuity equation to the known sources. A formal calculation would require the consideration of dynamic dipoles from the very start, because their acceleration can generate radiation-related terms (or, in other words, the solution to the continuity equation might not be unique). Besides, the concept of retarded time must also be included to assure physical causality. Such calculation will be presented in next section, and it will be shown the sources obtained here are indeed correct.

3.1.1 Time-dependent dipoles

It is well-known that in the Lorenz gauge the electromagnetic potentials φ and $\mathbf{A}$ are described by non-homogeneous wave equations whose formal solutions are [120]

$$\varphi(\mathbf{r},t) = \frac{1}{4\pi\varepsilon_0}\int \frac{\rho(\mathbf{r}',t_r)}{|\mathbf{r}-\mathbf{r}'|}\,\mathrm{d}^3\mathbf{r}' \tag{3.9}$$

and

$$\mathbf{A}(\mathbf{r},t) = \frac{\mu_0}{4\pi}\int \frac{\mathbf{J}(\mathbf{r}',t_r)}{|\mathbf{r}-\mathbf{r}'|}\,\mathrm{d}^3\mathbf{r}', \tag{3.10}$$

where $t_r = t - |\mathbf{r}-\mathbf{r}'|/c$ is the retarded time.

Under the dipolar approximation, the electromagnetic potentials of dynamic ideal dipoles are given by [128]

$$\varphi(\mathbf{r},t) = \frac{1}{4\pi\varepsilon_0}\left[\mathbf{p}(t_0) + \frac{r}{c}\dot{\mathbf{p}}(t_0)\right]\cdot\frac{\hat{\mathbf{r}}}{r^2} \tag{3.11}$$

and

$$\mathbf{A}(\mathbf{r},t) = \frac{\mu_0}{4\pi}\left[\frac{\dot{\mathbf{p}}(t_0)}{r} + \frac{\mathbf{m}(t_0)\times\hat{\mathbf{r}}}{r^2} + \frac{\dot{\mathbf{m}}(t_0)\times\hat{\mathbf{r}}}{cr}\right], \tag{3.12}$$

where $\mathbf{p}$ and $\mathbf{m}$ are the now time-dependent electric and magnetic dipole moments, respectively, and $t_0 = t - r/c$ is the retarded time at the origin.

The electromagnetic fields are given in terms of the potentials as $\mathbf{E} = -\boldsymbol{\nabla}\varphi - \partial_t\mathbf{A}$ and $\mathbf{B} = \boldsymbol{\nabla}\times\mathbf{A}$. We can use Gauss' Law and Ampère-Maxwell's law to obtain the time-dependent charge and current densities as

$$\rho(\mathbf{r},t) = -\varepsilon_0\nabla^2\varphi - \varepsilon_0\boldsymbol{\nabla}\cdot\partial_t\mathbf{A} \tag{3.13}$$

and

$$\mathbf{J}(\mathbf{r},t) = \frac{1}{\mu_0}\boldsymbol{\nabla}\times\boldsymbol{\nabla}\times\mathbf{A}. \tag{3.14}$$

However, this is not a very convenient procedure, because the implicit dependence of t_0 in $\mathbf{r}$ makes the calculation much more difficult[1]. Therefore, it is sufficient to show that the sources adopted in the last section, namely $\rho(\mathbf{r},t) = -(\mathbf{p}(t)\cdot\boldsymbol{\nabla})\delta^3(\mathbf{r})$ and $\mathbf{J}(\mathbf{r},t) = \dot{\mathbf{p}}(t)\delta^3(\mathbf{r}) - (\mathbf{m}(t)\times\boldsymbol{\nabla})\delta^3(\mathbf{r})$, generate the correct electromagnetic potentials given in Eqs.

[1]This calculation was performed in Ref. [71], but for the effective bound sources, which is analogous, but easier.

(3.11) and (3.12) when calculated using Eqs. (3.9) and (3.10).

We start by calculating the electric potential as

$$\varphi(\mathbf{r},t) = -\frac{1}{4\pi\varepsilon_0}\int \frac{(\mathbf{p}(t_r)\cdot\boldsymbol{\nabla}')\delta^3(\mathbf{r}')}{|\mathbf{r}-\mathbf{r}'|}\,\mathrm{d}^3\mathbf{r}'. \tag{3.15}$$

Using the property $\int f(x)\delta'(x-x_0)\,\mathrm{d}x = -f'(x_0)$, we have

$$\varphi(\mathbf{r},t) = \frac{1}{4\pi\varepsilon_0}\boldsymbol{\nabla}'\cdot\left(\frac{\mathbf{p}(t_r)}{|\mathbf{r}-\mathbf{r}'|}\right)_{\mathbf{r}'=0}. \tag{3.16}$$

Notice that, due to the implicit dependence of t_r on r, we have $\boldsymbol{\nabla}'\cdot\mathbf{p}(t_r)|_{\mathbf{r}'=0} = \tilde{\boldsymbol{\nabla}}'\cdot\mathbf{p}(t_0) + (\hat{\mathbf{r}}/c)\cdot\dot{\mathbf{p}}(t_0)$, where $\tilde{\boldsymbol{\nabla}}'$ denotes the nabla operator acting only on the spatial coordinates. Specifically, in the ideal dipole approximation we have $\tilde{\boldsymbol{\nabla}}'\cdot\mathbf{p}(t_0) = 0$, so that the electric potential is

$$\varphi(\mathbf{r},t) = \frac{1}{4\pi\varepsilon_0}\left[\frac{\mathbf{p}(t_0)\cdot\hat{\mathbf{r}}}{r^2} + \frac{\dot{\mathbf{p}}(t_0)\cdot\hat{\mathbf{r}}}{cr}\right], \tag{3.17}$$

which is indeed the same as Eq. (3.11).

For $\mathbf{A}$, we initially have

$$\mathbf{A}(\mathbf{r},t) = \frac{\mu_0}{4\pi}\int \frac{\dot{\mathbf{p}}(t_r)\delta^3(\mathbf{r}') - (\mathbf{m}(t_r)\times\boldsymbol{\nabla}')\delta^3(\mathbf{r}')}{|\mathbf{r}-\mathbf{r}'|}\,\mathrm{d}^3\mathbf{r}'. \tag{3.18}$$

The first term is trivially integrated to $(\mu_0/4\pi r)\dot{\mathbf{p}}(t_0)$. The second term is analogous to Eq. (3.16), with $\mathbf{p}\to\mathbf{m}$ and divergence operator $\to$ curl operator. Thus,

$$\mathbf{A}(\mathbf{r},t) = \frac{\mu_0}{4\pi}\left[\frac{\dot{\mathbf{p}}(t_0)}{r} + \frac{\mathbf{m}(t_0)\times\hat{\mathbf{r}}}{r^2} + \frac{\dot{\mathbf{m}}(t_0)\times\hat{\mathbf{r}}}{cr}\right], \tag{3.19}$$

which is equal to Eq. (3.12) and completes our calculation.

The proof shown here tells us that, even in the dynamic regime, if the dipolar approximation can be suitably applied, the microscopic electromagnetic sources obtained in the last section are indeed the correct ones. Consequently, by employing the Lorentz force density to these sources, we should be able to obtain the appropriate force density distribution inside matter within the adopted approximations.

Lastly, notice that in our system the correction term $|\mathbf{r}-\mathbf{r}'|/c$ of the retarded time t_r will be extremely small (typically of order $\lambda/c \sim 10^{-15}$ s), so the fields and forces can safely be evaluated at the regular time t.

3.2 Electromagnetic force density

We will consider electromagnetic fields inside dielectric materials within the optical bandwidth. We suppose here that at this optical length scale the microscopic sources are well described by the dipolar approximation, as discussed in the last section.

Initially, we want to derive the electromagnetic force spatio-temporal distribution acting on dielectric media with no free charges or currents. Mathematically, we obtained the electric charge and current densities for ideal dipoles located at the origin as

$$\rho(\mathbf{r},t) = -(\mathbf{p}(t)\cdot\boldsymbol{\nabla})\delta^3(\mathbf{r}) \tag{3.20}$$

and

$$\mathbf{J}(\mathbf{r},t) = \dot{\mathbf{p}}(t)\delta^3(\mathbf{r}) - (\mathbf{m}(t)\times\boldsymbol{\nabla})\delta^3(\mathbf{r}), \tag{3.21}$$

where $\mathbf{p}(t)$ and $\mathbf{m}(t)$ are the dipole's time-dependent electric and magnetic moment, respectively.

As discussed in Section 2.1 , the force acting on charged matter is unambiguously given by the continuous version of the Lorentz force law,

$$\mathbf{F} = \int (\rho\mathbf{E} + \mathbf{J}\times\mathbf{B})\,\mathrm{d}^3\mathbf{r}, \tag{3.22}$$

which in our case yields

$$\mathbf{F} = \int \big(\left[-(\mathbf{p}\cdot\boldsymbol{\nabla})\delta^3(\mathbf{r})\right]\mathbf{E} + \dot{\mathbf{p}}\delta^3(\mathbf{r})\times\mathbf{B} - \left[(\mathbf{m}\times\boldsymbol{\nabla})\delta^3(\mathbf{r})\right]\times\mathbf{B}\big)\,\mathrm{d}^3\mathbf{r}. \tag{3.23}$$

We must now calculate Eq. (3.23), which gives the total force on the dielectric. Each term of the integral will be treated separately. The first term is

$$\mathbf{F}_1 = -\int [(\mathbf{p}\cdot\boldsymbol{\nabla})\delta^3(\mathbf{r})]\mathbf{E}\,\mathrm{d}^3\mathbf{r}. \tag{3.24}$$

Writing explicitly the components of the term inside the brackets, we have

$$\begin{aligned}\mathbf{F}_1 = -\int [&p_x\delta(y)\delta(z)\delta'(x) + p_y\delta(x)\delta(z)\delta'(y) + \\ &p_z\delta(x)\delta(y)\delta'(z)]\mathbf{E}\,\mathrm{d}^3\mathbf{r}.\end{aligned} \tag{3.25}$$

Integrating each term by parts we obtain

$$\begin{aligned}\mathbf{F}_1 &= \partial_x(p_x\mathbf{E}) + \partial_y(p_y\mathbf{E}) + \partial_z(p_z\mathbf{E}) \\ &= (\mathbf{p}\cdot\boldsymbol{\nabla})\mathbf{E} + (\boldsymbol{\nabla}\cdot\mathbf{p})\mathbf{E}. \end{aligned} \tag{3.26}$$

Under the ideal dipolar approximation, the last term can be neglected – so, $\mathbf{F}_1 = (\mathbf{p}\cdot\boldsymbol{\nabla})\mathbf{E}$.

The second term of Eq. (3.23) is integrated trivially:

$$\mathbf{F}_2 = \int [\dot{\mathbf{p}}\delta^3(\mathbf{r})] \times \mathbf{B}\,\mathrm{d}^3\mathbf{r} = \dot{\mathbf{p}} \times \mathbf{B}. \tag{3.27}$$

The last term of Eq. (3.23) is

$$\begin{aligned}\mathbf{F}_3 &= -\int [(\mathbf{m}\times\boldsymbol{\nabla})\delta^3(\mathbf{r})] \times \mathbf{B}\,\mathrm{d}^3\mathbf{r} \\ &= -\int \{[\delta(x)\delta(y)m_y\delta'(z) - \delta(x)\delta(z)m_z\delta'(y)]\hat{\mathbf{i}} \\ &+ [\delta(y)\delta(z)m_z\delta'(x) - \delta(x)\delta(y)m_x\delta'(z)]\hat{\mathbf{j}} \\ &+ [\delta(x)\delta(z)m_x\delta'(y) - \delta(y)\delta(z)m_y\delta'(x)]\hat{\mathbf{k}}\} \times \mathbf{B}\,\mathrm{d}^3\mathbf{r} \\ &= -\int \mathbf{C}\times\mathbf{B}\,\mathrm{d}^3\mathbf{r}, \end{aligned} \tag{3.28}$$

where the auxiliary vector $\mathbf{C}$ has been implicitly defined for simplicity and $\hat{\mathbf{i}}, \hat{\mathbf{j}}, \hat{\mathbf{k}}$ denote the cartesian unit vectors. Performing the cross product, we have

$$\mathbf{F}_3 = -\int [(C_yB_z - C_zB_y)\hat{\mathbf{i}} + (C_zB_x - C_xB_z)\hat{\mathbf{j}} + (C_xB_y - C_yB_x)\hat{\mathbf{k}}]\,\mathrm{d}^3\mathbf{r}. \tag{3.29}$$

The x component of $\mathbf{F}_3$ is then

$$\begin{aligned}F_{3,x} &= -\int [\delta(y)\delta(z)m_z\delta'(x)B_z - \delta(x)\delta(y)m_x\delta'(z)B_z \\ &- \delta(x)\delta(z)m_x\delta'(y)B_y + \delta(y)\delta(z)m_y\delta'(x)B_y]\,\mathrm{d}^3\mathbf{r} \\ &= m_z\partial_xB_z - m_x\partial_zB_z - m_x\partial_yB_y + m_y\partial_xB_y, \end{aligned} \tag{3.30}$$

where we have integrated by parts again. The y and z components are obtained analogously, yielding

$$F_{3,y} = m_x\partial_yB_x - m_y\partial_xB_x - m_y\partial_zB_z + m_z\partial_yB_z, \tag{3.31}$$

$$F_{3,z} = m_y\partial_zB_y - m_z\partial_yB_y - m_z\partial_xB_x + m_x\partial_zB_x. \tag{3.32}$$

To obtain a more compact result, notice that

$$
\begin{aligned}
F_{3,x} - [\mathbf{m}\times(\boldsymbol{\nabla}\times\mathbf{B})]_x - [(\mathbf{m}\cdot\boldsymbol{\nabla})\mathbf{B}]_x &= -m_x\partial_z B_z - m_x\partial_y B_y + m_y\partial_y B_x \\
&+ \; m_z\partial_z B_x - m_x\partial_x B_x - m_y\partial_y B_x - m_z\partial_z B_x \\
&= -m_x(\boldsymbol{\nabla}\cdot\mathbf{B}) = 0. \qquad (3.33)
\end{aligned}
$$

This means that $F_{3,x} = [\mathbf{m}\times(\boldsymbol{\nabla}\times\mathbf{B})]_x + [(\mathbf{m}\cdot\boldsymbol{\nabla})\mathbf{B}]_x$, and, consequently,

$$\mathbf{F}_3 = \mathbf{m}\times(\boldsymbol{\nabla}\times\mathbf{B}) + (\mathbf{m}\cdot\boldsymbol{\nabla})\mathbf{B}, \qquad (3.34)$$

which completes our calculation.

Summing the three contributions to the force and dividing by the dielectric's volume, we obtain the position- and time-dependent force density in the so called Microscopic Ampère (MA) formulation

$$\mathbf{f}_{\mathrm{MA}} = (\mathbf{P}\cdot\boldsymbol{\nabla})\,\mathbf{E} + \dot{\mathbf{P}}\times\mathbf{B} + \mathbf{M}\times(\boldsymbol{\nabla}\times\mathbf{B}) + (\mathbf{M}\cdot\boldsymbol{\nabla})\,\mathbf{B}, \qquad (3.35)$$

where the fields are the macroscopic ones evaluated at the location of the dipoles.

Eq. (3.35) was first given, to our knowledge, in Ref. [71] – but it was not explored in the context of the Abraham-Minkowski controversy. It is compatible with a pure, ideal dipole located at the origin and at rest in its own frame. Explicitly, the time derivative term is

$$\dot{\mathbf{P}}\times\mathbf{B} = \frac{\partial\mathbf{P}}{\partial t}\times\mathbf{B}, \qquad (3.36)$$

as the dipole is assumed to be at rest.

Now, we want to rewrite Eq. (3.35) in a form which it is most conveniently interpreted in the context of the Abraham-Minkowski controversy. This task will require a lot of vector algebra. We start by using the vector property $\boldsymbol{\nabla}(\mathbf{U}\cdot\mathbf{V}) = (\mathbf{U}\cdot\boldsymbol{\nabla})\mathbf{V} + (\mathbf{V}\cdot\boldsymbol{\nabla})\mathbf{U} + \mathbf{U}\times(\boldsymbol{\nabla}\times\mathbf{V}) + \mathbf{V}\times(\boldsymbol{\nabla}\times\mathbf{U})$, which allows us to write

$$(\mathbf{P}\cdot\boldsymbol{\nabla})\,\mathbf{E} = \boldsymbol{\nabla}(\mathbf{P}\cdot\mathbf{E}) - (\mathbf{E}\cdot\boldsymbol{\nabla})\,\mathbf{P} - \mathbf{E}\times(\boldsymbol{\nabla}\times\mathbf{P}) - \mathbf{P}\times(\boldsymbol{\nabla}\times\mathbf{E}) \qquad (3.37)$$

and

$$\mathbf{M}\times(\boldsymbol{\nabla}\times\mathbf{B}) + (\mathbf{M}\cdot\boldsymbol{\nabla})\,\mathbf{B} = \boldsymbol{\nabla}(\mathbf{M}\cdot\mathbf{B}) - \mathbf{B}\times(\boldsymbol{\nabla}\times\mathbf{M}) - (\mathbf{B}\cdot\boldsymbol{\nabla})\,\mathbf{M}. \qquad (3.38)$$

For linear isotropic media, the medium responses are given by $\mathbf{P} = \varepsilon_0\chi_{\mathrm{e}}\mathbf{E}$ and $\mathbf{M} = \chi_{\mathrm{m}}\mathbf{H}$, where χ_{e} and χ_{m} are the electric and magnetic susceptibilities, respectively.

Working on Eq. (3.37), we have

$$(\mathbf{P}\cdot\boldsymbol{\nabla})\,\mathbf{E} = \varepsilon_0\boldsymbol{\nabla}\left(\chi_\mathrm{e}|\mathbf{E}|^2\right) - \varepsilon_0\,(\mathbf{E}\cdot\boldsymbol{\nabla})\,(\chi_\mathrm{e}\mathbf{E}) - \varepsilon_0\mathbf{E}\times(\boldsymbol{\nabla}\times(\chi_\mathrm{e}\mathbf{E})) \\ -\varepsilon_0\chi_\mathrm{e}\mathbf{E}\times(\boldsymbol{\nabla}\times\mathbf{E})\,. \tag{3.39}$$

The first term on the right hand side of this equation is

$$\varepsilon_0\boldsymbol{\nabla}\left(\chi_\mathrm{e}|\mathbf{E}|^2\right) = \varepsilon_0|\mathbf{E}|^2\boldsymbol{\nabla}\chi_\mathrm{e} + \varepsilon_0\chi_\mathrm{e}\boldsymbol{\nabla}|\mathbf{E}|^2. \tag{3.40}$$

The second term is

$$\varepsilon_0\,(\mathbf{E}\cdot\boldsymbol{\nabla})\,(\chi_\mathrm{e}\mathbf{E}) = \varepsilon_0\chi_\mathrm{e}\,(\mathbf{E}\cdot\boldsymbol{\nabla})\,\mathbf{E} + \varepsilon_0\,(\mathbf{E}\cdot\boldsymbol{\nabla}\chi_\mathrm{e})\,\mathbf{E}. \tag{3.41}$$

The third term is

$$\begin{aligned}\varepsilon_0\mathbf{E}\times(\boldsymbol{\nabla}\times(\chi_\mathrm{e}\mathbf{E})) &= \varepsilon_0\mathbf{E}\times(\chi_\mathrm{e}\boldsymbol{\nabla}\times\mathbf{E} + (\boldsymbol{\nabla}\chi_\mathrm{e})\times\mathbf{E}) \\ &= -\mathbf{P}\times\frac{\partial\mathbf{B}}{\partial t} + \varepsilon_0|\mathbf{E}|^2\boldsymbol{\nabla}\chi_\mathrm{e} - \varepsilon_0\,(\mathbf{E}\cdot\boldsymbol{\nabla}\chi_\mathrm{e})\,\mathbf{E},\end{aligned} \tag{3.42}$$

where the vector property $\mathbf{a}\times(\mathbf{b}\times\mathbf{c}) = (\mathbf{a}\cdot\mathbf{c})\mathbf{b} - (\mathbf{a}\cdot\mathbf{b})\mathbf{c}$ was used.

The last term on Eq. (3.39) can be described by Faraday's law as well, so that

$$\begin{aligned}(\mathbf{P}\cdot\boldsymbol{\nabla})\,\mathbf{E} &= \varepsilon_0|\mathbf{E}|^2\boldsymbol{\nabla}\chi_\mathrm{e} + \varepsilon_0\chi_\mathrm{e}\boldsymbol{\nabla}|\mathbf{E}|^2 - \varepsilon_0\chi_\mathrm{e}\,(\mathbf{E}\cdot\boldsymbol{\nabla})\,\mathbf{E} - \varepsilon_0\,(\mathbf{E}\cdot\boldsymbol{\nabla}\chi_\mathrm{e})\,\mathbf{E} \\ &+ \mathbf{P}\times\frac{\partial\mathbf{B}}{\partial t} - \varepsilon_0|\mathbf{E}|^2\boldsymbol{\nabla}\chi_\mathrm{e} + \varepsilon_0\,(\mathbf{E}\cdot\boldsymbol{\nabla}\chi_\mathrm{e})\,\mathbf{E} + \mathbf{P}\times\frac{\partial\mathbf{B}}{\partial t}.\end{aligned} \tag{3.43}$$

Simplifying the last equation, we obtain

$$(\mathbf{P}\cdot\boldsymbol{\nabla})\,\mathbf{E} = \frac{\varepsilon_0(\varepsilon_\mathrm{r}-1)}{2}\boldsymbol{\nabla}|\mathbf{E}|^2 + \mathbf{P}\times\frac{\partial\mathbf{B}}{\partial t}, \tag{3.44}$$

where we used $\boldsymbol{\nabla}|\mathbf{E}|^2/2 = (\mathbf{E}\cdot\boldsymbol{\nabla})\mathbf{E} + \mathbf{E}\times(\boldsymbol{\nabla}\times\mathbf{E})$.

Adding Eq. (3.36) to last equation yields

$$(\mathbf{P}\cdot\boldsymbol{\nabla})\,\mathbf{E} + \dot{\mathbf{P}}\times\mathbf{B} = \frac{\varepsilon_0(\varepsilon_\mathrm{r}-1)}{2}\boldsymbol{\nabla}|\mathbf{E}|^2 + \frac{\partial}{\partial t}\,(\mathbf{P}\times\mathbf{B})\,. \tag{3.45}$$

Proceeding analogously for Eq. (3.38), we have

$$\mathbf{M}\times(\boldsymbol{\nabla}\times\mathbf{B}) + (\mathbf{M}\cdot\boldsymbol{\nabla})\,\mathbf{B} = \boldsymbol{\nabla}\,(\chi_\mathrm{m}\mathbf{H}\cdot\mu\mathbf{H}) - \mu\mathbf{H}\times(\boldsymbol{\nabla}\times\chi_\mathrm{m}\mathbf{H}) \\ -(\mu\mathbf{H}\cdot\boldsymbol{\nabla})\,(\chi_\mathrm{m}\mathbf{H})\,, \tag{3.46}$$

where $\mathbf{B} = \mu_0(\mathbf{H}+\mathbf{M}) = \mu\mathbf{H}$ was used.

The first term on the right hand side of last equation is

$$\boldsymbol{\nabla}\left(\chi_{\mathrm{m}}\mathbf{H}\cdot\mu\mathbf{H}\right)=(2\mu_{\mathrm{r}}-1)|\mathbf{H}|^{2}\boldsymbol{\nabla}\mu+\mu(\mu_{\mathrm{r}}-1)\boldsymbol{\nabla}|\mathbf{H}|^{2}. \tag{3.47}$$

The second term is

$$\begin{aligned}\mu\mathbf{H}\times(\boldsymbol{\nabla}\times\chi_{\mathrm{m}}\mathbf{H}) &= \mu\mathbf{H}\times\left(\chi_{\mathrm{m}}\boldsymbol{\nabla}\times\mathbf{H}+(\boldsymbol{\nabla}\chi_{\mathrm{m}})\times\mathbf{H}\right)\\ &= \mu\chi_{\mathrm{m}}\mathbf{H}\times(\boldsymbol{\nabla}\times\mathbf{H})+\mu\mathbf{H}\times(\boldsymbol{\nabla}\chi_{\mathrm{m}}\times\mathbf{H})\\ &= \mu\chi_{\mathrm{m}}\mathbf{H}\times(\boldsymbol{\nabla}\times\mathbf{H})+\mu|\mathbf{H}|^{2}\boldsymbol{\nabla}\chi_{\mathrm{m}}-(\mu\mathbf{H}\cdot\boldsymbol{\nabla}\chi_{\mathrm{m}})\,\mathbf{H}.\end{aligned} \tag{3.48}$$

The third term is

$$(\mu\mathbf{H}\cdot\boldsymbol{\nabla})\,(\chi_{\mathrm{m}}\mathbf{H})=\mu\,(\mathbf{H}\cdot\boldsymbol{\nabla}\chi_{\mathrm{m}})\,\mathbf{H}+\mu\chi_{\mathrm{m}}\,(\mathbf{H}\cdot\boldsymbol{\nabla})\,\mathbf{H}. \tag{3.49}$$

Summing the three terms, Eq. (3.38) becomes

$$\begin{aligned}\mathbf{M}\times(\boldsymbol{\nabla}\times\mathbf{B})+(\mathbf{M}\cdot\boldsymbol{\nabla})\,\mathbf{B} &= \mu(\mu_{\mathrm{r}}-1)\boldsymbol{\nabla}|\mathbf{H}|^{2}-\mu(\mu_{\mathrm{r}}-1)\,(\mathbf{H}\cdot\boldsymbol{\nabla})\mathbf{H}\\ &- \mu(\mu_{\mathrm{r}}-1)\mathbf{H}\times(\boldsymbol{\nabla}\times\mathbf{H})+(\mu_{\mathrm{r}}-1)|\mathbf{H}|^{2}\boldsymbol{\nabla}\mu,\end{aligned} \tag{3.50}$$

which, using $\boldsymbol{\nabla}|\mathbf{H}|^{2}/2=(\mathbf{H}\cdot\boldsymbol{\nabla})\mathbf{H}+\mathbf{H}\times(\boldsymbol{\nabla}\times\mathbf{H})$, is simplified to

$$\mathbf{M}\times(\boldsymbol{\nabla}\times\mathbf{B})+(\mathbf{M}\cdot\boldsymbol{\nabla})\,\mathbf{B}=(\mu_{\mathrm{r}}-1)|\mathbf{H}|^{2}\boldsymbol{\nabla}\mu+\frac{\mu(\mu_{\mathrm{r}}-1)}{2}\boldsymbol{\nabla}|\mathbf{H}|^{2}. \tag{3.51}$$

The force density in linear media is then the sum of Eqs. (3.45) and (3.51), namely

$$\mathbf{f}_{\mathrm{MA}}=\frac{\varepsilon_{0}(\varepsilon_{\mathrm{r}}-1)}{2}\boldsymbol{\nabla}|\mathbf{E}|^{2}+(\mu_{\mathrm{r}}-1)|\mathbf{H}|^{2}\boldsymbol{\nabla}\mu+\frac{\mu(\mu_{\mathrm{r}}-1)}{2}\boldsymbol{\nabla}|\mathbf{H}|^{2}+\frac{\partial}{\partial t}\left(\mathbf{P}\times\mathbf{B}\right). \tag{3.52}$$

The last term in this equation is the Röntgen interaction, which naturally appeared in our non-relativistic derivation for a dipole at rest, as anticipated in Section 2.2. If we employed a relativistic derivation for a moving dipole from the very beginning, there would be an extra contribution – the hidden momentum –, as shown in Ref. [82]. An alternative non-relativistic derivation for the force density (in non-magnetic media) where the dipole is moving can be found in Ref. [92].

As discussed in Section 2.2, when switching to the laboratory frame we need to add the hidden momentum contribution to Eq. (3.52) as $\mathbf{f}_{\mathrm{h}}\approx\partial_{t}(\mathbf{E}\times\mathbf{M})/c^{2}$, where the time derivative approximation takes place because the dipole's velocity (as measured in the laboratory frame) is much smaller than c. The force density is then

$$\mathbf{f}_{\mathrm{MA}} = \frac{\varepsilon_0(\varepsilon_{\mathrm{r}}-1)}{2}\boldsymbol{\nabla}|\mathbf{E}|^2 + (\mu_{\mathrm{r}}-1)|\mathbf{H}|^2\boldsymbol{\nabla}\mu + \frac{\mu(\mu_{\mathrm{r}}-1)}{2}\boldsymbol{\nabla}|\mathbf{H}|^2 + \frac{n^2-1}{c^2}\frac{\partial}{\partial t}(\mathbf{E}\times\mathbf{H})\,, \tag{3.53}$$

where it is assumed that ε and μ do not depend on time. A simple rearrangement of the gradients as products yields, at last,

$$\mathbf{f}_{\mathrm{MA}} = \frac{1}{2}\boldsymbol{\nabla}(\mathbf{P}\cdot\mathbf{E}) + \frac{1}{2}\boldsymbol{\nabla}(\mathbf{M}\cdot\mathbf{B}) - \frac{1}{2}|\mathbf{E}|^2\boldsymbol{\nabla}\varepsilon - \frac{1}{2}|\mathbf{H}|^2\boldsymbol{\nabla}\mu + \frac{n^2-1}{c^2}\frac{\partial}{\partial t}(\mathbf{E}\times\mathbf{H})\,. \tag{3.54}$$

This force density equation is given in the laboratory frame. It is valid for linear, isotropic inhomogeneous media, with ε and μ independent of time (i.e., no dispersion). The presence of free sources would generate the extra terms $\rho_{\mathrm{f}}\mathbf{E}$ and $\mathbf{J}_{\mathrm{f}}\times\mathbf{B}$ in Eq. (3.22), and can be included if necessary. We can identify the first and second terms as the electrostriction and magnetostriction force densities, respectively. The third and fourth terms are the usual Abraham-Minkowski force, which occur in non-homogeneous regions, and the last term is the famous Abraham force. This equation contemplates almost every aspect of the reported experiments (as will be discussed in Sec. 3.3), and arises naturally from a clear and simple microscopic model, with no need for phenomenological approaches. Table 3.1 compares the electromagnetic force density described in this section with the main existing electromagnetic formulations.

Table 3.1: Comparison between the Microscopic Ampère force density and other formulations.

Formulation	**Difference in force density**
Minkowski	$\mathbf{f}_{\mathrm{M}} - \mathbf{f}_{\mathrm{MA}} = -\frac{1}{2}\boldsymbol{\nabla}(\mathbf{P}\cdot\mathbf{E}) - \frac{1}{2}\boldsymbol{\nabla}(\mathbf{M}\cdot\mathbf{B}) - \frac{n^2-1}{c^2}\frac{\partial}{\partial t}(\mathbf{E}\times\mathbf{H})$
Abraham	$\mathbf{f}_{\mathrm{Ab}} - \mathbf{f}_{\mathrm{MA}} = -\frac{1}{2}\boldsymbol{\nabla}(\mathbf{P}\cdot\mathbf{E}) - \frac{1}{2}\boldsymbol{\nabla}(\mathbf{M}\cdot\mathbf{B})$
Conventional Ampère	$\mathbf{f}_{\mathrm{A}} - \mathbf{f}_{\mathrm{MA}} = -\overleftrightarrow{\boldsymbol{\nabla}}\cdot(\mathbf{P}\otimes\mathbf{E}) + \overleftrightarrow{\boldsymbol{\nabla}}\cdot(\mathbf{B}\otimes\mathbf{M}) - \boldsymbol{\nabla}(\mathbf{M}\cdot\mathbf{B})$
Einstein-Laub[a]	$\mathbf{f}_{\mathrm{EL}} - \mathbf{f}_{\mathrm{MA}} = -\frac{\mu_0}{2}\boldsymbol{\nabla}|\mathbf{M}|^2$
Chu[b]	$\mathbf{f}_{\mathrm{C}} - \mathbf{f}_{\mathrm{MA}} = -\frac{\mu_0}{2}\boldsymbol{\nabla}|\mathbf{M}|^2$
Mass-polariton[c]	$\mathbf{f}_{\mathrm{Ab}} - \mathbf{f}_{\mathrm{MA}} = -\frac{1}{2}\boldsymbol{\nabla}(\mathbf{P}\cdot\mathbf{E}) - \frac{1}{2}\boldsymbol{\nabla}(\mathbf{M}\cdot\mathbf{B})$

[a] Here it is convenient to use $\mathbf{f}_{\mathrm{EL}}$ in the form $\mathbf{f}_{\mathrm{EL}} = \mathbf{f}_{\mathrm{Ab}} + \boldsymbol{\nabla}(\mathbf{P}\cdot\mathbf{E} + \mu_0\mathbf{M}\cdot\mathbf{H})/2$ [116].
[b] Considering the total stress-energy tensor of field plus matter.
[c] Obtained from the field part of the total mass-polariton stress–energy tensor.

3.2.1 Radiation pressure

We will now calculate the radiation pressure, $\mathcal{P}_{\mathrm{rad}}$, at a flat dielectric interface assuming a laser beam with azimuthal symmetry about the propagation axis. Notice the deformations induced by radiation pressure in dielectric liquids are typically bulges of height of order 10 nm [44, 48, 50, 56, 129], rapidly decreasing over a length of about one beam waist w_0, which is usually of order 100 μm. Thus, considering the interface flat even when the fields are acting on it is certainly a good approximation.

Being an isotropic quantity, the radiation pressure will have two contributions in this case: one due to the discontinuity of refractive index and $\mathbf{P}$ and $\mathbf{M}$ in the direction normal to the interface and another one due to the difference in the radial forces (electro- and magnetostriction effects) in each medium. The first contribution can be obtained from Eq. (3.54) by properly integrating the normal component of the force density. For example, for a beam propagating in z direction incident from a non-magnetic, linear and isotropic dielectric medium into another one through a flat interface at $z_0 = 0$, as illustrated in Fig. (3.1a), we have

$$\begin{aligned}
\mathcal{P}_z &= \lim_{\delta\to 0}\int_{-\delta}^{+\delta} f_z \,\mathrm{d}z \\
&= \lim_{\delta\to 0}\int_{-\delta}^{+\delta} \left[\frac{1}{2}\frac{\partial}{\partial z}\left(\mathbf{P}\cdot\mathbf{E}\right) - \frac{1}{2}|\mathbf{E}|^2\frac{\partial \varepsilon}{\partial z}\right] \mathrm{d}z \\
&= \left[\frac{1}{2}(\mathbf{P}\cdot\mathbf{E})\right]_{z=0^-}^{z=0^+} - \frac{\varepsilon_2-\varepsilon_1}{2}\left(|\mathbf{E}|^2_{\mathrm{avg}}\right). \qquad (3.55)
\end{aligned}$$

We assumed in Eq. (3.55) there are no free charges at the dielectric interface. Here, $|\mathbf{E}|^2_{\mathrm{avg}}$ is the average of the squared electric field magnitude across the interface.

The second term of the radiation pressure at the interface is related to the radial direction, and for normal incidence is given by

$$\mathcal{P}_r = -\left[\int f_r \,\mathrm{d}r\right]_{z=0^-}^{z=0^+} = -\left[\frac{1}{2}\left(\mathbf{P}\cdot\mathbf{E}\right)\right]_{z=0^-}^{z=0^+} \qquad (3.56)$$

where the same assumptions were used again and the function inside the brackets was implicitly calculated at fixed r.

Summing the two contributions, we have the radiation pressure at the flat dielectric interface as

$$\mathcal{P}_{\mathrm{rad}} = \mathcal{P}_z + \mathcal{P}_r = -\frac{(\varepsilon_2-\varepsilon_1)}{2}|\mathbf{E}|^2_{\mathrm{avg}}. \qquad (3.57)$$

Applying Maxwell's equations boundary conditions, we have then

$$\mathcal{P}_{\mathrm{rad}} = -\frac{(\varepsilon_2 - \varepsilon_1)}{2}\left[E_x^2 + E_y^2 + \left(1 + \frac{\varepsilon_{\mathrm{t}}^2}{\varepsilon_{\mathrm{i}}^2}\right)\frac{E_{z,\mathrm{t}}^2}{2}\right]. \tag{3.58}$$

Here $E_{z,\mathrm{t}}$ is the transmitted field component normal to the interface. As this component is not continuous across the interface, we averaged its squared magnitude with a simple arithmetic mean. The tangential components E_x and E_y are continuous across the interface, and therefore do not need the subscript indicating the current medium. Notice a very important subtlety introduced by this equation: the permittivities ε_1 and ε_2 are related to the direction of z, which in our convention always points from medium 1 to medium 2. The gradient $\boldsymbol{\nabla}\varepsilon$ is calculated accordingly, resulting in the term outside the brackets in Eq. (3.58). On the other hand, the permittivities ε_{i} and ε_{t} are related to the beam propagation direction – i.e., they refer to incident and transmitted components. Thus, if the beam is propagating in the z direction, we have $\varepsilon_{\mathrm{i}} = \varepsilon_1$ and $\varepsilon_{\mathrm{t}} = \varepsilon_2$, as in Fig. 3.1a; if the propagation direction is reversed, we have $\varepsilon_{\mathrm{t}} = \varepsilon_1$ and $\varepsilon_{\mathrm{i}} = \varepsilon_2$, as in Fig. 3.1b.

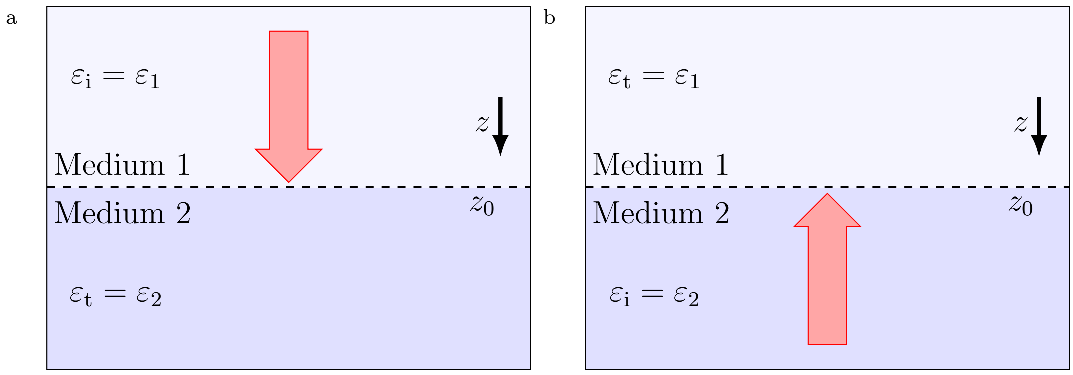

Figure 3.1: Convention for permittivities used in radiation pressure equation, Eq. (3.58), according to beam incidence direction. In (a), the beam propagates in z direction, while in (b) the propagation direction is reversed.

By using the conventions just described, Eq. (3.58) is then valid for any beam polarization, incidence angle and propagation direction. Specifically, for normal incidences we have $E_z^2 \ll E_x^2 + E_y^2$, even for typical focused gaussian beams. This leads to $\mathcal{P}_{\mathrm{rad}} \approx -(\varepsilon_2 - \varepsilon_1)(E_x^2 + E_y^2)/2$, which is the widely known Abraham-Minkowski radiation pressure. Also, we see that keeping normal incidence and reversing beam propagation direction would generate the same pressure equation.

For oblique beam incidences, we must properly account the different reflection and transmission coefficients for each polarization. We will consider the beam is locally a plane wave – which is a good approximation, since even for focused gaussian beams the field components in directions other than the polarization one are typically negligible. In this condition, we can apply the widely known Fresnel equations to describe the reflected and transmitted field amplitudes (see Appendix B). First, for s polarization, the field is by definition perpendicular to the plane of incidence. In this case, we have in our convention $E_z = 0$, which generates

$$\mathcal{P}_{\mathrm{rad}}^{(\mathrm{s})} = -\frac{(\varepsilon_2 - \varepsilon_1)}{2} t_{\mathrm{s}}^2(\theta_{\mathrm{i}}) E_0^2, \tag{3.59}$$

where E_0 is the field amplitude, t_{s} is the transmission coefficient for s polarization and θ_{i} is the incident angle relative to the interface's normal direction.

For p polarized beams, we have a non-zero normal component, so that the radiation pressure becomes

$$\mathcal{P}_{\mathrm{rad}}^{(\mathrm{p})} = -\frac{(\varepsilon_2 - \varepsilon_1)}{2} E_0^2 \left[t_{\mathrm{p}}^2(\theta_{\mathrm{i}}) \cos^2\theta_{\mathrm{t}} + \frac{(1 + r_{\mathrm{p}}(\theta_{\mathrm{i}}))^2 \sin^2\theta_{\mathrm{i}} + t_{\mathrm{p}}^2(\theta_{\mathrm{i}}) \sin^2\theta_{\mathrm{t}}}{2} \right], \tag{3.60}$$

where t_{p} and r_{p} are the transmission and reflection coefficients for p polarization, respectively, and $\theta_{\mathrm{t}} = \sin^{-1}((n_1/n_2)\sin\theta_{\mathrm{i}})$ is the transmitted (refracted) angle.

Notice that when considering a fluid incompressible we are assuming any information about deformations in the fluid propagates instantaneously – thus, no transient response is present. Indeed, at equilibrium, applying the divergence operator to the Navier-Stokes equation for an incompressible fluid at rest yields [130]

$$\nabla^2 \mathcal{P} = \boldsymbol{\nabla} \cdot \mathbf{f}_{\mathrm{em}}, \tag{3.61}$$

where $\mathbf{f}_{\mathrm{em}}$ is the electromagnetic body force and $\mathcal{P}$ is the fluid's pressure. This is an elliptic partial differential equation for $\mathcal{P}$, known as Poisson's equation. It is well-known to possess unique solutions (up to an additive constant) for a very broad class of boundary conditions. Thus, in this situation, the Abraham-Minkowski pressure, Eq. (3.58) with $E_z = 0$, arises naturally as a boundary condition uniquely related to the divergence of the body force density from Eq. (3.54). On the other hand, if the fluid develops a position-dependent velocity field, the pressure at the surface can not be uniquely related to the body force anymore, as there will be another source term in Eq. (3.61). In fact, the pressure (and consequently the surface deformation) can even change signs, as shown in Ref. [46]. This is a possible explanation to the Abraham-type deformation of a free fluid surface reported in Ref. [45].

3.3 Comparison to experiments

As we have seen in Section 3.2, the MA formulation accounts for the electro- and magnetostriction effects, presents a radiation pressure of the Abraham-Minkowski form and has an Abraham-type momentum density. These fundamental properties will be used to analyze the main existing experiments related to electromagnetic force density. For better organization, these experiments are grouped in four categories: radiation pressure experiments, photon momentum experiments, bulk force experiments and total force experiments.

3.3.1 Radiation pressure experiments

The surface deformation of water under normal laser incidence was successfully explained using the radiation pressure given in Eq. (3.58), both in old and recent measurements [30, 44, 47] – specifically, in Ref. [30] the reversed beam propagation direction was also considered. An interface of different fluids close to the critical point was studied in Ref. [33] and the observed surface deformations were also well described by Eq. (3.58).

The radiation pressure for oblique incidence adopted in the literature is [111, 131–133]

$$\mathcal{P}_{\mathrm{rad}} = \frac{n_{\mathrm{i}} I}{c} \cos^2 \theta_{\mathrm{i}} \left[1 + R(\theta_{\mathrm{i}}) - \frac{\tan \theta_{\mathrm{i}}}{\tan \theta_{\mathrm{t}}} T(\theta_{\mathrm{i}}) \right] , \tag{3.62}$$

where n_{i} is the incidence medium's refractive index, I is the beam intensity and R and T are the interface's reflectance and transmittance, respectively. This equation contemplates both polarizations in a single equation by using the appropriate R and T, and has been applied to explain the experiments reported in Refs. [48, 50, 55, 111, 131]. However, this equation does not account properly for the discontinuity of the normal field at the interface for p polarization, as shown in Appendix C.

For an air-water interface, Fig. (3.2) shows the radiation pressures from Eqs. (3.60) and (3.62) for both incidence directions. The behavior is qualitatively the same, but the magnitude of the corrected version is about 5–10% larger. At first sight, our suggestion seems to be compatible with the deformations observed in Refs. [48, 50, 55], but further investigations are necessary.

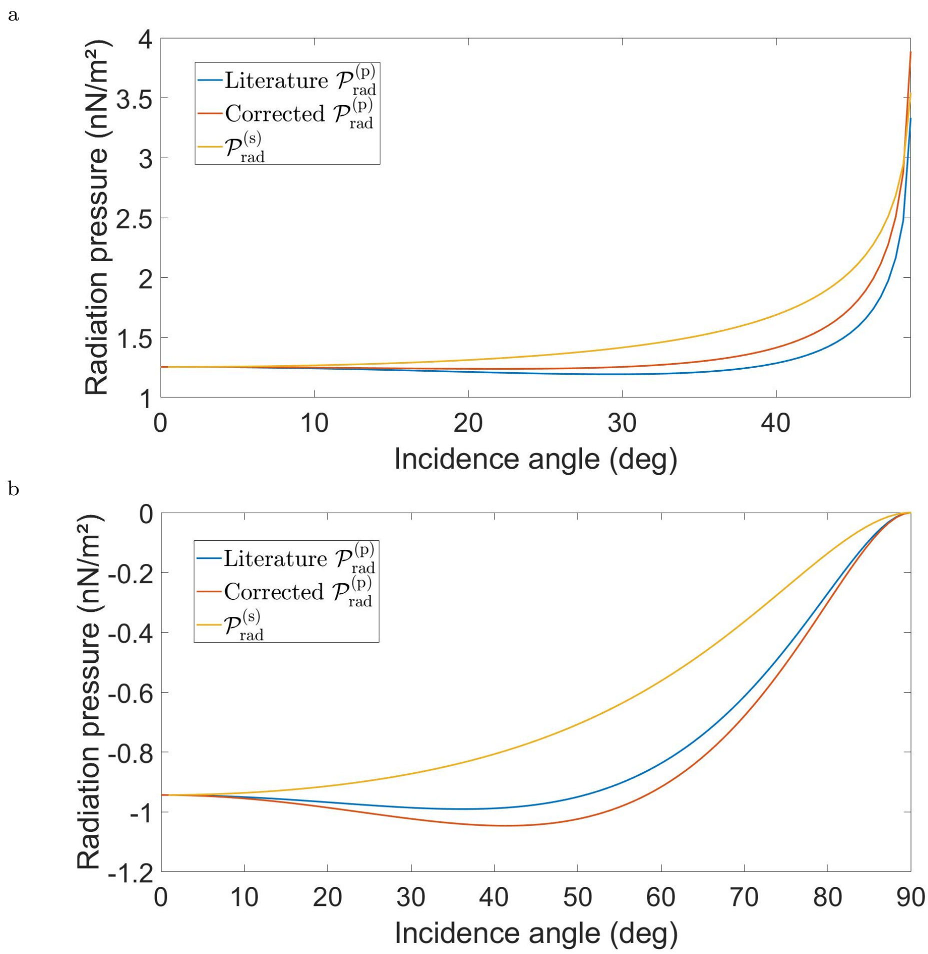

Figure 3.2: Radiation pressure for oblique incidence and p-polarized beams according to the literature, Eq. (3.62), and to our suggestion, Eq. (3.60). In (a) we have an water-to-air incidence and the radiation pressure is calculated for angles smaller than the critical angle for total internal reflection, $\theta_c \approx 48.77\,°$. In (b) we have an air-to-water incidence. The result for s polarization is also shown for completeness. Beam intensity is 1.0 W/m². The relative permittivities used for water and air were 1.769 and 1.0, respectively.

3.3.2 Photon momentum experiments

The recoil due to the radiation pressure on a submerged mirror was measured twice [28, 29], and the results were directly proportional to the refractive index of the background dielectric media – i.e., of Minkowski's form. This can effectively be explained by the Doppler-shifted recoil of the mirror, while the field retains Abraham's form of momentum [101]. To show this, consider an atom of mass m moving inside a dielectric with velocity v. The atom is assumed to have a sharp transition frequency ω_0 and to be moving away from the source of electromagnetic fields. In the reference frame of the atom, the electromagnetic field is observed to have a Doppler-shifted frequency $\omega(1 - nv/c)$, where n is the host dielectric refractive index and ω is the frequency of the excitation field. The atom can then absorb a photon only if $\omega(1 - nv/c) = \omega_0$. Now, if the velocity v of the atom is not relativistic – which is typically the case –, we can expand $(1 - nv/c)^{-1}$ as a geometric series, obtaining, to order nv/c,

$$\omega \approx \omega_0(1 + nv/c). \tag{3.63}$$

The non-relativistic conservation of energy tells us that $\hbar\omega + mv^2/2 = \hbar\omega_0 + mv'^2/2$, where v' is the velocity of the atom after the absorption of the photon. We have then

$$\frac{m}{2}\left(v'^2 - v^2\right) \approx mv(v' - v) = \hbar(\omega - \omega_0). \tag{3.64}$$

In the above equation, we approximated $(v'^2 - v^2)/2$ as $v(v' - v)$, i.e, we took $v' + v \approx 2v$. The momentum conservation in this case is simply $p + mv = mv'$, where p is the photon momentum. From this we have $p/m = (v' - v)$, which is inserted in Eq. (3.64), yielding $\omega \approx \omega_0 + pv/\hbar$. Using this result and Eq. (3.63), we obtain

$$p = \frac{n\hbar\omega_0}{c}. \tag{3.65}$$

At last, considering $\omega \approx \omega_0$ in the last equation, we see the photon momentum is, to first order in nv/c, linear in n. Recall that this is also exactly the momentum of the mass-polariton quasi-particle proposed by the formulation described in Section 2.3.6. The Doppler-shifted recoil approach can also be applied to Ref. [34], where the recoil of ultra cold atoms in a Bose-Einstein condensate due to radiation pressure was observed to be compatible with Minkowski momentum.

There is an old measurement of the photon drag effect in semiconductors that agreed with Minkowski's momentum [32], and the Doppler-shifted recoil explanation seems to again be in place. This also applies to most cases reported in Ref. [54], where the same effect was measured in thin metal films. It is important to notice, however, that one specific measurement in this last reference showed a negative dependence on Minkowski's momentum – a result that, according to the authors, still lacks theoretical explanation regarding the optical transduction and microscopic momentum exchange mechanisms.

3.3.3 Bulk force experiments

The electrostriction effect was measured inside a fluid in Refs. [121, 122] using high-intensity static fields (the latter one in a microgravity environment) and the results agreed with Helmholtz formulation [116, 118, 119]. These results can also be explained by the MA formulation if we consider the local-field correction in the form of the Clausius-Mossotti relation [114, 120, 134, 135]. For optical excitation, the local-field correction is typically given as the Lorentz-Lorenz relation [136]. However, a recent measurement of the the electrostriction effect in water for laser excitation at optical frequency was very well described by the MA formulation without the Lorentz-Lorenz correction to the local-field [129]. This result can be justified by a phenomenological argumentation presented in Ref. [137], where this local-field correction is absent due to the optical electrostriction effect causing energetically non-conservative changes in the dipole moments through the variation of the material's local mass density. Notice that, as shown in the last appendix of Ref. [129], for linear media we have $\rho_\mathrm{m}\partial\varepsilon_\mathrm{r}/\partial\rho_\mathrm{m} = \varepsilon_\mathrm{r} - 1$, which generates $\varepsilon_0 \boldsymbol{\nabla}\left[(\rho_\mathrm{m}\partial\varepsilon_\mathrm{r}/\partial\rho_\mathrm{m})_T\,|\mathbf{E}|^2/2\right] = \boldsymbol{\nabla}\left(\mathbf{P}\cdot\mathbf{E}\right)/2$. We stress, however, that this is just an accidental coincidence – although the electrostriction effect would in this case end up with the same mathematical form in both Helmholtz and MA formulations, the two equations are built under very different assumptions.

A quite intricate measurement of the electromagnetic force inside optical fibers was reported recently in Ref. [57]. It was concluded that the force density has a different symmetry than the expected from MA formulation for this case. It should be mentioned that the irregular position-dependent refractive index in the optical fiber due to its fabrication process may play a significant role in the force density symmetry through the terms proportional to $\boldsymbol{\nabla}\varepsilon$ and $\boldsymbol{\nabla}\mu$.

In Ref. [49] the observation of the Abraham force was reported in a liquid-filled hollow optical fiber, where the Abraham-Minkowski pressure at the free liquid surface was claimed to be carefully suppressed by the geometry of the waveguide. We notice that striction forces were not considered in the analysis of the results, where it is expected they would generate deformations with contrary direction to the observed one. We also notice there would be an additional Abraham-Minkowski force at the ring core/liquid interface, and adhesion effects are also expected to be important – indeed, these last two forces should partially cancel the striction force. If this cancellation is significant, the remaining force term according to MA formulation would be Abraham's one, in agreement with the authors' conclusions. Alternatively, all the effects but Abraham's force could also be relatively very small. The presence of more than one mode in the excitation wave can also be relevant.

3.3.4 Total force experiments

Recall that electro- and magnetostriction effects should not contribute to the macroscopic movement of the body, as discussed in Section 2.4. Thus, the total force acting on a dielectric body should be composed of only the time-derivative term in Eq. (3.54), i.e., Abraham's force. The movement of a torsion pendulum induced by the simultaneous application of low frequency time-dependent electric fields and static magnetic fields was measured in Ref. [31], and agreed with Abraham's force. The experiment and results reported in Ref. [43] are similar, but more detailed as it also covered the case of electromagnetic forces generated by static electric fields together with time-varying magnetic fields. At last, in Ref. [42], the pressure variation of a confined gas due to the presence of electromagnetic fields was measured to be compatible with Abraham's force. All these results are in agreement with MA formulation.

3.4 Stress-energy tensor

The MA force density was derived in Section 3.2 using three covariant elements: Maxwell's equations, the Lorentz force density and the dipolar four-current – thus, it is expected the resultant force and energy continuity equations can be associated to a true electromagnetic tensor. This same argument is valid for the conventional Ampère formulation as well, as we have the same three elements, but with a different four-current. In fact, the derivation from Section 2.3.3 can be applied to any four-current configuration, as we can always substitute the sources in Lorentz force law by the electromagnetic fields through Gauss' and Ampère-Maxwell's law. We therefore argue that Maxwell's stress-energy tensor must be valid for any four-current configuration. In particular, for MA formulation we have then

$$\overleftrightarrow{\mathbf{T}}_{\mathrm{MA}} = \frac{1}{2}\left(\epsilon_0|\mathbf{E}|^2 + \mu_0^{-1}|\mathbf{B}|^2\right)\overleftrightarrow{\mathbf{I}} - \epsilon_0\mathbf{E}\otimes\mathbf{E} - \mu_0^{-1}\mathbf{B}\otimes\mathbf{B}, \tag{3.66}$$

$$\mathbf{g}_{\mathrm{MA}} = \varepsilon_0\mathbf{E}\times\mathbf{B}, \tag{3.67}$$

$$\mathbf{S}_{\mathrm{MA}} = \mu_0^{-1}\mathbf{E}\times\mathbf{B}, \tag{3.68}$$

$$W_{\mathrm{MA}} = \frac{1}{2}\left(\epsilon_0|\mathbf{E}|^2 + \mu_0^{-1}|\mathbf{B}|^2\right). \tag{3.69}$$

Notice the hidden momentum does not need to be explicitly added to the stress-energy tensor components, as it arises naturally from the correct relativistic derivation of the continuity equations from them – indeed, explicitly adding the hidden momentum to these components would make the stress-energy tensor not invariant.

These last four equations are equal to Ampère's conventional formulation – the difference is, of course, in the continuity equations: the force density $\mathbf{f}_{\mathrm{MA}}$ given in Eq. (3.54) and the power density $\phi_{\mathrm{MA}} = \mathbf{E}\cdot\mathbf{J}$, with $\mathbf{J}$ given in Eq. (3.21). This last equation still lacks its explicit form in terms of the fields, which will be calculated now. We start by writing the total power as

$$\Phi_{\mathrm{MA}} = \int \mathbf{E}\cdot\left[\dot{\mathbf{p}}\delta^3(\mathbf{r}) - \mathbf{m}\times\boldsymbol{\nabla}\delta^3(\mathbf{r})\right]\,\mathrm{d}^3\mathbf{r}. \tag{3.70}$$

Adopting index notation for the last term, this equation is given by

$$\Phi_{\mathrm{MA}} = \dot{\mathbf{p}} \cdot \mathbf{E} - \int E_i \epsilon_{ijk} m_j \partial_k \delta^3(\mathbf{r}) \, \mathrm{d}^3\mathbf{r}, \tag{3.71}$$

where ϵ_{ijk} is the Levi-Civita symbol and the summations in repeated indices are implied. Integrating by parts we obtain

$$\Phi_{\mathrm{MA}} = \dot{\mathbf{p}} \cdot \mathbf{E} + \epsilon_{ijk} m_j \partial_k E_i, \tag{3.72}$$

where the fields are calculated at the dipole's position. The second term in the right hand side is, in vector notation, equal to $\mathbf{m} \cdot (\boldsymbol{\nabla} \times \mathbf{E})$. Invoking Faraday's law, we have $\Phi_{\mathrm{MA}} = \dot{\mathbf{p}} \cdot \mathbf{E} - \mathbf{m} \cdot \partial_t \mathbf{B}$ and, consequently,

$$\phi_{\mathrm{MA}} = \dot{\mathbf{P}} \cdot \mathbf{E} - \mathbf{M} \cdot \frac{\partial}{\partial t} \mathbf{B}. \tag{3.73}$$

As before, we take $\mathrm{d}\mathbf{P}/\,\mathrm{d}t \approx \partial_t \mathbf{P}$. Recalling the medium is assumed non-dispersive, we have then

$$\phi_{\mathrm{MA}} = \frac{1}{2} \frac{\partial}{\partial t} \left(\mathbf{P} \cdot \mathbf{E} - \mathbf{M} \cdot \mathbf{B} \right). \tag{3.74}$$

The four-continuity equation associated to MA formulation, $-\partial_\nu \mathcal{T}_{\mathrm{MA}}^{\mu\nu} = f_{\mathrm{MA}}^{\mu}$, is then completely defined.

3.4.1 Relation to MP formulation

From the discussion developed in Section 3.3, we can see the MA force density is capable of describing the vast majority of experiments up to date. It also has the advantage of being derived from a well-known microscopic model – the dipolar sources. On the other hand, we have seen in Section 2.3.6 that, in order to fulfill the covariance requirements, there must be a coupled state of field and matter propagating through the dielectric. This is, of course, the basis of the MP formulation. However, MP formulation was built using Abraham's force density, which does not contemplate striction effects, and thus can not explain experiments such as the one reported in Ref. [129]. Another important fact is that the few experiments that were able to measure the photon momentum in matter, discussed in Section 3.3.2, showed a linear dependence on the medium's refractive index, exactly as predicted by the coupled mass-polariton state. Thus, it seems natural to consider the possibility of properly incorporating the MA force density into the MP formulation.

As we know, the MP formulation adopts, in the laboratory frame, Abraham's force density and the stress-energy tensor relation $\mathcal{T}_{\mathrm{MP}} = \mathcal{T}_{\mathrm{Ab}} + \mathcal{T}_{\mathrm{MDW}}$, assuming the medium is in mechanical equilibrium. On the other hand, as shown in Table 3.1, MA force density is the sum of Abraham's force density plus electro- and magnetostriction effects, i.e.,

$$\mathbf{f}_{\mathrm{MA}} = \mathbf{f}_{\mathrm{Ab}} + \boldsymbol{\nabla}(\mathbf{P}\cdot\mathbf{E})/2 + \boldsymbol{\nabla}(\mathbf{M}\cdot\mathbf{B})/2. \tag{3.75}$$

This last equation should be equivalent to

$$\overleftrightarrow{\boldsymbol{\nabla}} \cdot \left(\overleftrightarrow{\mathbf{T}}_{\mathrm{Ab}} - \overleftrightarrow{\mathbf{T}}_{\mathrm{MA}}\right) + \frac{\partial}{\partial t}\left(\mathbf{g}_{\mathrm{Ab}} - \mathbf{g}_{\mathrm{MA}}\right) = \frac{1}{2}\overleftrightarrow{\boldsymbol{\nabla}} \cdot \left[(\mathbf{P}\cdot\mathbf{E})\overleftrightarrow{\mathbf{I}} + (\mathbf{M}\cdot\mathbf{B})\overleftrightarrow{\mathbf{I}}\right]. \tag{3.76}$$

It can be verified that Eq. (3.76) does not hold. What is the problem? In the process of obtaining $\mathbf{f}_{\mathrm{Ab}}$ from $\mathbf{f}_{\mathrm{Ab}} = -\overleftrightarrow{\boldsymbol{\nabla}} \cdot \overleftrightarrow{\mathbf{T}}_{\mathrm{Ab}} - \partial\mathbf{g}_{\mathrm{Ab}}/\partial t$, Gauss' and Ampère-Maxwell's laws are used in their macroscopic forms, Eqs. (2.5) and (2.7) respectively. These forms can not be applied for microscopic forces, as effective bound sources are automatically assumed. They are only suitable for the macroscopic (conventional) Ampère formulation, described in Section 2.3.3. Thus, in general, we have $\mathbf{f}_{\mathrm{Ab}} \neq -\overleftrightarrow{\boldsymbol{\nabla}} \cdot \overleftrightarrow{\mathbf{T}}_{\mathrm{Ab}} - \partial\mathbf{g}_{\mathrm{Ab}}/\partial t$. This problem also happens to Einstein-Laub formulation, i.e., in general $\mathbf{f}_{\mathrm{EL}} \neq -\overleftrightarrow{\boldsymbol{\nabla}} \cdot \overleftrightarrow{\mathbf{T}}_{\mathrm{EL}} - \partial\mathbf{g}_{\mathrm{EL}}/\partial t$, as previously pointed out in the last paragraph of Section 2.3.4. Again, we stress the only way to treat the sources generically, be them bound and/or free, is by means of Maxwell's stress-energy tensor, as discussed in Section 3.4.

In the context presented, we propose the correct form of the MP tensor should be

$$\mathcal{T}_{\mathrm{MP}} = \mathcal{T}_{\mathrm{MA}} + \mathcal{T}_{\mathrm{MDW}}. \tag{3.77}$$

Here, $\mathcal{T}_{\mathrm{MDW}}$ represents the difference in the material's stress-energy tensor after and before the electromagnetic fields are applied, as described in Section 2.3.6. For example, if the medium is a perfect fluid in thermodynamical equilibrium, its stress-energy tensor in flat space-time is [138]

$$\mathcal{T}^{\mu\nu}_{\mathrm{mat}} = \rho_0 U^\mu U^\nu + \mathcal{P}\left(\eta^{\mu\nu} + \frac{U^\mu U^\nu}{c^2}\right), \tag{3.78}$$

where ρ_0 is the proper mass density, $\mathcal{P}$ is the pressure and $U^\mu = \gamma(c, \mathbf{u})$ is the four-velocity, with $\gamma = (1 - |\mathbf{u}|^2/c^2)^{-1/2}$. For a solid elastic medium, the spatial part of $\mathcal{T}_{\mathrm{mat}}$ is given in a more complicate way in terms of the material's strain – see Ref. [139] for example.

The electromagnetic field and the material must, in our case, form a closed system. From Section 3.4, we know the electromagnetic fields deliver energy to the dielectric through ϕ_{MA} given in Eq. (3.74). As we have in this equation a partial time derivative, we can then conveniently assign to the material the amount of energy density $(\mathbf{P}\cdot\mathbf{E}-\mathbf{M}\cdot\mathbf{B})/2$. With this choice, by summing the field and the material energy density we obtain, apart from the rest energy term, $(\varepsilon_0|\mathbf{E}|^2 + \mu_0^{-1}|\mathbf{B}|^2 + \mathbf{P}\cdot\mathbf{E} - \mathbf{M}\cdot\mathbf{B})/2$, which is exactly $W_{\mathrm{Ab}} = (\mathbf{D}\cdot\mathbf{E}+\mathbf{B}\cdot\mathbf{H})/2$, the well-known electromagnetic energy density inside linear, lossless and non-dispersive dielectrics. With the aid of Eq. (2.80), the continuity equation for energy becomes

$$\partial_\nu \mathcal{T}^{0\nu}_{\mathrm{MP}} = \frac{\partial}{\partial t}\left(\frac{1}{2}\mathbf{D}\cdot\mathbf{E} + \frac{1}{2}\mathbf{B}\cdot\mathbf{H} + \rho_{\mathrm{MDW}}c^2\right) + \boldsymbol{\nabla}\cdot\left(\mathbf{E}\times\mathbf{H} + \rho_{\mathrm{MDW}}\mathbf{v}_{\mathrm{MDW}}c^2\right) = 0. \quad (3.79)$$

Here, the hidden momentum has been added to the electromagnetic part of $\mathbf{S}$ by the same reasoning as in Eq. (3.53). This means we are working with quantities as measured in the laboratory frame, initially keeping contributions only to order $|\mathbf{v}_{\mathrm{a}}|/c$, where $\mathbf{v}_{\mathrm{a}}$ is the atomic velocity. This approximation is also applied to the MDW tensor. Notice that, as the motion of the atoms is accelerated due to the external forces, their proper frames are not inertial reference frames – the velocity $\mathbf{v}_{\mathrm{a}}$ is actually the relative velocity between a local inertial reference frame, moving along with the atoms, and the laboratory frame [99]. Also notice that Eq. (3.79) has the same form of the original MP formulation, but its interpretation is slightly different, as we will shortly see. The momentum continuity equation, on its turn, is now given by

$$\sum_{i=1}^{3}\partial_\nu \mathcal{T}^{i\nu}_{\mathrm{MP}} = \mathbf{f}_{\mathrm{MA}} + \mathbf{f}_{\mathrm{b}} + \overleftrightarrow{\boldsymbol{\nabla}}\cdot(\rho_{\mathrm{MDW}}\mathbf{v}_{\mathrm{MDW}}\otimes\mathbf{v}_{\mathrm{a}}) + \frac{\partial}{\partial t}(\rho_{\mathrm{MDW}}\mathbf{v}_{\mathrm{MDW}}) = 0, \quad (3.80)$$

where $\mathbf{f}_{\mathrm{b}}$ denotes the internal body force density in the medium – in our context, typically elastic forces for solid media and pressure gradients for fluid media. The difference to the original MP formulation is, of course, the electro- and magnetostriction forces contained in $\mathbf{f}_{\mathrm{MA}}$.

What role do the striction forces play in the energy continuity equation? From the definition of potential energy, the stress acting inside the material due to the electromagnetic fields can be found from the derivative of W_{Ab} with respect to the associated strain component in solid media [140]. It can be shown [137] such calculation leads to the force density $\boldsymbol{\nabla}(\mathbf{P}\cdot\mathbf{E} + \mathbf{M}\cdot\mathbf{B})/2$, i.e., the work done by the electromagnetic field generates strain inside the material, which is manifested through the electro- and magnetostricion effects. The same occurs for fluid media, with strain being substituted by a local pressure increase. We can then see that striction effects are essentially pure stresses, and so they do not change the momentum transfer inside the material, which occurs exclusively in the pulse propagation direction. This is consistent with the discrete picture of light, where every incident photon on the dielectric has its momentum in the propagation direction.

Eq. (3.77) is compatible with the opto-elastic simulations from Ref. [95] – striction effects would be balanced by elastic forces, while the remaining force density is the dynamical part, equal to $\mathbf{f}_{\mathrm{Ab}}$. In turn, this force density is responsible for the previously unrecognized mass density wave propagating along with the light pulse. Besides, as both

$\mathcal{T}_{\mathrm{MA}}$ and $\mathcal{T}_{\mathrm{MDW}}$ are true tensors, the covariance of the proposed theory would remain intact.

Note that, as just shown, in mechanical equilibrium the equations for energy, force and momentum in the dielectric are equal to Abraham's formulation – however, we emphasize they do not originate from Abraham's stress-energy tensor, as this tensor necessarily employs macroscopic sources in its application. Therefore, the argumentation developed here clarifies the true origin of Abraham's force density in linear, isotropic, lossless and non-dispersive dielectric media: it results from the electromagnetic force acting on moving induced dipoles partially counter-balanced by internal mechanical stresses.

CHAPTER 4

Numerical calculation of the electromagnetic force density

Although much can be qualitatively inferred from the MA force density as given in Eq. (3.54), quantitative investigations are also of great interest. Specifically, knowing the relative magnitude of the momentum term (the Abraham force) compared to the internal stress (striction effects) is very important to design experiments aiming to measure the former inside materials. Recall that knowing this contribution is necessary to obtain the mass transferred, δm, and the MP momentum, p_{MP}, and eventually confirm our proposed theory.

Due to the broad control possibility of the generated excitation, it is a very common practice in experimental investigations of light-matter interactions to employ laser sources. These laser beams are frequently applied as focused beams on the dielectric to provide greater intensities and, therefore, enhance the desired effects. To calculate the electromagnetic force density inside the sample material we must, of course, know the electromagnetic fields as a function of position and time. As analytical solutions of Maxwell's equations are available only in very specific circumstances, we must resort to numerical calculations. This chapter will describe the main numerical techniques employed to obtain such fields and discuss some of the related computational aspects. We will first derive equations for monochromatic focused laser beams propagating in a homogeneous dielectric medium, later adding an interface and a second dielectric medium. An extension to quasi-monochromatic beams is then presented, providing a full numerical procedure to calculate the time- and position-dependent electromagnetic fields associated to focused laser beams in optical regime. From these fields, we show lastly a new method to obtain the related numerical electromagnetic force density in a semi-analytical way.

4.1 Angular Spectrum Representation

The Angular Spectrum Representation (ASR), also known as Angular Spectrum Method, is a formalism developed for the description of wave propagation in homogeneous media. It can be used for both electromagnetic and acoustic waves (see Refs. [141–144] for example). In particular, for applications in optics, the electromagnetic fields are obtained through sums of plane waves and evanescent waves, which are simple solutions of Maxwell's equations. The theoretical description of this method and its development is based on Refs. [145–147].

Let us consider a monochromatic electric field with angular frequency ω, according to the convention

$$\mathbf{E}(\mathbf{r}, t) = \mathrm{Re}\{\mathbf{E}(\mathbf{r})\,\mathrm{e}^{-\,\mathrm{i}\omega t}\}, \tag{4.1}$$

occupying the homogeneous region $z \geq 0$ of refractive index n real and constant. If all the electromagnetic sources are outside this region, the field $\mathbf{E}(\mathbf{r})$ must satisfy the homogeneous wave equation – which, in this case, reduces to the Helmholtz equation as

$$\left(\nabla^2 + k^2\right)\mathbf{E}(\mathbf{r}) = 0, \tag{4.2}$$

where $k = (\omega/c)n$ is the wavenumber and c is the speed of light in vacuum. Let $z =$ constant be an arbitrary plane inside the region $z \geq 0$. At this plane, the field $\mathbf{E}(\mathbf{r})$ can be described in terms of a two-dimensional Fourier transform

$$\mathbf{E}(x, y, z) = \iint\limits_{-\infty}^{+\infty} \hat{\mathbf{E}}(k_x, k_y; z)\,\mathrm{e}^{\mathrm{i}(k_x x + k_y y)}\,\mathrm{d}k_x\,\mathrm{d}k_y, \tag{4.3}$$

where x and y are the transverse coordinates to z and k_x and k_y are their reciprocal coordinates, respectively. The term $\hat{\mathbf{E}}(k_x, k_y; z)$ is given by the usual Fourier transform relations

$$\hat{\mathbf{E}}(k_x, k_y; z) = \frac{1}{4\pi^2}\iint\limits_{-\infty}^{+\infty} \mathbf{E}(x, y, z)\,\mathrm{e}^{-\,\mathrm{i}(k_x x + k_y y)}\,\mathrm{d}x\,\mathrm{d}y. \tag{4.4}$$

Eq. (4.2) can be written in terms of Eq. (4.3) as

$$\iint\limits_{-\infty}^{+\infty} (\nabla^2 + k^2)\,\hat{\mathbf{E}}(k_x, k_y; z)\,\mathrm{e}^{\mathrm{i}(k_x x + k_y y)}\mathrm{d}k_x\mathrm{d}k_y = 0, \tag{4.5}$$

yielding

$$\iint_{-\infty}^{+\infty} \left[\frac{\partial^2 \hat{E}_j(k_x, k_y; z)}{\partial z^2} + (k^2 - k_x^2 - k_y^2)\hat{E}_j(k_x, k_y; z) \right] \mathrm{e}^{\,\mathrm{i}(k_x x + k_y y)} \,\mathrm{d}k_x \,\mathrm{d}k_y = 0, \tag{4.6}$$

where $j = x, y, z$ is used to denote the three components of $\hat{\mathbf{E}}(k_x, k_y; z)$. As Eq. (4.6) must be valid for all x and y, its integrand must then be zero, yielding

$$\frac{\partial^2 \hat{E}_j(k_x, k_y; z)}{\partial z^2} + (k^2 - k_x^2 - k_y^2)\hat{E}_j(k_x, k_y; z) = 0. \tag{4.7}$$

The general solution of Eq. (4.7) is

$$\hat{\mathbf{E}}(k_x, k_y; z) = \mathbf{A}(k_x, k_y)\,\mathrm{e}^{\mathrm{i}k_z(k_x,k_y)z} + \mathbf{B}(k_x, k_y)\,\mathrm{e}^{-\,\mathrm{i}k_z(k_x,k_y)z}, \tag{4.8}$$

with

$$k_z(k_x, k_y) = \sqrt{k^2 - k_x^2 - k_y^2} \tag{4.9}$$

as the reciprocal coordinate of z. Substituting Eq. (4.8) into Eq. (4.3), the integral form for the electric field reads

$$\begin{aligned} \mathbf{E}(x, y, z) = &\iint_{-\infty}^{+\infty} \mathbf{A}(k_x, k_y)\,\mathrm{e}^{\,\mathrm{i}(k_x x + k_y y + k_z z)} \mathrm{d}k_x \,\mathrm{d}k_y \\ &+ \iint_{-\infty}^{+\infty} \mathbf{B}(k_x, k_y)\,\mathrm{e}^{\,\mathrm{i}(k_x x + k_y y - k_z z)} \mathrm{d}k_x \,\mathrm{d}k_y. \end{aligned} \tag{4.10}$$

The first integral in Eq. (4.10) represents a superposition of waves propagating in $+z$ direction, while the second integral represents a superposition of waves propagating in $-z$ direction. Within the region of interest, $z \geq 0$, the asymptotic form of the electric field must represent an outgoing wave and be a square integrable function. These boundary conditions lead to $\mathbf{B}(k_x, k_y) = 0$, and Eq. (4.10) reduces to

$$\mathbf{E}(x, y, z) = \iint_{-\infty}^{+\infty} \mathbf{A}(k_x, k_y)\,\mathrm{e}^{\,\mathrm{i}(k_x x + k_y y + k_z z)} \,\mathrm{d}k_x \,\mathrm{d}k_y. \tag{4.11}$$

This form resembles an usual Fourier transform description – however, notice that only two coordinates were transformed and Eq. (4.9) imposes a restriction on the k_z domain.

Comparing Eqs. (4.11) and (4.8), the amplitude $\mathbf{A}(k_x, k_y)$ can be written as

$$\mathbf{A}(k_x, k_y) = \hat{\mathbf{E}}(k_x, k_y; z = 0), \tag{4.12}$$

leading to

$$\hat{\mathbf{E}}(k_x, k_y; z) = \hat{\mathbf{E}}(k_x, k_y; z = 0)\, \mathrm{e}^{\mathrm{i}k_z z}. \tag{4.13}$$

This equation shows how the spatial Fourier spectrum in an arbitrary plane $z =$ constant can be obtained through the multiplication of the spatial Fourier spectrum at the boundary $z = 0$ by the term $\mathrm{e}^{\mathrm{i}k_z z}$, which in this context is known as optical propagator. Substituting Eq. (4.12) into Eq. (4.10), $\mathbf{E}(x, y, z)$ is given by

$$\mathbf{E}(x, y, z) = \iint\limits_{-\infty}^{+\infty} \hat{\mathbf{E}}(k_x, k_y; 0)\, \mathrm{e}^{\mathrm{i}(k_x x + k_y y + k_z z)} \mathrm{d}k_x\, \mathrm{d}k_y, \tag{4.14}$$

which is known as Angular Spectrum Representation. This equation tells us how the electric field spectrum at the boundary $z = 0$ can be transformed into the propagated electric field at any point (x, y, z) for $z > 0$. Notice that, as seen in Fig. (4.1), the optical propagator has two distinct behaviors depending on k_z: for $k^2 \leq k_x^2 + k_y^2$, the propagator is represented by an oscillatory function, while for $k^2 > k_x^2 + k_y^2$ it decays exponentially. If we consider planes sufficiently far from $z = 0$, only the oscillatory contribution of the propagator will be non-zero. Thus, in this situation the domain of integration of Eqs. (4.14) and (4.15) can be restricted to the circle $k^2 \leq k_x^2 + k_y^2$. Physically, this restriction is commonly satisfied in optical systems.

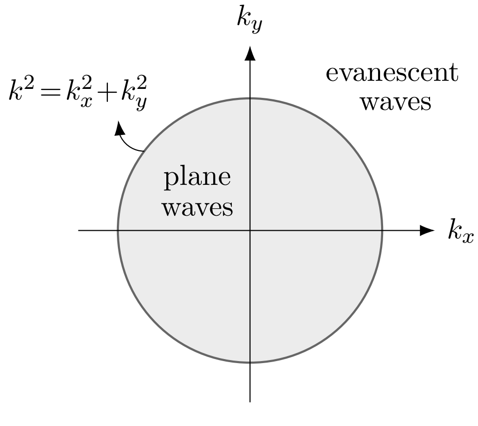

Figure 4.1: Optical propagator behavior.

Using the same approach employed to describe the electric field, the magnetic field

$\mathbf{H}(x, y, z)$ can be obtained as

$$\mathbf{H}(x, y, z) = \iint_{-\infty}^{+\infty} \hat{\mathbf{H}}(k_x, k_y; 0)\, \mathrm{e}^{\mathrm{i}(k_x x + k_y y + k_z z)} \mathrm{d}k_x\, \mathrm{d}k_y. \tag{4.15}$$

4.1.1 Far field regime

Let us consider now a general problem in which the electric field distribution is known at $z = 0$ and we wish to know the behavior of the field at a distant plane z. In this scenario, the electric field has initially the form

$$\mathbf{E}(x, y, z) = \iint_{k_x^2 + k_y^2 \leq k^2} \hat{\mathbf{E}}(k_x, k_y; 0)\, \mathrm{e}^{\mathrm{i}(k_x x + k_y y + k_z z)}\, \mathrm{d}k_x\, \mathrm{d}k_y, \tag{4.16}$$

where the domain of integration has already been restricted to the circle $k_x^2 + k_y^2 \leq k^2$. Let $\mathbf{r}$ be the point where we want the field to be calculated. We define the unit vector $\hat{\mathbf{s}}$ that gives the direction of $\mathbf{r}$ as

$$\hat{\mathbf{s}} = (s_x, s_y, s_z) = \left(\frac{x}{r}, \frac{y}{r}, \frac{z}{r} \right), \tag{4.17}$$

where $r = \sqrt{x^2 + y^2 + z^2}$. For calculating the distant field, denoted by $\mathbf{E}_\infty$, the limit $r \to \infty$ must be taken in Eq. (4.16); besides, (x, y, z) are written in terms of (s_x, s_y, s_z), using Eq. (4.17). This yields

$$\mathbf{E}_\infty(s_x, s_y) = \lim_{kr \to \infty} \iint_{k_x^2 + k_y^2 \leq k^2} \hat{\mathbf{E}}(k_x, k_y; 0)\; \mathrm{e}^{\mathrm{i}kr\left(\frac{k_x}{k} s_x + \frac{k_y}{k} s_y + \frac{k_z}{k} s_z\right)}\, \mathrm{d}k_x\, \mathrm{d}k_y, \tag{4.18}$$

with $s_z = \sqrt{1 - s_x^2 - s_y^2}$. This integral can be solved using the stationary phase method, resulting in [146]

$$\mathbf{E}_\infty(s_x, s_y) = -2\pi\, \mathrm{i}k s_z \hat{\mathbf{E}}(k s_x, k s_y; 0) \frac{\mathrm{e}^{\mathrm{i}kr}}{r}. \tag{4.19}$$

This result shows that the electric field in the far field regime is completely described by the spatial spectrum $\hat{\mathbf{E}}(k_x, k_y; 0)$ assuming $k_x \to k s_x$ and $k_y \to k s_y$. This implies that the unit vector $\hat{\mathbf{s}}$ satisfies the relation

$$\hat{\mathbf{s}} = \left(\frac{k_x}{k}, \frac{k_y}{k}, \frac{k_z}{k} \right). \tag{4.20}$$

In fact, only the plane wave with wavevector $\mathbf{k} = (k_x, k_y, k_z)$ from the angular spectrum at $z = 0$ contributes to the far field in a point located in the direction $\hat{\mathbf{s}}$. The contribution from all other plane waves is carefully cancelled out by destructive interference. The far field can then be effectively treated as a set of optical rays, where each ray is associated to only one specific plane wave from the initial angular spectrum – i.e., the familiar geometrical optics regime is obtained. Using Eqs. (4.19) and (4.20), we can relate the initial spatial spectrum to the far field as

$$\hat{\mathbf{E}}(k_x, k_y; 0) = \frac{\mathrm{i}r\,\mathrm{e}^{-\,\mathrm{i}kr}}{2\pi k_z}\mathbf{E}_\infty\left(\frac{k_x}{k}, \frac{k_y}{k}\right). \tag{4.21}$$

and, using Eq. (4.16),

$$\mathbf{E}(x, y, z) = \frac{\mathrm{i}r\,\mathrm{e}^{-\,\mathrm{i}kr}}{2\pi} \iint\limits_{k_x^2+k_y^2\leq k^2} \mathbf{E}_\infty\left(\frac{k_x}{k}, \frac{k_y}{k}\right) \mathrm{e}^{\,\mathrm{i}(k_x x+k_y y+k_z z)}\frac{1}{k_z}\,\mathrm{d}k_x\,\mathrm{d}k_y. \tag{4.22}$$

4.2 Focused laser beams

In this section, we describe the electromagnetic fields generated through the incidence of a collimated laser beam on an ideal lens. The treatment is based on Refs. [145] and [148].

The characteristics of a focused laser beam are determined exclusively from the incident beam and the focusing optical element. In the following derivation, we consider the incidence of an arbitrarily polarized and collimated gaussian beam on an ideal biconvex lens. We assume that the source is far from the lens, so that we may use the geometrical optics regime. In order to describe the action of the lens in this regime, two factors must be taken into account: the so-called Abbe sine condition and the energy conservation principle.

The Abbe sine condition corresponds to a restriction necessary for the magnification factor of the lens to be independent of the incident angles [149]. This condition implies, in our case, that the focused beam has spherical wavefronts of radius f equal to the focal distance of the system, as illustrated in Fig. 4.2a. For this reason, the theoretical sphere of radius f and centered at the focal spot of the system is known as reference sphere and will be used in our calculations.

A complete treatment of the refractions by the lens would require the application of the Fresnel coefficients for transmission and reflection. Experimentally, however, it is possible to utilize lenses with efficient anti-reflection coatings, making the transmission approximately total. This condition, together with the geometrical optics regime, allow us to apply the energy conservation principle only at the reference sphere.

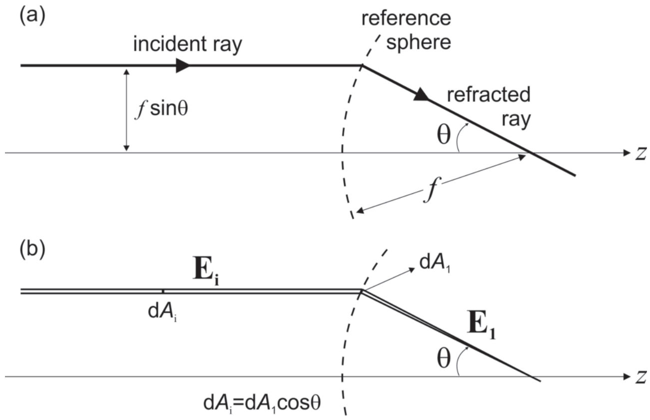

Figure 4.2: a) Abbe sine condition for geometrical optics. The refraction of the incident beam is effectively described at the reference sphere. b) Energy conservation in the geometrical optics regime. The energy transported by each ray must remain constant.

The power transmitted by an arbitrary beam is given by

$$P = \langle \mathbf{S} \rangle \cdot \mathrm{d}\mathbf{A}, \tag{4.23}$$

where $\mathrm{d}\mathbf{A}$ is the infinitesimal area element of the cross section of the beam and $\langle \mathbf{S} \rangle$ is the average value (in time) of the Poynting vector. Considering well collimated beams, we have, approximately,

$$\langle S \rangle = \frac{1}{2Z} |\mathbf{E}|^2, \tag{4.24}$$

with Z being the wave impedance of the medium.

As reflections on the lens surface were assumed negligible, the energy conservation principle requires that the power as given by Eq. (4.23) remains constant after the beam leaves the lens. Applying this condition for the refraction at the reference sphere (Fig. 4.2b), we get

$$|\mathbf{E}_\mathrm{l}| = \sqrt{\cos\theta} |\mathbf{E}_\mathrm{i}|, \tag{4.25}$$

where θ is the angle that the propagation direction of the refracted beam makes with the optical axis and $\mathbf{E}_\mathrm{i}$ and $\mathbf{E}_\mathrm{l}$ are the incident and refracted fields, respectively.

The optical system will transform an incoming beam with cylindrical symmetry into a refracted beam with spherical symmetry. Therefore, it is convenient for us to introduce spherical coordinates for the reference sphere (f, θ, ϕ), as well as the unit vectors $\hat{\mathbf{n}}_\rho$, $\hat{\mathbf{n}}_\theta$ and $\hat{\mathbf{n}}_\phi$. The unit vectors $\hat{\mathbf{n}}_\rho$ and $\hat{\mathbf{n}}_\phi$ refer to the cylindrical coordinate system, while $\hat{\mathbf{n}}_\theta$ and $\hat{\mathbf{n}}_\phi$ refer to the spherical coordinate system. Besides, as different polarizations are refracted differently, the incident electric field $\mathbf{E}_\mathrm{i}$ will be decomposed into the generic s and p polarizations as

$$\mathbf{E}_\mathrm{i} = \mathbf{E}_\mathrm{i}^{(\mathrm{s})} + \mathbf{E}_\mathrm{i}^{(\mathrm{p})}, \tag{4.26}$$

where $\mathbf{E}_{\mathrm{i}}^{(\mathrm{s})} = [\mathbf{E}_{\mathrm{i}} \cdot \hat{\mathbf{n}}_\phi]\, \hat{\mathbf{n}}_\phi$ e $\mathbf{E}_{\mathrm{i}}^{(\mathrm{p})} = [\mathbf{E}_{\mathrm{i}} \cdot \hat{\mathbf{n}}_\rho]\, \hat{\mathbf{n}}_\rho$.

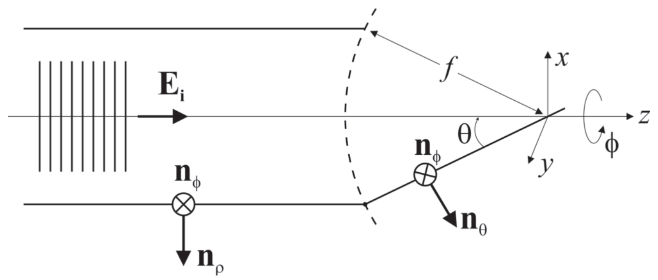

Figure 4.3: Coordinate systems for beam refraction at the lens.

The refraction keeps the unit vector $\hat{\mathbf{n}}_\phi$ unaltered, but transforms the unit vector $\hat{\mathbf{n}}_\rho$ into $\hat{\mathbf{n}}_\theta$, as seen in Fig. 4.3. Thus, using Eq. (4.25), the refracted electric field is given by

$$\mathbf{E}_{\mathrm{l}} = (\,[\,\mathbf{E}_{\mathrm{i}} \cdot \hat{\mathbf{n}}_\phi]\, \hat{\mathbf{n}}_\phi + [\,\mathbf{E}_{\mathrm{i}} \cdot \hat{\mathbf{n}}_\rho]\, \hat{\mathbf{n}}_\theta)\, \sqrt{\cos\theta}. \tag{4.27}$$

The focal distances f of lenses in typical optical setups are of order of centimeters. Besides, for incident fields within the optical band, the wavelengths are of order of $0.1\,\mu$m. Therefore, we have $f \gg \lambda$, and fields at the surface of the reference sphere and at its center (the focal spot) can be considered as an incident-field/far-field pair, so Eq. (4.22) may be applied. For such, we consider $\mathbf{E}_{\mathrm{l}}$ calculated on the surface of the reference sphere as the far field $\mathbf{E}_\infty$, allowing the field in the focal region to be obtained by

$$\mathbf{E}_{\mathrm{f}}(x, y, z) = \frac{f\,\mathrm{e}^{-\,\mathrm{i}kf}}{2\pi\,\mathrm{i}} \iint\limits_{k_x^2 + k_y^2 \leq k^2} \mathbf{E}_{\mathrm{l}}\left(\frac{k_x}{k}, \frac{k_y}{k}\right) \frac{1}{k_z}\, \mathrm{e}^{\,\mathrm{i}(k_x x + k_y y + k_z z)}\, \mathrm{d}k_x\, \mathrm{d}k_y, \tag{4.28}$$

where a negative sign was added due to the far field being implicitly calculated at $z \to -\infty$ in this case, which changes s_z sign. The origin of the coordinate system is conveniently chosen to be at the focal spot.

We now only need to determine the complete form of the integrand, considering the cylindrical and spherical symmetries present in our system. For this, we will initially write down the components of the wavevector in spherical coordinates:

$$k_x = k \sin\theta \cos\phi, \tag{4.29}$$

$$k_y = k \sin\theta \sin\phi, \tag{4.30}$$

$$k_z = k \cos\theta. \tag{4.31}$$

The electric field in the focal region, on its turn, will be described in cylindrical coordinates, where the following transformations will be used

$$x = \rho \cos\varphi, \tag{4.32}$$

$$y = \rho \sin\varphi, \tag{4.33}$$

with $\rho = \sqrt{x^2+y^2}$ and $\varphi = \tan^{-1}(y/x)$. Notice that the angle φ refers to the azimuthal angle of the cylindrical coordinates, and corresponds to a coordinate of the electric field in the focal region ($\mathbf{E}_\mathrm{f}$), while the angle ϕ refers to the azimuthal angle of the spherical coordinates and is related to the wavevector of the refracted field at the reference sphere ($\mathbf{E}_\mathrm{l}$).

Using Eqs. (4.29) to (4.33), we have

$$\begin{aligned} k_x x + k_y y + k_z z &= k\left[\rho \sin\theta \cos\phi \cos\varphi + \rho \sin\theta \sin\phi \sin\varphi + z\cos\theta\right] \\ &= k\rho \sin\theta \cos(\phi-\varphi) + kz\cos\theta. \end{aligned} \tag{4.34}$$

The remaining factor of the integrand is related to the Jacobian determinant of the transformation,

$$\begin{vmatrix} \dfrac{\partial k_x}{\partial \theta} & \dfrac{\partial k_x}{\partial \phi} \\ \dfrac{\partial k_y}{\partial \theta} & \dfrac{\partial k_y}{\partial \phi} \end{vmatrix} = k^2 \sin\theta \cos\theta, \tag{4.35}$$

and yields

$$\frac{1}{k_z}\,\mathrm{d}k_x\,\mathrm{d}k_y = k \sin\theta \,\mathrm{d}\theta\,\mathrm{d}\phi. \tag{4.36}$$

Finally, in cylindrical coordinates the field in the focal region is then given by

$$\mathbf{E}_\mathrm{f}(\rho,\varphi,z) = \frac{kf\,\mathrm{e}^{-\mathrm{i}kf}}{2\pi\,\mathrm{i}} \int_0^{\theta_\mathrm{max}} \int_0^{2\pi} \mathbf{E}_\mathrm{l}(\theta,\phi)\,\mathrm{e}^{\mathrm{i}kz\cos\theta}\,\mathrm{e}^{\mathrm{i}k\rho\sin\theta\cos(\phi-\varphi)} \sin\theta\,\mathrm{d}\theta\,\mathrm{d}\phi, \tag{4.37}$$

where θ_max denotes the maximum focusing angle of the lens. This equation is capable of describing a tightly focused laser beam, provided that the incident beam on the lens is well collimated and that the lens itself has a good anti-reflection coating. To obtain a more explicit form, we would only need to choose the specific form of the incident field $\mathbf{E}_\mathrm{i}$; this would allow the description of the refracted field at the reference sphere $\mathbf{E}_\mathrm{l}$ in terms of the angles ϕ and θ, and will be developed in the following section.

4.2.1 Focused gaussian beam

In our applications, the incident electric field will be the fundamental mode of a linearly polarized gaussian beam in the x direction. Such beam can be described by (see Appendix D for more details)

$$\mathbf{E}_{\mathrm{i}}(x,y,z) = E_0\,\mathrm{e}^{-\frac{x^2+y^2}{w_0^2}}\,\mathrm{e}^{\mathrm{i}kz}\hat{\mathbf{n}}_x, \tag{4.38}$$

where w_0 is the beam waist of the field on the lens and E_0 is the amplitude, given by

$$E_0 = \sqrt{4\eta P/\pi w_0^2}, \tag{4.39}$$

where $\eta = \sqrt{\mu/\epsilon}$ is the wave impedance of the medium and P is the beam power in continuous wave (cw) regime for a monochromatic source. The curvature is taken to be plane because the beam is collimated. The phase factor was arbitrarily set to one, and the harmonic time dependence is implicit, according to the convention given in Eq. (4.1).

In terms of the cartesian unit vectors $\hat{\mathbf{n}}_x$, $\hat{\mathbf{n}}_y$ and $\hat{\mathbf{n}}_z$, the unit vectors $\hat{\mathbf{n}}_\rho$, $\hat{\mathbf{n}}_\phi$ and $\hat{\mathbf{n}}_\theta$ are given by

$$\hat{\mathbf{n}}_\rho = \cos\phi\,\hat{\mathbf{n}}_x + \sin\phi\,\hat{\mathbf{n}}_y, \tag{4.40}$$

$$\hat{\mathbf{n}}_\phi = -\sin\phi\,\hat{\mathbf{n}}_x + \cos\phi\,\hat{\mathbf{n}}_y, \tag{4.41}$$

$$\hat{\mathbf{n}}_\theta = \cos\theta\cos\phi\,\hat{\mathbf{n}}_x + \cos\theta\sin\phi\,\hat{\mathbf{n}}_y - \sin\theta\,\hat{\mathbf{n}}_z. \tag{4.42}$$

At the reference sphere, the magnitude of the incident field (already rewritten in terms of ϕ and θ) is then

$$|\mathbf{E}_{\mathrm{i}}(\theta,\phi)| = E_0\,\mathrm{e}^{-\frac{f^2\sin^2\theta}{w_0^2}}\,\hat{\mathbf{n}}_x, \tag{4.43}$$

with the ϕ dependence implicitly contained in the unit vector. Notice that the focal distance f is now treated only as a parameter.

Eqs. (4.40) to (4.43) must be inserted into Eq. (4.27) for the explicit calculation of $\mathbf{E}_{\mathrm{l}}(\theta,\phi)$. Performing the dot products, the components of $\mathbf{E}_{\mathrm{l}}(\theta,\phi)$ are given by:

$$E_{\mathrm{l},x}(\theta,\phi) = A_1(\theta)\left[\sin^2\phi + \cos^2\phi\cos\theta\right], \tag{4.44}$$

$$E_{\mathrm{l},y}(\theta,\phi) = A_1(\theta)\left[-\sin\phi\cos\phi + \sin\phi\cos\phi\cos\theta\right], \tag{4.45}$$

$$E_{\mathrm{l},z}(\theta,\phi) = A_1(\theta)\left[-\cos\phi\sin\theta\right], \tag{4.46}$$

with $A_1(\theta) = E_0\,\mathrm{e}^{-\frac{f^2\sin^2\theta}{w_0^2}}\sqrt{\cos\theta}$. Eq. (4.37) can then be finally applied, yielding the components of the electric field in the focal region:

$$E_{\mathrm{f},x}(\rho,\varphi,z) = \int_0^{\theta_{\max}}\int_0^{2\pi} A_2(\theta)\,\mathrm{e}^{\mathrm{i}k\rho\sin\theta\cos(\phi-\varphi)}[\sin^2\phi + \cos^2\phi\cos\theta] \times \mathrm{e}^{\mathrm{i}kz\cos\theta}\sin\theta\,\mathrm{d}\theta\,\mathrm{d}\phi, \tag{4.47}$$

$$E_{\mathrm{f},y}(\rho,\varphi,z) = \int_0^{\theta_{\max}}\int_0^{2\pi} A_2(\theta)\,\mathrm{e}^{\mathrm{i}k\rho\sin\theta\cos(\phi-\varphi)}[\sin\phi\cos\phi\cos\theta - \sin\phi\cos\phi] \times \mathrm{e}^{\mathrm{i}kz\cos\theta}\sin\theta\,\mathrm{d}\theta\,\mathrm{d}\phi, \quad (4.48)$$

$$E_{\mathrm{f},z}(\rho,\varphi,z) = -\int_0^{\theta_{\max}}\int_0^{2\pi} A_2(\theta)\cos\phi\sin\theta\mathrm{e}^{\mathrm{i}kz\cos\theta}\mathrm{e}^{\mathrm{i}k\rho\sin\theta\cos(\phi-\varphi)}\sin\theta\,\mathrm{d}\theta\mathrm{d}\phi, \quad (4.49)$$

where $A_2(\theta) = A_1(\theta)kf\,\mathrm{e}^{-\mathrm{i}kf}/(2\pi\,\mathrm{i})$.

The integrals in ϕ can be analytically calculated using the relations [148]

$$\int_0^{2\pi}\cos(n\phi)\,\mathrm{e}^{\mathrm{i}x\cos(\phi-\varphi)}\,\mathrm{d}\phi = 2\pi(\,\mathrm{i})^n J_n(x)\cos(n\varphi), \quad (4.50)$$

$$\int_0^{2\pi}\sin(n\phi)\,\mathrm{e}^{\mathrm{i}x\cos(\phi-\varphi)}\,\mathrm{d}\phi = 2\pi(\,\mathrm{i})^n J_n(x)\sin(n\varphi), \quad (4.51)$$

where $J_n(x)$ represents the n-th order Bessel function of the first kind.

Integrating in ϕ and grouping the terms, the components of the electric field in the focal region become

$$E_{\mathrm{f},x}(\rho,\varphi,z) = \frac{kf\,\mathrm{e}^{-\mathrm{i}kf}E_0}{2\,\mathrm{i}}\left[I_0(\rho,z) + I_2(\rho,z)\cos 2\varphi\right], \quad (4.52)$$

$$E_{\mathrm{f},y}(\rho,\varphi,z) = \frac{kf\,\mathrm{e}^{-\mathrm{i}kf}E_0}{2\,\mathrm{i}} I_2(\rho,z)\sin 2\varphi, \quad (4.53)$$

$$E_{\mathrm{f},z}(\rho,\varphi,z) = -kf\,\mathrm{e}^{-\mathrm{i}kf}E_0 I_1(\rho,z)\cos\varphi, \quad (4.54)$$

where the integrals $I_0(\rho,z)$, $I_1(\rho,z)$ and $I_2(\rho,z)$ are given by

$$I_0(\rho,z) = \int_0^{\theta_{\max}} \mathrm{e}^{-\frac{f^2\sin^2\theta}{w_0^2}}\sqrt{\cos\theta}\,\mathrm{e}^{\mathrm{i}kz\cos\theta}J_0(\rho k\sin\theta) \times(1+\cos\theta)\sin\theta\,\mathrm{d}\theta, \quad (4.55)$$

$$I_1(\rho,z) = \int_0^{\theta_{\max}} \mathrm{e}^{-\frac{f^2\sin^2\theta}{w_0^2}}\sqrt{\cos\theta}\,\mathrm{e}^{\mathrm{i}kz\cos\theta}J_1(\rho k\sin\theta)\sin^2\theta\,\mathrm{d}\theta, \quad (4.56)$$

$$I_2(\rho,z) = \int_0^{\theta_{\max}} \mathrm{e}^{-\frac{f^2\sin^2\theta}{w_0^2}}\sqrt{\cos\theta}\,\mathrm{e}^{\mathrm{i}kz\cos\theta}J_2(\rho k\sin\theta)(1-\cos\theta)\sin\theta\,\mathrm{d}\theta. \quad (4.57)$$

We see the electric field $\mathbf{E}_{\mathrm{f}}(\rho,\varphi,z)$ can be obtained at any point through, at maximum, four one-dimensional numerical integrations. These operations are not expected to be computationally expensive, making the ASR as described here a suitable approach to numerical treatments of tightly focused laser beams.

4.2.2 Gaussian beams focused on planar dielectric interfaces

For the calculation of the electromagnetic force densities, we will introduce now two linear, isotropic, homogeneous, non-magnetic dielectric materials of real refractive indexes $n_1 = \sqrt{\epsilon_{1r}}$ and $n_2 = \sqrt{\epsilon_{2r}}$, where ϵ_{1r} and ϵ_{2r} are the relative permittivities. The interface between them will be assumed planar and located at $z = z_0$. The lens will be totally immersed in medium 1, while medium 2 will be the sample medium, where the forces will be calculated.

The origin of the coordinate system is, again, chosen to be at the focal spot that the system would have if the space was homogeneous (i.e., no media 2 present). This clarification is necessary because the refraction at the surface will naturally change the focal spot if the beam is being focused on medium 2 surface. With this convention, we can conveniently generalize our formalism to also describe defocusing beams – we only need to shift the interface position z_0 (see Fig. 4.4). If $z_0 \leq 0$, the beam is being focused on medium 2 surface, and if $z_0 > 0$ the beam is being defocused on medium 2 surface. This allows further investigation possibilities of the electromagnetic force densities.

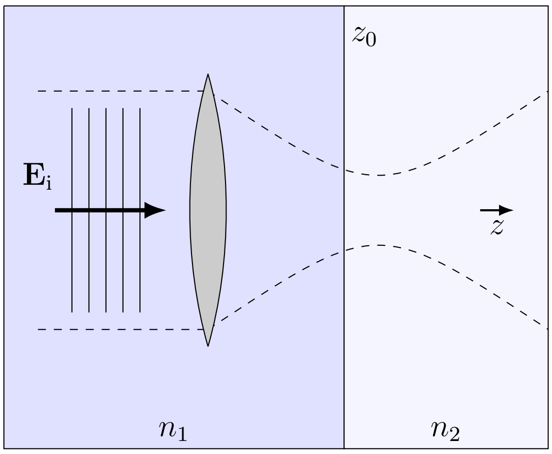

Figure 4.4: Laser beam focused on a planar dielectric interface located at $z = z_0$. By shifting the z_0 position, the beam can be defocused on the interface. Notice that the refraction at the surface is not shown.

The incidence of the focused beam on the interface will, naturally, generates a reflected beam and a transmitted beam, so that

$$\mathbf{E} = \begin{cases} \mathbf{E}_\mathrm{f} + \mathbf{E}_\mathrm{r}, & z < z_0, \\ \mathbf{E}_\mathrm{t}, & z \geq z_0, \end{cases} \tag{4.58}$$

where f, r and t denote the focused (incident), reflected and transmitted fields, respectively.

The fields in Eq. (4.58) must satisfy the boundary conditions imposed by Maxwell's equations. Such conditions lead to the well-known Fresnel transmission and reflection coefficients $r(\theta)$ and $t(\theta)$ for each polarization (see Appendix B for more details), yielding

$$\mathbf{E} = \begin{cases} (1+r_\mathrm{s})\mathbf{E}_\mathrm{f}^{(\mathrm{s})} + (1+r_\mathrm{p})\mathbf{E}_\mathrm{f}^{(\mathrm{p})}, & z < z_0, \\ t_\mathrm{s}\mathbf{E}_\mathrm{f}^{(\mathrm{s})} + t_\mathrm{p}\mathbf{E}_\mathrm{f}^{(\mathrm{p})}, & z \geq z_0. \end{cases} \tag{4.59}$$

The ASR can be extended to describe this inhomogeneous space [145, 150]. In analogy with the former section, the electric field components are again given in terms of one-dimensional integrals. As we will be interested in the electromagnetic forces arising on medium 2, from now on we need only to treat the transmitted field, which is given by

$$E_{\mathrm{t},x}(\rho,\varphi,z) = \frac{k_1 f E_0 \mathrm{e}^{-\,\mathrm{i}k_1 f}}{2\,\mathrm{i}}[I_{0\mathrm{t}}(\rho,z) + I_{2\mathrm{t}}(\rho,z)\cos 2\varphi], \tag{4.60}$$

$$E_{\mathrm{t},y}(\rho,\varphi,z) = \frac{k_1 f E_0 \mathrm{e}^{-\,\mathrm{i}k_1 f}}{2\,\mathrm{i}} I_{2\mathrm{t}}(\rho,z)\sin 2\varphi, \tag{4.61}$$

$$E_{\mathrm{t},z}(\rho,\varphi,z) = -k_1 f E_0 \mathrm{e}^{-\,\mathrm{i}k_1 f} I_{1\mathrm{t}}(\rho,z)\cos\varphi. \tag{4.62}$$

The new one-dimensional integrals are

$$I_{0\mathrm{t}}(\rho,z) = \int_0^{\theta_\mathrm{max}} \mathrm{e}^{\mathrm{i}(k_1\cos\theta - k_2\cos\theta_\mathrm{t})z_0} \mathrm{e}^{-\frac{f^2\sin^2\theta}{w_0^2}} \sqrt{\cos\theta}\,(t_\mathrm{s}(\theta) + t_\mathrm{p}(\theta)\cos\theta_\mathrm{t}) \times \sin\theta \mathrm{e}^{\mathrm{i}k_2 z\cos\theta_\mathrm{t}} J_0(\rho k_1\sin\theta)\mathrm{d}\theta, \tag{4.63}$$

$$I_{1\mathrm{t}}(\rho,z) = \int_0^{\theta_\mathrm{max}} \mathrm{e}^{\mathrm{i}(k_1\cos\theta - k_2\cos\theta_\mathrm{t})z_0} \mathrm{e}^{-\frac{f^2\sin^2\theta}{w_0^2}} \sqrt{\cos\theta}\sin\theta \mathrm{e}^{\mathrm{i}k_2 z\cos\theta_\mathrm{t}} t_\mathrm{p}(\theta) \times \sin\theta_\mathrm{t} J_1(\rho k_1\sin\theta)\mathrm{d}\theta, \tag{4.64}$$

$$I_{2\mathrm{t}}(\rho,z) = \int_0^{\theta_\mathrm{max}} \mathrm{e}^{\mathrm{i}(k_1\cos\theta - k_2\cos\theta_\mathrm{t})z_0} \mathrm{e}^{-\frac{f^2\sin^2\theta}{w_0^2}} \sqrt{\cos\theta}\,(t_\mathrm{s}(\theta) - t_\mathrm{p}(\theta)\cos\theta_\mathrm{t}) \times \sin\theta \mathrm{e}^{\mathrm{i}k_2 z\cos\theta_\mathrm{t}} J_2(\rho k_1\sin\theta)\mathrm{d}\theta. \tag{4.65}$$

In the above integrals, $\theta_\mathrm{t} = \sin^{-1}((n_1/n_2)\sin\theta)$ is the transmitted angle at the dielectric interface and $k_1 = n_1(\omega/c)$ and $k_2 = n_2(\omega/c)$ are the wavevector magnitudes in each medium. The first term of the integrands guarantees that the phase is continuous when changing media.

Having all the electric field components, the magnetic field can be determined through Faraday's law (using numerical derivatives) or applying again the ASR – i.e., using numerical integrations. The latter is chosen here due to potential increased numerical accuracy and stability. The resulting integrals for the magnetic field are given in the same way as for the electric field – only the transmission coefficients for the s and p polarizations must be swapped. Besides, there is a factor $\sqrt{\epsilon/\mu}$ that must be multiplied, corresponding to the inverse of the wave impedance in the medium. The full description is given in Appendix E.

4.3 Pulsed gaussian beam and momentum density

The ASR framework was developed in the last sections for monochromatic beams. Here, we will show how to extend it properly for numerical calculations considering quasi-monochromatic beams at optical frequencies.

We want to calculate the amplitude of a pulsed gaussian beam propagating in z direction when its energy is known. For applications within the ASR, we only need the amplitude E_0 of the electric field incident on the lens located at $z = z_l$, where

$$\mathbf{E} = \mathrm{Re}\{\mathbf{E}_0\, \mathrm{e}^{-\frac{x^2+y^2}{w_0^2}}\, \mathrm{e}^{-\frac{(t-\xi)^2}{\tau^2}}\, \mathrm{e}^{-\,\mathrm{i}\omega t}\}, \tag{4.66}$$

with the term $\mathrm{e}^{\mathrm{i}kz_l}$ being arbitrarily set to one, $w_0 = w(z = z_l)$ is the beam width[1] at the lens and τ and ξ are parameters describing the gaussian temporal dependence of the pulse.

The instantaneous power transferred by the beam at a cross section S is given by the surface integral

$$P(t) = \int_S (\mathbf{E} \times \mathbf{H}) \cdot \mathrm{d}\mathbf{A}, \tag{4.67}$$

where $\mathrm{d}\mathbf{A} = \hat{\mathbf{z}}\, \mathrm{d}x\, \mathrm{d}y$. The magnetic field $\mathbf{H}$ has the same functional form of the electric field $\mathbf{E}$ (apart from a multiplicative constant) provided $k \gg w_0^{-1}$ and $\omega \gg \tau^{-1}$, which are conditions usually satisfied for gaussian beams at optical frequencies. The cross product in the integrand is then

$$\begin{aligned} \mathbf{E} \times \mathbf{H} &= \mathrm{Re}\{\mathbf{E}_0\, \mathrm{e}^{-\frac{x^2+y^2}{w_0^2}}\, \mathrm{e}^{-\frac{(t-\xi)^2}{\tau^2}}\, \mathrm{e}^{-\,\mathrm{i}\omega t}\} \times \mathrm{Re}\{\mathbf{H}_0\, \mathrm{e}^{-\frac{x^2+y^2}{w_0^2}}\, \mathrm{e}^{-\frac{(t-\xi)^2}{\tau^2}}\, \mathrm{e}^{-\,\mathrm{i}\omega t}\} \\ &= \hat{\mathbf{z}}\frac{E_0^2}{\eta}\, \mathrm{e}^{-2\frac{x^2+y^2}{w_0^2}}\, \mathrm{e}^{-2\frac{(t-\xi)^2}{\tau^2}} \cos^2(\omega t), \end{aligned} \tag{4.68}$$

where $\mathbf{H}_0 = \hat{\mathbf{z}} \times \mathbf{E}_0/\eta$ and η is the wave impedance of the medium, given by $\eta = \sqrt{\mu/\epsilon}$.

[1] Recall the convention that w_0 here is the beam waist parameter of the field, and not of the intensity.

Returning to Eq. (4.67) and using polar coordinates (r, θ), we have

$$\begin{aligned} P(t) &= \frac{E_0^2}{2\eta}\,\mathrm{e}^{-2\frac{(t-\xi)^2}{\tau^2}}\left[1+\cos\left(2\omega t\right)\right]\int_0^{2\pi}\int_0^{\infty}\mathrm{e}^{\frac{-2r^2}{w_0^2}}\,r\,\mathrm{d}r\,\mathrm{d}\theta \\ &= \frac{\pi E_0^2 w_0^2}{4\eta}\,\mathrm{e}^{-2\frac{(t-\xi)^2}{\tau^2}}\left[1+\cos\left(2\omega t\right)\right]. \end{aligned} \tag{4.69}$$

Integrating the power in time, we find the (assumed known) total energy of pulse:

$$Q = \int_0^{\infty} P(t)\,\mathrm{d}t. \tag{4.70}$$

The integral containing the cosine term is null for this domain of integration, so that

$$Q = \frac{\pi E_0^2 w_0^2}{4\eta}\int_0^{\infty}\mathrm{e}^{-2\frac{(t-\xi)^2}{\tau^2}}\,\mathrm{d}t. \tag{4.71}$$

The amplitude E_0 is then given is terms of Q as

$$E_0 = \sqrt{\frac{4\eta Q}{\pi w_0^2 t_0}}, \tag{4.72}$$

where t_0 is given in terms of the error function (erf):

$$t_0 = \frac{\sqrt{\pi}\tau}{2\sqrt{2}}\left[\operatorname{erf}\left(\frac{\sqrt{2}\xi}{\tau}\right)+1\right]. \tag{4.73}$$

In fact, typical pulses have $\xi \geq 2\tau$, which generates $t_0 \approx \sqrt{\pi/2}\tau$, and consequently

$$E_0 \approx \sqrt{\frac{4\sqrt{2}\eta Q}{\pi^{3/2} w_0^2 \tau}}, \tag{4.74}$$

if the amplitude is calculated in air, as usual.

The time-derivative term of MA force density is the Abraham force, given by $c^{-2}(n^2 - 1)\partial_t(\mathbf{E}\times\mathbf{H})$. To calculate this term, notice that we know from Eq. (4.68) that, generally,

$$\mathbf{E}\times\mathbf{H} = \mathbf{C}(\mathbf{r})\,\mathrm{e}^{-2\frac{(t-\xi)^2}{\tau^2}}\left[1+\cos\left(2kz - 2\omega t\right)\right], \tag{4.75}$$

for some function $\mathbf{C}(\mathbf{r})$ related to the spatial dependence of the fields, which is given numerically by the ASR. Notice that the z dependence has been restored, except for phase terms. The time derivative of $\mathbf{E}\times\mathbf{H}$ is then:

$$\frac{\partial(\mathbf{E}\times\mathbf{H})}{\partial t}=\mathbf{C}(\mathbf{r})\,\mathrm{e}^{-2\frac{(t-\xi)^2}{\tau^2}}\left[-4\frac{(t-\xi)}{\tau^2}\left[1+\cos\left(2kz-2\omega t\right)\right]+2\omega\sin\left(2kz-2\omega t\right)\right]. \tag{4.76}$$

The sine term dominates over the remaining ones, due to the large values of ω at optical regime; however, we know that oscillations at optical time scale can only be measured as cycle-averages – thus, the cosine and sine terms can be neglected here as they average to zero, and we obtain

$$\frac{\partial(\mathbf{E}\times\mathbf{H})}{\partial t}=-4\mathbf{C}(\mathbf{r})\frac{(t-\xi)}{\tau^2}\,\mathrm{e}^{-2\frac{(t-\xi)^2}{\tau^2}}. \tag{4.77}$$

As already stated, by using the ASR implementation we are able to directly determine only the stationary force densities. According to the analysis just presented, we can generalize the ASR and add the time dependence for the force densities as[2]

$$\mathbf{f}(\mathbf{r},t)=\mathbf{f}_{\mathrm{ASR}}(\mathbf{r})\,\mathrm{e}^{-2\frac{(t-\xi)^2}{\tau^2}}+4\frac{n^2-1}{c^2}\mathrm{Re}\left[\mathbf{E}(\mathbf{r})\times\mathbf{H}^*(\mathbf{r})\right]_{\mathrm{ASR}}\frac{(t-\xi)}{\tau^2}\,\mathrm{e}^{-2\frac{(t-\xi)^2}{\tau^2}}. \tag{4.78}$$

Here, the subscript "ASR" means the term is calculated using the standard ASR fields, which depend only on spatial coordinates. The cycle-average argument for optical time scales has been used again for the time dependence of the first term. The function $\mathbf{C}(\mathbf{r})$ from Eq. (4.77) is implicitly contained in the ASR fields.

In realistic experiments, the time modulation is often not exactly gaussian; thus, it is convenient for the numerical implementations to describe Eq. (4.78) explicitly in terms of Q, τ and ξ. This allows a more accurate fit to the experimental temporal profile, where we can use, for example, the sum of two different gaussian functions. Recalling that the amplitude of a monochromatic gaussian beam with unitary power is given by $\sqrt{4\eta/\pi w_0^2}$, we can rewrite Eq. (4.78) as

$$\mathbf{f}(\mathbf{r},t)=\frac{Q}{t_0}\mathbf{f}_{\mathrm{ASR,m}}(\mathbf{r})h(t)-\frac{Q}{t_0}\left(\frac{n^2-1}{c^2}\right)\mathrm{Re}\left[\mathbf{E}(\mathbf{r})\times\mathbf{H}^*(\mathbf{r})\right]_{\mathrm{ASR,m}}h'(t). \tag{4.79}$$

Here, $h(t)$ is the gaussian-like time modulation of the beam, fitted from the experimental laser source, and the subscript "ASR, m" means the fields are calculated in the ASR with the monochromatic amplitude of unitary power.

Lastly, notice that if the pulsed beam is very short, the frequency bandwidth will be large – so, one ASR simulation must be carried out for each discrete frequency component. This happens because the ASR integrals depend on the wavenumber k, even for non-dispersive media. For example, for a typical beam with $\tau = 10$ ns and $\lambda = 532.0$ nm,

[2]The product of $\mathbf{E}$ with $\mathbf{H}^*$ (instead of $\mathbf{H}$) eliminates the oscillatory part, automatically yielding the correct form.

we can safely consider the beam monochromatic in frequency space[3,4] (or, more formally, quasi-monochromatic), because $\omega^{-1} \ll \tau$. In this case, a single ASR simulation should be enough to completely describe the pulsed beam, according to Eq. (4.79).

4.4 Force densities

As we have seen, the electromagnetic force density is quadratic in the fields and involves a linear combination of first-order time and spatial derivatives. Specifically, the introduction of the time dependence within the ASR framework was described in the last section; now, we present a way to numerically calculate any of the relevant spatial derivatives using, again, a combination of one-dimensional integrals. This is done by simply differentiating the transmitted field equations from Section. 4.2.2 with respect to the spatial coordinates. This approach is computationally faster, more accurate and more stable than the standard numerical derivative calculation.

With the auxiliary functions

$$C_1 \equiv \frac{k_1 f E_0\, \mathrm{e}^{-\,\mathrm{i}k_1 f}}{2\,\mathrm{i}} \tag{4.80}$$

and

$$C_2(\theta, z) \equiv \mathrm{e}^{\,\mathrm{i}(k_1\cos\theta - k_2\cos\theta_\mathrm{t})z_0}\,\mathrm{e}^{\frac{-f^2\sin^2\theta}{w_0^2}}\sqrt{\cos\theta}\,\mathrm{e}^{\,\mathrm{i}k_2 z\cos\theta_\mathrm{t}}, \tag{4.81}$$

the electric field derivatives for polarization x needed to describe the force densities within the dielectric material are given by

$$\begin{aligned}\frac{\partial E_{\mathrm{t},x}}{\partial x} &= C_1 k_1\left[-\cos\varphi I_{0\mathrm{t}}^{(x)}(\rho,z) + \frac{\cos\varphi}{2}\cos 2\varphi I_{2\mathrm{t}}^{(x)}(\rho,z)\right.\\ &+ \left.\frac{2\sin\varphi}{k_1\rho}\sin 2\varphi I_{2\mathrm{t}}(\rho,z)\right],\end{aligned} \tag{4.82}$$

$$\begin{aligned}\frac{\partial E_{\mathrm{t},x}}{\partial y} &= C_1 k_1\left[-\sin\varphi I_{0\mathrm{t}}^{(y)}(\rho,z) + \frac{\sin\varphi}{2}\cos 2\varphi I_{2\mathrm{t}}^{(y)}(\rho,z)\right.\\ &- \left.\frac{2\cos\varphi}{k_1\rho}\sin 2\varphi I_{2\mathrm{t}}(\rho,z)\right],\end{aligned} \tag{4.83}$$

[3]The formal quantitative analysis must, of course, be carried in frequency domain.

[4]Notice that relatively short pulses can break the gaussian approximation in time, i.e., the magnetic and electric fields would not have the same time-dependence, making the analysis much more difficult.

$$\frac{\partial E_{\mathrm{t},x}}{\partial z} = \mathrm{i}k_2 C_1 \left[I_{0\mathrm{t}}^{(z)}(\rho,z) + \cos 2\varphi I_{2\mathrm{t}}^{(z)}(\rho,z) \right], \tag{4.84}$$

$$\frac{\partial E_{\mathrm{t},y}}{\partial x} = C_1 \left[\frac{k_1 \cos\varphi}{2} \sin 2\varphi I_{2\mathrm{t}}^{(x)}(\rho,z) - \frac{2\sin\varphi}{\rho} \cos 2\varphi I_{2\mathrm{t}}(\rho,z) \right], \tag{4.85}$$

$$\frac{\partial E_{\mathrm{t},y}}{\partial y} = C_1 \left[\frac{k_1 \sin\varphi}{2} \sin 2\varphi I_{2\mathrm{t}}^{(y)}(\rho,z) \ + \frac{2\cos\varphi}{\rho} \cos 2\varphi I_{2\mathrm{t}}(\rho,z) \right], \tag{4.86}$$

$$\frac{\partial E_{\mathrm{t},y}}{\partial z} = \mathrm{i}k_2 C_1 \sin 2\varphi I_{2\mathrm{t}}^{(z)}(\rho,z), \tag{4.87}$$

$$\frac{\partial E_{\mathrm{t},z}}{\partial x} = -2\,\mathrm{i}C_1 \left[\frac{k_1 \cos\varphi}{2} \cos\varphi I_{1\mathrm{t}}^{(x)}(\rho,z) + \frac{\sin\varphi}{\rho} \sin\varphi I_{1\mathrm{t}}(\rho,z) \right], \tag{4.88}$$

$$\frac{\partial E_{\mathrm{t},z}}{\partial y} = -2\,\mathrm{i}C_1 \left[\frac{k_1 \sin\varphi}{2} \cos\varphi I_{1\mathrm{t}}^{(y)}(\rho,z) - \frac{\cos\varphi}{\rho} \sin\varphi I_{1\mathrm{t}}(\rho,z) \right], \tag{4.89}$$

$$\frac{\partial E_{\mathrm{t},z}}{\partial z} = 2k_2 C_1 \cos\varphi I_{1\mathrm{t}}^{(z)}(\rho,z). \tag{4.90}$$

The new one-dimensional integrals appearing are given by

$$I_{0\mathrm{t}}^{(x)}(\rho,z) = \int_0^{\theta_{\max}} C_2(\theta,z) \sin^2\theta (t_\mathrm{s}(\theta) + t_\mathrm{p}(\theta) \times \cos\theta_\mathrm{t}) J_1(\rho k_1 \sin\theta)\,\mathrm{d}\theta, \tag{4.91}$$

$$I_{0\mathrm{t}}^{(y)}(\rho,z) = I_{0\mathrm{t}}^{(x)}(\rho,z), \tag{4.92}$$

$$I_{1\mathrm{t}}^{(x)}(\rho,z) = \int_0^{\theta_{\max}} C_2(\theta,z) \sin^2\theta \sin\theta_\mathrm{t}\, t_\mathrm{p}(\theta) (J_0(\rho k_1 \sin\theta) - J_2(\rho k_1 \sin\theta))\,\mathrm{d}\theta, \tag{4.93}$$

$$I_{1\mathrm{t}}^{(y)}(\rho,z) = I_{1\mathrm{t}}^{(x)}(\rho,z), \tag{4.94}$$

$$\begin{aligned} I_{2\mathrm{t}}^{(x)}(\rho,z) = \int_0^{\theta_{\max}} & C_2(\theta,z) \sin^2\theta (t_\mathrm{s}(\theta) - t_\mathrm{p}(\theta) \cos\theta_\mathrm{t}) \\ & \times (J_1(\rho k_1 \sin\theta) - J_3(\rho k_1 \sin\theta))\,\mathrm{d}\theta, \end{aligned} \tag{4.95}$$

$$I_{2\mathrm{t}}^{(y)}(\rho, z) = I_{2\mathrm{t}}^{(x)}(\rho, z), \tag{4.96}$$

$$I_{0\mathrm{t}}^{(z)}(\rho, z) = \int_0^{\theta_{\max}} C_2(\theta, z) \cos\theta_\mathrm{t} \sin\theta (t_\mathrm{s}(\theta) + t_\mathrm{p}(\theta)\cos\theta_\mathrm{t}) J_0(\rho k_1 \sin\theta)\, \mathrm{d}\theta, \tag{4.97}$$

$$I_{1\mathrm{t}}^{(z)}(\rho, z) = \int_0^{\theta_{\max}} C_2(\theta, z) \cos\theta_\mathrm{t} \sin\theta \sin\theta_\mathrm{t}\, t_\mathrm{p}(\theta) J_1(\rho k_1 \sin\theta)\, \mathrm{d}\theta, \tag{4.98}$$

$$I_{2\mathrm{t}}^{(z)}(\rho, z) = \int_0^{\theta_{\max}} C_2(\theta, z) \cos\theta_\mathrm{t} \sin\theta (t_\mathrm{s}(\theta) - t_\mathrm{p}(\theta)\cos\theta_\mathrm{t}) J_2(\rho k_1 \sin\theta)\, \mathrm{d}\theta. \tag{4.99}$$

In deriving these integrals, the properties $J_n'(x) = 1/2\,[J_{n-1}(x) - J_{n+1}(x)]$ and $J_{-n}(x) = (-1)^n J_n(x)$ of Bessel functions were used. Also, we recall that the transmitted angle is $\theta_\mathrm{t} = \sin^{-1}((n_1/n_2)\sin\theta)$. The derivatives for the magnetic field components are given in the same manner, and are not shown here for brevity.

Notice that there is an apparent divergence at the origin for some terms due to ρ appearing in the denominator. It can be shown that this factor is actually cancelled by the Bessel functions present in the integrals, so no divergence occurs, as expected. Still, care should be taken with this point when performing numerical simulations.

For clarity, we show as an example the form of the x component of the time-averaged force density inside a non-magnetic material according to our numerical description for a monochromatic beam excitation. From Eq. (3.54), this term is analytically given as $\langle f_x \rangle = (1/2)\langle \partial_x(\mathbf{P}\cdot\mathbf{E})\rangle$, which results in $\langle f_x \rangle = (\varepsilon_0(n^2-1)/4)\mathrm{Re}[\partial_x(\mathbf{E}\cdot\mathbf{E}^*)]$, or, equivalently, $\langle f_x \rangle = (\varepsilon_0(n^2-1)/2)\mathrm{Re}[\mathbf{E}\cdot\partial_x\mathbf{E}^*]$. The force density can then be numerically obtained from the real part of the following equation:

$$\langle f_x \rangle = \frac{\varepsilon_0(n^2-1)}{2}\left[E_{x,\mathrm{t}}\frac{\partial E_{x,\mathrm{t}}^*}{\partial x} + E_{y,\mathrm{t}}\frac{\partial E_{y,\mathrm{t}}^*}{\partial x} + E_{z,\mathrm{t}}\frac{\partial E_{z,\mathrm{t}}^*}{\partial x}\right], \tag{4.100}$$

where each field term inside the brackets is given through ASR equations – specifically, Eqs. (4.60) to (4.62), (4.82), (4.85) and (4.88) and their related one-dimensional integrals, Eqs. (4.63) to (4.65), (4.91), (4.93) and (4.95).

4.5 Simulations

The numerical simulations were performed considering air, with $n_1 = 1.0003$, and water, with $n_2 = 1.33$, as the dielectrics. The gaussian laser beam has wavelength in air $\lambda = 532.0$ nm and beam waist at the lens $w_0 = 0.39$ mm. The biconvex lens has a focal distance

$f = 5.0$ cm and maximum focusing angle $\theta_{\max} \approx 14.7°$. The water domain is chosen to be a column with $L = 10.0$ mm height in z, and the interface air-water is placed at $z_0 = -5.0$ mm. The values chosen for the parameters f, w_0, $\theta_{\max}$ and L are all realistic in available experiments, as well as the beam power (for continuous excitation) and beam energy (for pulsed excitation) in the next two sections. The geometry of the problem is illustrated in Fig. (4.5).

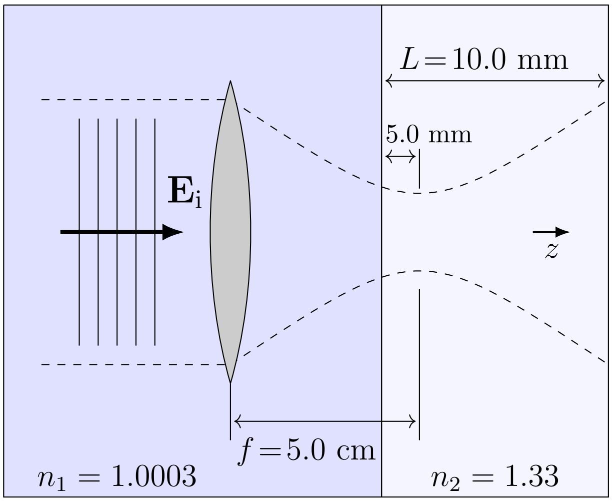

Figure 4.5: Geometry of the simulated problem (not to scale).

4.5.1 Continuous excitation

For the continuous monochromatic beam excitation, we choose a power of 1.0 W – which corresponds to an approximate amplitude $E_0 \approx 5.6 \cdot 10^4$ V/m. Figs. (4.6a) to (4.6f) show the beam intensity at planes $z = -5.0, -3.0, -1.0, 1.0, 3.0, 5.0$ mm respectively. We can see that even after the focusing by the lens and transmission through the dielectric interface, the beam retains its gaussian intensity profile. Typically, non-gaussian corrections are three orders of magnitude smaller. This allows us to maintain the definition of beam waist inside the dielectric, which is shown in Fig. (4.7) as function of z. We can see its value decreases linearly until a focal spot is reached approximately at $z = -2.0$ mm. Then, the beam starts to linearly diverge, as expected.

The MA time-averaged radial force densities $\langle f_r \rangle$ are seen in Fig. (4.8) for the same selected cross sections. The electrostriction effect is clearly manifested, generating radial forces which always point towards the center of the beam. The longitudinal component $\langle f_z \rangle$, on the other hand, is positive before the focal spot, and negative after it – it is, however, two orders of magnitude smaller than the radial force, as seen in Fig. (4.9). This is in accordance with electrostriction effects being typically observed only in the direction transversal to the electromagnetic wave propagation. Arrows qualitatively indicating the

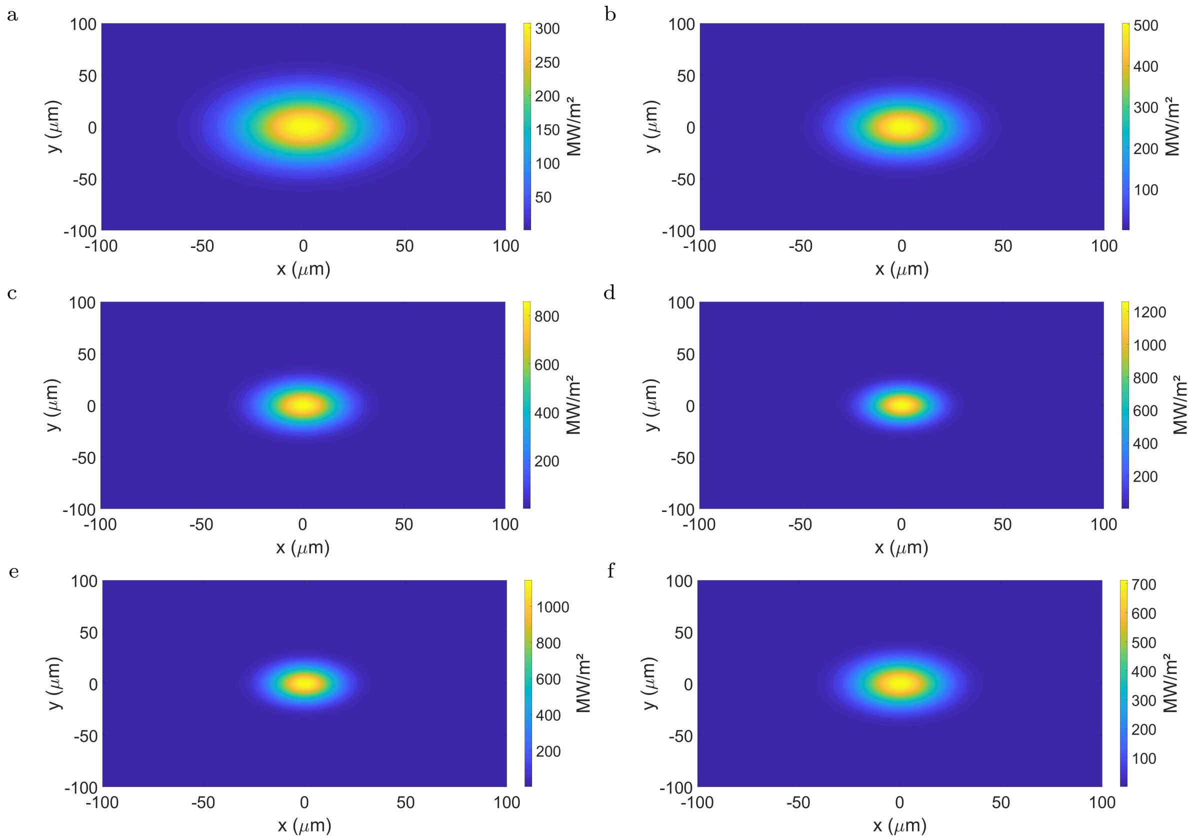

Figure 4.6: Beam intensity at planes z = −5.0, −3.0, −1.0, 1.0, 3.0, 5.0 mm, respectively, from (a) to (f).

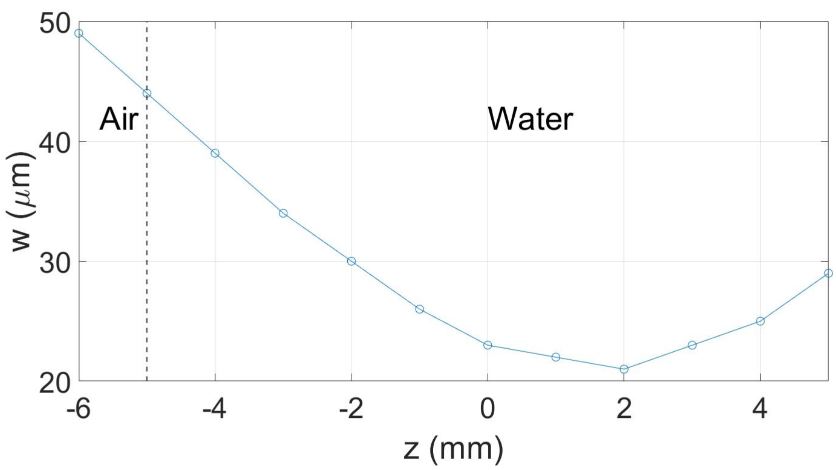

Figure 4.7: Beam waist as a function of distance propagated of the approximate gaussian beam focused inside the dielectric material.

radial force direction are also included. At last, the radiation pressure at the air-water interface is illustrated in Fig. (4.10). The pressure presents a gaussian profile and is strictly negative. In the coordinate system adopted, this corresponds to a force pointing towards the air region – which should generate a bulge in the water surface, as observed in the vast majority of experiments.

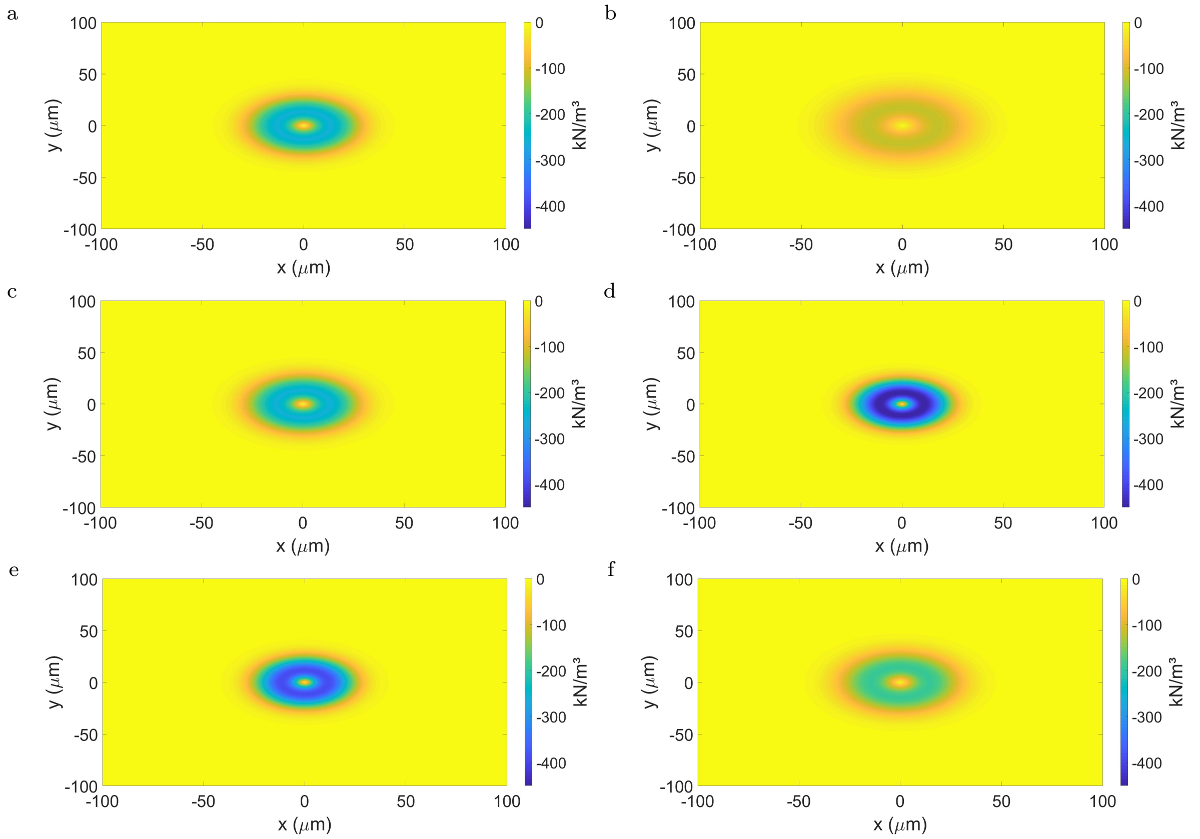

Figure 4.8: Time-averaged radial electromagnetic force densities $\langle f_r \rangle$ at planes $z = -5.0, -3.0, -1.0, 1.0, 3.0, 5.0$ mm, respectively, from (a) to (f).

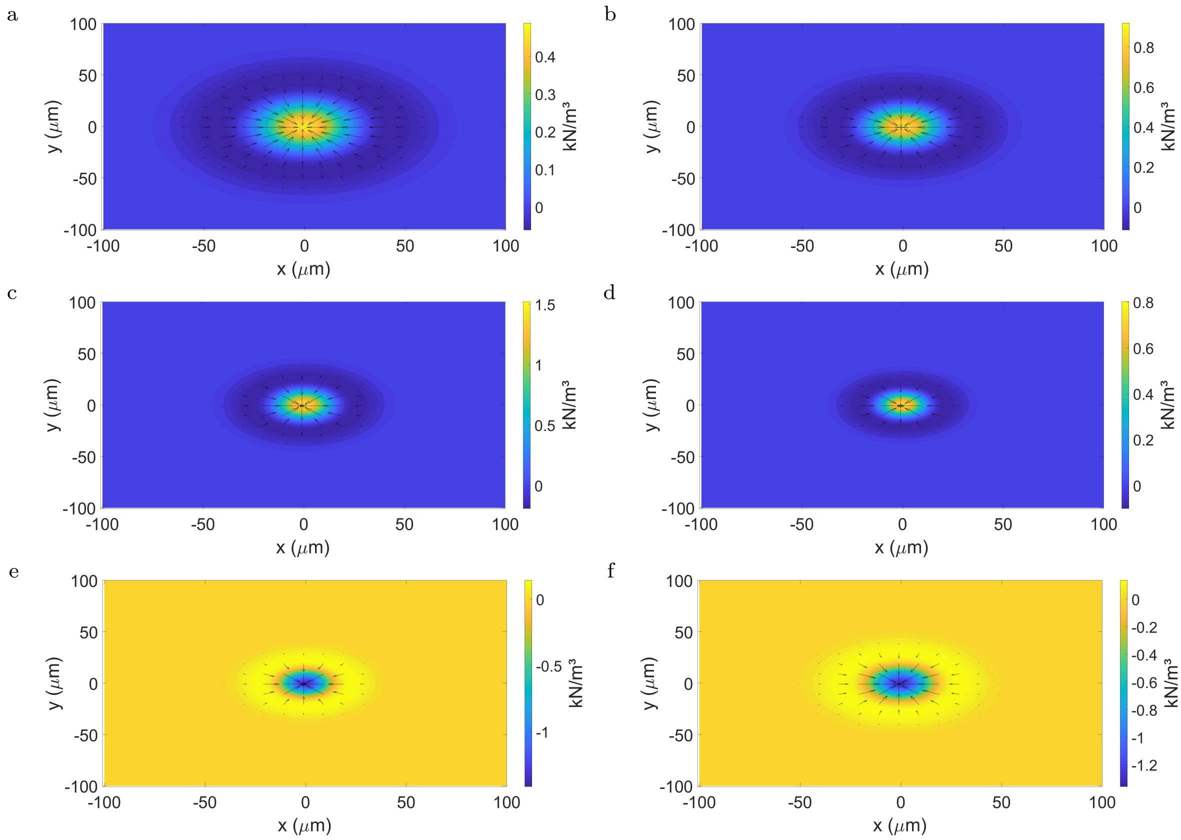

Figure 4.9: Time-averaged longitudinal electromagnetic force densities $\langle f_z \rangle$ (contour plot) and radial force direction (arrows) at planes $z = -5.0$, -3.0, -1.0, 1.0, 3.0, 5.0 mm, respectively, from (a) to (f).

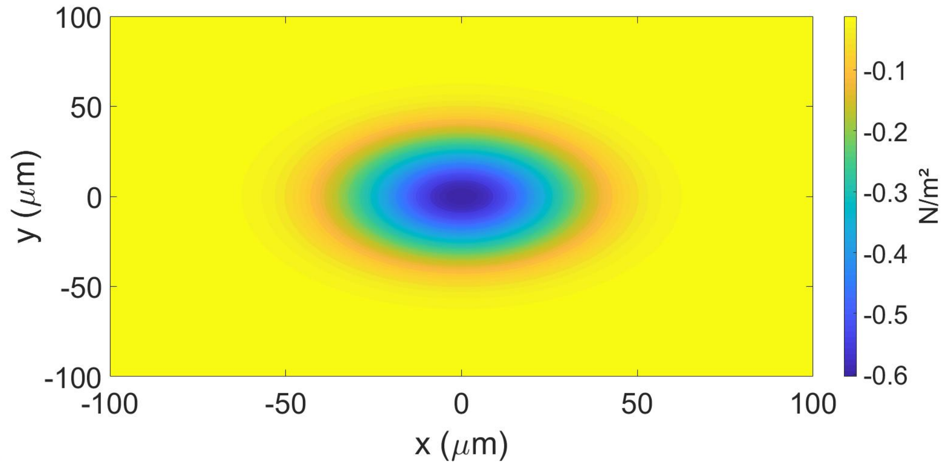

Figure 4.10: Time-averaged radiation pressure $\langle \mathcal{P}_{\text{rad}} \rangle$ at the air-water interface.

4.5.2 Pulsed excitation

For the pulsed beam excitation, we use a gaussian time-modulation as illustrated in Fig. (4.11), defined by $\tau = 4.5$ ns and $\xi = 15.0$ ns. The beam energy is $Q = 1.0$ mJ, which generates $E_0 \approx 2.4 \cdot 10^7$ V/m. The spatial profile is the same as the continuous case – however, notice the field amplitude is approximately 420 times bigger, according to Eq. (4.72). Higher beam amplitudes are characteristic of short pulsed beams, and therefore can provide bigger force densities. In fact, the peak instantaneous intensity for pulsed beam would be $420^2 \approx 1.8 \cdot 10^5$ times bigger than the continuous wave intensity. As the force density scales linearly with beam intensity, the instantaneous force components f_r and f_z for the pulsed excitation would then be multiplied by this factor. Apart from this numerical factor and the gaussian modulation time dependence, their behavior would be exactly the same as the continuous excitation case, and therefore are not shown here.

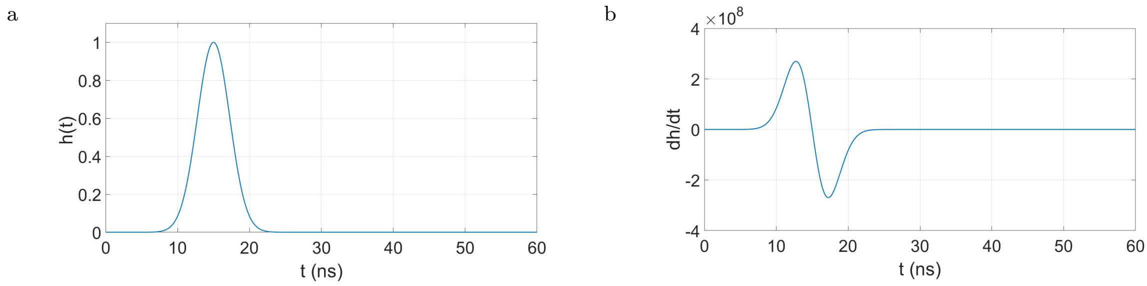

Figure 4.11: Normalized gaussian time modulation for pulsed excitation (a) and its time derivative (b). The parameters are $\tau = 4.5$ ns and $\xi = 15.0$ ns.

The new force density term in the pulsed case is the Abraham force. This term has maximum magnitude at times $t = \xi \pm \tau/2$, and the positive maximum is shown in Fig. (4.12) at $z = 1.0$ mm. We can see it has a gaussian behavior, as expected, but is 4 orders of magnitude smaller, at peak value in time, than the radial force f_r at the same instant. This fact makes its detection extremely difficult to perform. Note that managing to measure this term isolated from other contributions is theoretically very important, for it is directly related to the momentum of the mass-polariton and its associated mass-density wave inside dielectrics. Recall that the few clear measurements of the Abraham force discussed in Section 3.3 are generally related to the total force in macroscopic bodies, and thus can not be associated to the mass-density wave.

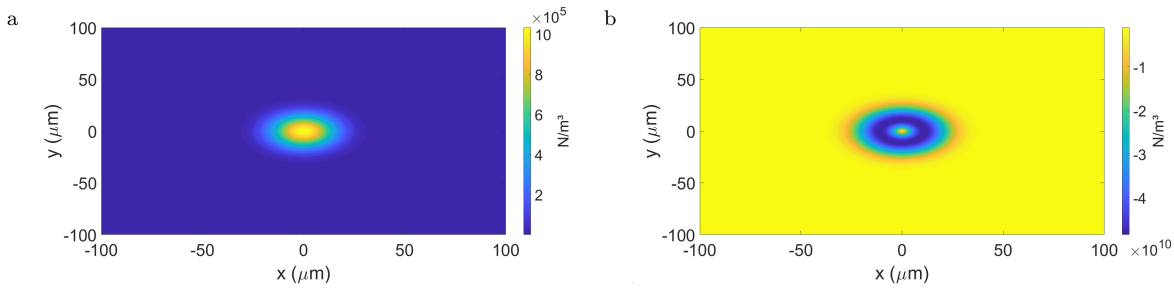

Figure 4.12: Abraham force at its peak value (a) and the radial force density f_r at the same time and location (b).

4.5.3 Fluid dynamics with electromagnetic forces

The presented numerical force densities can be used in fluid simulations to study the effects induced on the materials by the laser beams. However, the dynamics of fluids is long known to be one of the most complex topics in Physics. Even in Computational Physics, accurate simulations of fluid dynamics are usually very hard to be performed. In this context, we used in Ref. [129] our numerical MA force densities along with the commercial software Comsol Multiphysics (COMSOL Inc, Burlington, MA, USA). The forces were added as sources in a previously built Comsol script that solved the coupled thermal and fluid dynamics equations with the proper boundary conditions. The simulation was then compared to experimental results obtained with a photo-induced lens technique and were able to describe the observations with excellent agreement. Indeed, this work is the first to report measurements of the optical electrostriction as the dominant effect.

CHAPTER 5

Conclusions

As we have extensively discussed, there are basically two main problems related to the long-standing Abraham-Minkowski controversy from the theoretical side: first, the use of incorrect microscopic sources when dealing with local force densities and, second, the necessity to recognize the bound state of field and matter (the mass-polariton) arising from the coupling of the propagating field and the driven moving atoms. Although many works have been published recently addressing the latter, there are no works that contemplate both aspects simultaneously. In this scenario, for the first point we presented a new equation for the electromagnetic force densities inside linear, isotropic, non-dispersive and lossless dielectric material. This result is derived from the widely known dipolar approximation for electromagnetic sources and is capable of correctly describing the vast majority of experiments reported to date. The associated radiation pressure at oblique incidence for p polarized beams was shown to be different from the expression currently adopted in the literature. Initially, this result seems compatible with the reported experiments, but more detailed investigations are necessary. For the second point, we have proposed an alteration to the mass-polariton stress-energy tensor, where the Abraham stress-energy tensor is substituted by MA's stress-energy tensor. This allows the theory to describe electro- and magnetostriction effects as well, while maintaining its main characteristics. Theoretically, the momentum transfer of electromagnetic waves inside dielectrics can be consistently explained by this new enhanced formulation, providing a very promising candidate to settle the Abraham-Minkowski controversy.

From the experimental side, it is known that the electromagnetic forces are typically very small, being often suppressed by the existence of bigger effects, like absorption. Besides, measurements at optical frequencies can not provide the time dependence of the forces due to their extremely high frequency oscillations. This scenario leads to very few experimental works being actually capable of distinguishing between the different proposed momenta, as discussed in Ref. [69]. The eventual complete experimental confirmation of our new formulation still requires the measurement of the transferred mass δm and mass-polariton momentum p_{MP}, as discussed in Section 2.3.6.

Another important aspect addressed in this work is the hidden momentum contribution, which is also directly related to the Abraham-Minkowski controversy and has also been itself subject to misunderstandings. It appears naturally from a relativistic derivation of the equations of motion of ideal dipoles, as seen in the laboratory frame, when their center of mass-energy is properly described as a dynamical variable. This derivation was not presented here, but can concisely be found in Ref. [82]. As we have pointed out, the presence of hidden momentum should be recognized as essential even in elementary electromagnetic theory nowadays, as it keeps the smooth behavior of the electromagnetic energy flux across magnetic interfaces.

The numerical calculations of the electromagnetic forces generated in dielectric media by the incidence of tightly focused laser beams were also covered in this work. Notice that employing the usual finite-difference methods to solve Maxwell's equations under optical regime is typically unfeasible due to the relatively very small discretization needed; thus, following the literature on the Angular Spectrum Representation, we were able to write these forces in a semi-analytical form for both pulsed and continuous excitations, which is expected to provide faster and more stable numerical calculations. Such forces can be used to help designing new experimental investigations. Besides, they were obtained for the Microscopic Ampère formulation and successfully used in the simulations of Ref. [129].

The present work is by no means exhaustive – there are many possibilities that can be explored starting from it. One can, for example, try to extend the theory to more complex materials, where effects such as dispersion, absorption, anisotropy and nonlinearities can take place. Consideration of non-conservative optical forces can also be of interest [151]. The analysis of angular momentum distributions inside materials is also relevant, especially because light can have both spin and orbital angular momentum [152] – this has been simulated, for example, using the MP formulation and considering circular and linear polarizations in Ref. [96]. Additionally, one can search for a physically more fundamental formalism by fully working in the Quantum Mechanics regime. There are already some theoretical works in this regard, contemplating, for example, QED corrections to the Abraham force [153] and Casimir-like effects [154].

References

1. Minkowski, H. Die Grundgleichungen für die elektromagnetischen Vorgänge in bewegten Körpern [The fundamental equations for the electromagnetic processes of moving bodies]. *Nachr. Ges. Wiss. Göttn. Math.-Phys. Kl.* **1,** 53–111 (1908).
2. Abraham, M. Zur Elektrodynamik bewegter Körper [The electrodynamics of moving bodies]. *Rend. Circ. Matem. Palermo* **28,** 1–28 (1909).
3. Minenna, D. F. G., Elskens, Y., Doveil, F. & André, F. Electromagnetic momenta for wave-particle systems in vacuum waveguides. *Eur. Phys. J. D* **74,** 103 (1 2020).
4. Minenna, D. F. G., Elskens, Y., Doveil, F. & André, F. *Universality of the Abraham-Minkowski dilemma for photon momenta beyond dielectric* Pre-print available at `arxiv.org/abs/1902.06431`. 2019.
5. Bliokh, K. Y., Bliokh, Y. P. & Nori, F. Ponderomotive forces, Stokes drift, and momentum in acoustic and electromagnetic waves. *Phys. Rev. A* **106,** L021503 (2 2022).
6. Bliokh, K. Y., Bekshaev, A. Y. & Nori, F. Optical momentum, spin, and angular momentum in dispersive media. *Phys. Rev. Lett.* **119,** 073901 (7 2017).
7. Bliokh, K. Y., Bekshaev, A. Y. & Nori, F. Optical momentum and angular momentum in complex media: from the Abraham–Minkowski debate to unusual properties of surface plasmon-polaritons. *New J. Phys.* **19,** 123014 (2017).
8. Lobet, M. *et al.* Momentum considerations inside near-zero index materials. *Light Sci. Appl.* **11,** 1–8 (110 2022).
9. Ashkin, A. Trapping of atoms by resonance radiation pressure. *Phys. Rev. Lett.* **40,** 729–732 (12 1978).
10. Ashkin, A., Dziedzic, J. M., Bjorkholm, J. E. & Chu, S. Observation of a single-beam gradient force optical trap for dielectric particles. *Opt. Lett.* **11,** 288–290 (1986).
11. Mansuripur, M. Momentum exchange effect. *Nat. Photon.* **7,** 765–766 (10 2013).

12. Molloy, J. E. & Padgett, M. J. Lights, action: optical tweezers. *Contemp. Phys.* **43,** 241–258 (4 2010).

13. Gao, D. *et al.* Optical manipulation from the microscale to the nanoscale: fundamentals, advances and prospects. *Light Sci. Appl.* **6,** 1–15 (e17039 2017).

14. Neto, P. A. M. & Nussenzveig, H. M. Theory of optical tweezers. *Europhys. Lett.* **50,** 702–708 (5 2000).

15. Ashkin, A. Optical trapping and manipulation of neutral particles using lasers. *Proc. Natl. Acad. Sci. USA* **94,** 4853–4860 (10 1997).

16. Shi, Y. *et al.* Optical manipulation with metamaterial structures. *Appl. Phys. Rev.* **9,** 031303 (2022).

17. Li, H. *et al.* Optical pulling forces and their applications. *Adv. Opt. Photon.* **12,** 288–366 (2020).

18. Nieminen, T. A., Knöner, G., Heckenberg, N. R. & Rubinsztein-Dunlop, H. Physics of optical tweezers. *Methods Cell Biol.* **82,** 207–236 (6 2007).

19. Phillips, W. D. Nobel lecture: Laser cooling and trapping of neutral atoms. *Rev. Mod. Phys.* **70,** 721–741 (3 1998).

20. Yang, Y. *et al.* Optical forces in photonic Weyl system. *New J. Phys.* **24,** 043019 (4 2022).

21. Chin, L. K., Shi, Y. & Liu, A.-Q. Optical forces in silicon nanophotonics and optomechanical systems: science and applications. *Adv. Dev. Instrum.* **2020,** 1–14 (2020).

22. Wiederhecker, G. S., Chen, L., Gondarenko, A. & Lipson, M. Controlling photonic structures using optical forces. *Nature* **462,** 633–637 (2009).

23. Partanen, M. & Tulkki, J. Time-dependent optical force theory for optomechanics of dispersive 3D photonic materials and devices. *Opt. Express* **30,** 28577–28588 (2022).

24. Psaltis, D., Quake, S. R. & Yang, C. Developing optofluidic technology through the fusion of microfluidics and optics. *Nature* **442,** 381–386 (7101 2006).

25. Monat, C., Domachuk, P. & Eggleton, B. J. Integrated optofluidics: A new river of light. *Nat. Photon.* **1,** 106–114 (2007).

26. Garnier, N., Grigoriev, R. O. & Schatz, M. F. Optical manipulation of microscale fluid flow. *Phys. Rev. Lett.* **91,** 054501 (5 2003).

27. Lebedev, P. N. Experimental examination of light pressure. *Ann. der Physik* **6,** 1–26 (433 1901).

28. Jones, R. V. & Richards, J. C. S. The pressure of radiation in a refracting medium. *Proc. R. Soc. Lond. A* **221,** 480–498 (1147 1954).

29. Jones, R. V. & Leslie, B. The measurement of optical radiation pressure in dispersive media. *Proc. R. Soc. Lond. A* **360,** 347–363 (1702 1978).

30. Ashkin, A. & Dziedzic, J. M. Radiation pressure on a free liquid surface. *Phys. Rev. Lett.* **30,** 139–142 (4 1973).

31. Walker, G. B. & Lahoz, D. G. Experimental observation of Abraham force in a dielectric. *Nature* **253,** 339–340 (1975).

32. Gibson, A. F., Kimmit, M. F., Koohian, A. O., Evans, D. E. & Levy, G. F. D. A study of radiation pressure in a refractive medium by the photon drag effect. *Proc. R. Soc. Lond.* **370,** 303–311 (1980).

33. Casner, A. & Delville, J.-P. Giant deformations of a liquid-liquid interface induced by the optical radiation pressure. *Phys. Rev. Lett.* **87,** 054503 (5 2001).

34. Campbell, G. K. *et al.* Photon recoil momentum in dispersive media. *Phys. Rev. Lett.* **94,** 170403 (17 2005).

35. She, W., Yu, J. & Feng, R. Observation of a push force on the end face of a nanometer silica filament exerted by outgoing light. *Phys. Rev. Lett.* **101,** 243601 (24 2008).

36. Brevik, I. Comment on "Observation of a push force on the end face of a nanometer silica filament exerted by outgoing light". *Phys. Rev. Lett.* **103,** 219301 (21 2009).

37. Mansuripur, M. Comment on "Observation of a push force on the end face of a nanometer silica filament exerted by outgoing light". *Phys. Rev. Lett.* **103,** 019301 (1 2009).

38. Partanen, M., Lee, H. & Oh, K. Quantitative in situ measurement of optical force along a strand of cleaved silica optical fiber induced by the light guided therewithin. *Photonics Res.* **9,** 2016 (2021).

39. Emile, O. & Emile, J. Low-power laser deformation of an air-liquid interface. *Phys. Rev. Lett.* **106,** 183904 (18 2011).

40. Brasselet, E. Comment on "Low-Power laser deformation of an air-liquid interface". *Phys. Rev. Lett.* **108,** 269401 (26 2012).

41. Verma, G., Nair, J. & Singh, K. P. Comment on "Low-power laser deformation of an air-liquid interface". *Phys. Rev. Lett.* **110,** 079401 (7 2013).

42. Rikken, G. L. J. A. & van Tiggelen, B. A. Measurement of the Abraham force and its predicted QED corrections in crossed electric and magnetic fields. *Phys. Rev. Lett.* **107,** 170401 (17 2011).

43. Rikken, G. L. J. A. & van Tiggelen, B. A. Observation of the intrinsic Abraham force in time-varying magnetic and electric fields. *Phys. Rev. Lett.* **108,** 230402 (23 2012).

44. Astrath, N. G. C., Malacarne, L. C., Baesso, M. L., Lukasievicz, G. V. B. & Bialkowski, S. E. Unravelling the effects of radiation forces in water. *Nat. Commun.* **5,** 4363 (2014).

45. Zhang, L., She, W., Peng, N. & Leonhardt, U. Experimental evidence for Abraham pressure of light. *New J. Phys.* **17,** 053035 (2015).

46. Leonhardt, U. Abraham and Minkowski momenta in the optically induced motion of fluids. *Phys. Rev. A* **90,** 033801 (2014).

47. Capeloto, O. A. *et al.* Quantitative assessment of radiation force effect at the dielectric air-liquid interface. *Sci. Rep.* **6,** 20515 (2015).

48. Verma, G. & Singh, K. P. Universal long-range nanometric bending of water by light. *Phys. Rev. Lett.* **115,** 143902 (14 2015).

49. Choi, H., Park, M., Elliott, D. S. & Oh, K. Optomechanical measurement of the Abraham force in an adiabatic liquid-core optical-fiber waveguide. *Phys. Rev. A* **95,** 053817 (5 2017).

50. Verma, G., Chaudhary, K. & Singh, K. P. Nanomechanical effects of light unveil photons momentum in medium. *Sci. Rep.* **7,** 1–7 (2017).

51. Kundu, A., Rani, R. & Hazra, S. K. Graphene oxide demonstrates experimental confirmation of Abraham pressure on solid surface. *Sci. Rep.* **7,** 42538 (2017).

52. Brevik, I. Analysis of recent interpretations of the Abraham-Minkowski problem. *Phys. Rev. A* **98,** 043847 (4 2018).

53. Partanen, M. & Tulkki, J. Comment on "Analysis of recent interpretations of the Abraham-Minkowski problem". *Phys. Rev. A* **100,** 017801 (1 2019).

54. Strait, J. H. *et al.* Revisiting the photon-drag effect in metal films. *Phys. Rev. Lett.* **123,** 053903 (2019).

55. Schaberle, F. A., Reis, L. A., Serpa, C. & Arnaut, L. G. Photon momentum transfer at water/air interfaces under total internal reflection. *New J. Phys.* **21,** 033013 (2019).

56. Chaudhary, K. & Singh, K. P. Picometer resolved nanoscale optomechanics of micro-droplet. *Appl. Phys. Lett.* **115,** 251103 (2019).

57. Xi, X. *et al.* Experimental investigation of the angular symmetry of optical force in a solid dielectric. *Optica* **8,** 1435 (11 2021).

58. Balazs, N. L. The energy-momentum tensor of the electromagnetic field inside matter. *Phys. Rev.* **91,** 408–411 (2 1953).

59. Gordon, J. P. Radiation forces and momenta in dielectric media. *Phys. Rev. A.* **8,** 14–21 (1 1973).

60. Nelson, D. F. Momentum, pseudomomentum, and wave momentum: Toward resolving the Minkowski-Abraham controversy. *Phys. Rev. A* **44,** 3985–3996 (6 1991).

61. Leonhardt, U. Energy-momentum balance in quantum dielectrics. *Phys. Rev. A* **73,** 032108 (3 2006).

62. Pfeifer, R. N. C., Nieminen, T. A., Heckenberg, N. R. & Rubinsztein-Dunlop, H. Colloquium: Momentum of an electromagnetic wave in dielectric media. *Rev. Mod. Phys.* **79,** 1197–1216 (4 2007).

63. Padgett, M. J. On diffraction within a dielectric medium as an example of the Minkowski formulation of optical momentum. *Opt. Express* **16,** 20864–20868 (25 2008).

64. Barnett, S. M. Resolution of the Abraham-Minkowski dilemma. *Phys. Rev. Lett.* **104,** 070401 (7 2010).

65. Kemp, B. A. Resolution of the Abraham-Minkowski debate: Implications for the electromagnetic wave theory of light in matter. *J. Appl. Phys.* **109,** 111101 (11 2011).

66. Brevik, I. & Ellingsen, S. Å. Electromagnetic momentum conservation in media. *Ann. Phys.* **326,** 754–769 (2011).

67. Kemp, B. A. & Sheppard, C. J. Electromagnetic and material contributions to stress, energy, and momentum in metamaterials. *Adv. Electromagn.* **6,** 11–19 (1 2017).

68. Brevik, I. Minkowski momentum resulting from a vacuum–medium mapping procedure, and a brief review of Minkowski momentum experiments. *Ann. Phys.* **377,** 10–21 (2017).

69. Brevik, I. Radiation forces and the Abraham-Minkowski problem. *Mod. Phys. Lett. A* **33,** 1–15 (10-11 2018).

70. Silveirinha, M. G. Reexamination of the Abraham-Minkowski dilemma. *Phys. Rev. A* **96,** 033831 (2017).
71. Griffiths, D. J. & Hnizdo, V. *What's the use of bound charge?* Pre-print available at `arxiv.org/abs/1506.02590`. 2015.
72. Landau, L. D. & Lifshitz, E. M. *The classical theory of fields* 4th ed. (Butterworth Heinemann, 1987).
73. Maxwell, J. C. *A treatise on electricity and magnetism* (Clarendon Press, Oxford, 1873).
74. Griffiths, D. J. Resource Letter EM-1: electromagnetic momentum. *Am. J. Phys.* **80,** 7–18 (2012).
75. Shockley, W. & James, R. P. "Try simplest cases" discovery of "hidden momentum" forces on "magnetic currents". *Phys. Rev. Lett.* **18,** 876–879 (20 1967).
76. Corrêa, R. & Saldanha, P. L. Hidden momentum in continuous media and the Abraham-Minkowski debate. *Phys. Rev. A* **102,** 063510 (6 2020).
77. Babson, D., Reynolds, S. P., Bjorquist, R. & Griffiths, D. J. Hidden momentum, field momentum, and electromagnetic impulse. *Am. J. Phys.* **77,** 826–833 (9 2009).
78. McDonald, K. T. *No bootstrap spaceships via magnets in electric fields* available at `http://kirkmcd.princeton.edu/examples/redfern.pdf`. 2018.
79. McDonald, K. T. *On the definition of "hidden" momentum* available at `http://physics.princeton.edu/~mcdonald/examples/hiddendef.pdf`. 2020.
80. Hnizdo, V. Hidden momentum and the electromagnetic mass of a charge and current carrying body. *Am. J. Phys.* **65,** 55–65 (1 1997).
81. Vanzella, D. A. T. Relativistic paradox exposing the ubiquity of hidden momentum. *Phys. Rev. A* **102,** 042203 (4 2020).
82. Horsley, S. A. R. & Babiker, M. Power–Zienau–Woolley QED: centre of mass-energy and the Aharonov–Casher effect. *J. Phys. B: At. Mol. Opt. Phys.* **39,** S565–S571 (2006).
83. Sonnleitner, M. & Barnett, S. M. The Röntgen interaction and forces on dipoles in time-modulated optical field. *Eur. Phys. J. D* **71,** 1–13 (336 2017).
84. Hnizdo, V. Magnetic dipole moment of a moving electric dipole. *Am. J. Phys.* **80,** 645–647 (2012).
85. Aharonov, Y. & Casher, A. Topological quantum effects for neutral particles. *Phys. Rev. Lett.* **53,** 319–321 (4 1984).

86. Aharonov, Y. & Bohm, D. Significance of electromagnetic potentials in the quantum theory. *Phys. Rev.* **115,** 485–491 (3 1959).

87. Sangster, K., Hinds, E. A., Barnett, S. M., Riis, E. & Sinclair, A. G. Aharonov-Casher phase in an atomic system. *Phys. Rev. A* **51,** 1776–1786 (3 1995).

88. Pop, I. M. *et al.* Experimental demonstration of Aharonov-Casher interference in a Josephson junction circuit. *Phys. Rev. B* **85,** 094503 (2012).

89. Baxter, C., Babiker, M. & Loudon, R. Canonical approach to photon pressure. *Phys. Rev. A* **47,** 1278–1287 (2 1993).

90. Lembessis, V. E., Babiker, M., Baxter, C. & Loudon, R. Theory of radiation forces and momenta for mobile atoms in light fields. *Phys. Rev. A* **48,** 1594–1603 (2 1993).

91. Wilkens, M. Quantum phase of a moving dipole. *Phys. Rev. Lett.* **72,** 5–8 (1 1994).

92. Stenholm, S. The semiclassical theory of laser cooling. *Rev. Mod. Phys.* **58,** 699–739 (3 1986).

93. Einstein, A. & Laub, J. Über die im elektromagnetischen Felde auf ruhende Körper ausgeübten ponderomotorischen Kräfte [On the ponderomotive forces exerted on bodies at rest in the electromagnetic field]. *Ann. Phys.* **26,** 541 (1908).

94. Chu, L. J., Haus, H. & Jr, P. P. The force density in polarizable and magnetizable fluids. *Proc. IEEE* **54,** 7 (1966).

95. Partanen, M., Häyrynen, T., Oksanen, J. & Tulkki, J. Photon mass drag and the momentum of light in a medium. *Phys. Rev. A* **95,** 063850 (6 2017).

96. Partanen, M. & Tulkki, J. Mass-polariton theory of light in dispersive media. *Phys. Rev. A* **96,** 063834 (6 2017).

97. Partanen, M. & Tulkki, J. Mass-polariton theory of sharing the total angular momentum of light between the field and matter. *Phys. Rev. A* **98,** 033813 (3 2018).

98. Partanen, M. & Tulkki, J. Lorentz covariance of the mass-polariton theory of light. *Phys. Rev. A* **99,** 033852 (3 2019).

99. Partanen, M. & Tulkki, J. Lagrangian dynamics of the coupled field-medium state of light. *New J. Phys.* **21,** 073062 (2019).

100. Partanen, M. & Tulkki, J. Covariant theory of light in a dispersive medium. *Phys. Rev. A* **104,** 023510 (2 2021).

101. Milonni, P. W. & Boyd, R. W. Momentum of light in a dielectric medium. *Adv. Opt. Photon.* **2,** 519–553 (2010).

102. Jackson, J. D. *The nature of intrinsic magnetic dipole moments* CERN 77-17 Lecture. 1977.

103. McDonald, K. T. *Biot-Savart vs. Einstein-Laub force law* available at `http://kirkmcd.princeton.edu/examples/laub.pdf`. 2018.
104. Rasetti, F. Deflection of mesons in magnetized iron. *Phys. Rev.* **66,** 1–5 (1944).
105. Boyer, T. H. The force on a magnetic dipole. *Am. J. Phys.* **56,** 688–692 (8 1988).
106. Mansuripur, M. Resolution of the Abraham–Minkowski controversy. *Opt. Commun.* **283,** 1997–2005 (2010).
107. Mansuripur, M., Zakharian, A. R. & Wright, E. M. Electromagnetic-force distribution inside matter. *Phys. Rev. A* **88,** 023826 (2013).
108. Partanen, M. & Tulkki, J. Time-dependent optical force theory for optomechanics of dispersive 3D photonic materials and devices. *Opt. Express* **30** (16 2022).
109. Požar, T. *et al.* Isolated detection of elastic waves driven by the momentum of light. *Nat. Commun.* **9,** 1–11 (3340 2018).
110. Ellingsen, S. Å. & Brevik, I. Electrostrictive fluid pressure from a laser beam. *Phys. Fluids* **23,** 096101 (9 2011).
111. Casner, A. & Delville, J.-P. Laser-induced hydrodynamic instability of fluid interfaces. *Phys. Rev. Lett.* **90,** 144503 (14 2003).
112. Brueckner, K. A. & Jorna, S. Linear instability theory of laser propagation in fluids. *Phys. Rev. Lett.* **17,** 78–81 (2 1966).
113. Brevik, I. Fluids in electric and magnetic fields: Pressure variation and stability. *Can. J. Phys.* **60,** 449–455 (1982).
114. Boyd, R. W. *Nonlinear optics* 4th ed. (Academic Press, 2020).
115. Cachier, G. Laser excitation of microwave sound in solids. *J. Acoust. Soc. Am.* **49,** 974–978 (1971).
116. Brevik, I. Experiments in phenomenological electrodynamics and the electromagnetic energy-momentum tensor. *Phys. Rep.* **52,** 133–201 (1979).
117. Landau, L. D. & Lifshitz, E. M. *Electrodynamics of continuous media* 2nd ed. (Pergamon Press, Oxford, 1984).
118. Von Helmholtz, H. *Wied. Ann.* **13,** 385 (1881).
119. Lai, H. M., Shen, W. M. & Young, K. Microscopic derivation of the Helmholtz force density. *Phys. Rev. Lett.* **47,** 177–179 (3 1981).
120. Jackson, J. D. *Classical electrodynamics* 3rd ed. (Wiley, New York, 1999).

121. Hakim, S. S. & Higham, J. B. An experimental determination of the excess pressure produced in a liquid dielectric by an electric field. *Proc. Phys. Soc.* **80,** 190–198 (1 1962).

122. Zimmerli, G. A., Wilkinson, R. A., Ferrell, R. A. & Moldover, M. R. Electrostriction of a near-critical fluid in microgravity. *Phys. Rev. E* **59,** 5862–5869 (5 1999).

123. Buckland, E. L. & Boyd, R. W. Measurement of the frequency response of the electrostrictive nonlinearity in optical fibers. *Opt. Lett.* **22,** 676–678 (10 1997).

124. Borth, D. E. & Cain, C. A. Theoretical analysis of acoustic signal generation in materials irradiated with microwave energy. *IEEE Trans. Microw. Theory Tech.* **25,** 944–954 (11 1977).

125. Anghinoni, B. *et al.* On the formulations of the electromagnetic stress–energy tensor. *Ann. Phys.* **443,** 169004 (2022).

126. Partanen, M. & Tulkki, J. Covariant theory of light in a dispersive medium. *Phys. Rev. A* **104,** 023510 (2 2021).

127. Griffiths, D. J. Dipoles at rest. *Am. J. Phys.* **60,** 979–987 (11 1992).

128. Griffiths, D. J. Dynamic dipoles. *Am. J. Phys.* **79,** 867–872 (8 2011).

129. Astrath, N. G. C. *et al.* Unveiling bulk and surface radiation forces in a dielectric liquid. *Light Sci. Appl.* **11,** 1–10 (103 2022).

130. Batchelor, G. K. *An introduction to fluid dynamics* (Cambridge University Press, Cambridge, 2000).

131. Casner, A., Delville, J.-P. & Brevik, I. Asymmetric optical radiation pressure effects on liquid interfaces under intense illumination. *J. Opt. Soc. Am. B* **20,** 2355–2362 (2003).

132. Borzdov, G. N. An intrinsic tensor technique in Minkowski space with applications to boundary value problems. *J. Math. Phys.* **34,** 3162 (1993).

133. Hallanger, A., Brevik, I., Haaland, S. & Sollie, R. Nonlinear deformations of liquid-liquid interfaces induced by electromagnetic radiation pressure. *Phys. Rev. E* **71,** 056601 (5 2005).

134. Aspnes, D. E. Local-field effects and effective-medium theory: A microscopic perspective. *Am. J. Phys.* **50,** 704–709 (1982).

135. Ashcroft, N. W. & Mermin, D. N. *Solid state physics* 1st ed. (Harcourt College Publishers, 1976).

136. Kragh, H. The Lorenz-Lorentz formula: origin and early history. *Substantia* **2,** 7–18 (2018).

137. Partanen, M., Anghinoni, B., Astrath, N. G. C. & Tulkki, J. *Time-dependent theory of optical electro- and magnetostriction* Submitted. 2022.
138. Luscombe, J. H. *Core principles of special and general relativity* 1st ed. (CRC Press, Boca Raton, 2019).
139. Hernandez, W. C. Elasticity theory in general relativity. *Phys. Rev. D* **1,** 1013–1018 (4 1970).
140. Kittel, C. *Introduction to solid state physics* 7th ed., 80–85 (John Wiley & Sons, New York, 1996).
141. Yu, L. & Myuing, K. K. Wavelength-scanning digital interference holography for tomographic three-dimensional imaging by use of the angular spectrum method. *Opt. Lett.* **30,** 16 (2005).
142. Török, P. & Varga, P. Electromagnetic diffraction of light focused through a stratified medium. *Appl. Opt.* **26,** 11 (1997).
143. Zemp, R. J., Tavakkoli, J. & Coboold, R. S. C. Modeling of nonlinear ultrasound propagation in tissue from array transducers. *J. Acoust. Soc. Am.* **113,** 139 (2003).
144. Vecchio, C. J., Schager, M. E. & Lewin, P. A. Prediction of ultrasonic field propagation through layered media using the extended angular spectrum method. *Ultrasound Med. Biol.* **20,** 7 (1994).
145. Novotny, L. & Hecht, B. *Principles of nano-optics* 2nd ed., 12–85 (Cambridge University Press, 2012).
146. Mandel, L. & Wolf, E. *Optical coherence and quantum optics* 1st ed., 109–117 (Cambridge University Press, 1995).
147. Wolf, E. Electromagnetic diffraction in optical systems. I. An integral representation of the image field. *Proc. R. Soc. A* **253,** 1274 (1959).
148. Richards, B. & Wolf, E. Electromagnetic diffraction in optical systems. II. Structure of the image field in an aplanatic system. *Proc. R. Soc. A* **253,** 1274 (1959).
149. Small, A. Spherical aberration, coma, and the Abbe sine condition for physicists who don't design lenses. *Am. J. Phys* **86,** 7 (2018).
150. Török, P., Varga, P., Laczik, Z. & Booker, G. R. Electromagnetic diffraction of light focused through a planar interface between materials of mismatched refractive indices: an integral representation. *J. Opt. Soc. Am. A* **12,** 2 (1995).
151. Sukhov, S. & Dogariu, A. Non-conservative optical forces. *Rep. Prog. Phys.* **80,** 112001 (2017).

152. Bliokh, K., Rodríguez-Fortuño, F., Nori, F. & Zayats, A. V. Spin–orbit interactions of light. *Nat. Photon.* **9,** 796–808 (2015).

153. Le Fournis, R., van Tiggelen, B. A. & Donaire, M. QED corrections to the Abraham and Aharonov-Casher forces on Rydberg atoms. *Phys. Rev. A* **106,** 042817 (4 2022).

154. Feigel, A. Quantum vacuum contribution to the momentum of dielectric media. *Phys. Rev. Lett.* **92,** 020404 (2 2004).

155. Hecht, E. *Optics* 4th ed., 111–127 (Addison Wesley, San Francisco, CA, 2002).

APPENDIX A

Covariant electrodynamics in flat space-time

For an inertial system at rest with arbitrary electromagnetic sources ρ and $\mathbf{J}$, Maxwell's equations are given by

$$\varepsilon_0 \boldsymbol{\nabla} \cdot \mathbf{E} = \rho, \tag{A.1}$$

$$\boldsymbol{\nabla} \cdot \mathbf{B} = 0, \tag{A.2}$$

$$\frac{1}{\mu_0} \boldsymbol{\nabla} \times \mathbf{B} - \varepsilon_0 \frac{\partial \mathbf{E}}{\partial t} = \mathbf{J}, \tag{A.3}$$

$$\boldsymbol{\nabla} \times \mathbf{E} + \frac{\partial \mathbf{B}}{\partial t} = 0. \tag{A.4}$$

For a flat space-time, these equations can be compactly written in covariant form as [138]

$$\partial_\nu F^{\mu\nu} = \mu_0 J^\mu, \tag{A.5}$$

$$\epsilon^{\mu\nu\lambda\sigma} \partial_\nu F_{\lambda\sigma} = 0, \tag{A.6}$$

where $F^{\mu\nu}$ is the electromagnetic field tensor, given by $F^{\mu\nu} = \partial^\mu A^\nu - \partial^\nu A^\mu$, $\partial_\nu = \partial/\partial x^\nu$ is the covariant derivative, $A^\mu = (\varphi/c, \mathbf{A})$ is the electromagnetic four-potential, $\epsilon^{\mu\nu\lambda\sigma}$ is the total anti-symmetric tensor and $J^\mu = (c\rho, \mathbf{J})$ is the four-current.

For macroscopic bodies, it is possible to apply the conventional Ampère formulation, as discussed in Section 2.3.3. The macroscopic Maxwell's equations used in this formulation can also be written in covariant form. To see that, notice that the bound four-current is given by $J^\mu_{\mathrm{b}} = (c\rho_{\mathrm{b}}, \mathbf{J}_{\mathrm{b}}) = (-c\boldsymbol{\nabla} \cdot \mathbf{P}, \boldsymbol{\nabla} \times \mathbf{M} + \partial_t \mathbf{P})$, which can be conveniently packed into a continuity equation as

$$\partial_\nu M^{\mu\nu} = J^\mu_{\mathrm{b}}, \tag{A.7}$$

where $M^{\mu\nu}$ is an anti-symmetric tensor known as magnetization-polarization tensor and given by

$$M^{\mu\nu} = \begin{pmatrix} 0 & -cP_x & -cP_y & -cP_z \\ cP_x & 0 & M_z & -M_y \\ cP_y & -M_z & 0 & M_x \\ cP_z & M_y & -M_x & 0 \end{pmatrix}. \tag{A.8}$$

With this new tensor, we can also write $\mathbf{D} = \epsilon_0 \mathbf{E} + \mathbf{P}$ and $\mathbf{H} = \mathbf{B}/\mu_0 - \mathbf{M}$ in tensor form through $D^{\mu\nu} = F^{\mu\nu}/\mu_0 - M^{\mu\nu}$. Maxwell's macroscopic equations are then given in covariant form as

$$\partial_\nu D^{\mu\nu} = J^\mu, \tag{A.9}$$

$$\epsilon^{\mu\nu\lambda\sigma}\partial_\nu F_{\lambda\sigma} = 0, \tag{A.10}$$

where J^μ now contains both free and bound four-current sources, i.e., $J^\mu = J^\mu_{\mathrm{f}} + J^\mu_{\mathrm{b}}$.

Electromagnetic force

The covariant Lagrangian for a particle with electric charge q and mass m in flat space-time is given by [138]

$$L = -mc\sqrt{-\eta_{\mu\nu}U^\mu U^\nu} + qA_\mu U^\mu, \tag{A.11}$$

where $\eta_{\mu\nu}$ is the flat space-time metric tensor and U^ν is the four-velocity. The covariant Euler-Lagrange equation is

$$\frac{\mathrm{d}}{\mathrm{d}\tau}\frac{\partial L}{\partial U^\mu} = \frac{\partial L}{\partial x^\mu}, \tag{A.12}$$

where τ is the proper time. Inserting the Lagrangian from Eq. (A.11), we obtain the equations of motion as

$$m\frac{\mathrm{d}U_\mu}{\mathrm{d}\tau} + q\frac{\mathrm{d}A_\mu}{\mathrm{d}\tau} = qU^\alpha\frac{\partial A_\alpha}{\partial x^\mu}. \tag{A.13}$$

Using the chain rule, we can rewrite

$$\frac{\mathrm{d}A_\mu}{\mathrm{d}\tau} = \frac{\partial A_\mu}{\partial x^\nu}\frac{\mathrm{d}x^\nu}{\mathrm{d}\tau} = U^\nu\frac{\partial A_\mu}{\partial x^\nu}. \tag{A.14}$$

Combining the last two equations, we have

$$m\frac{\mathrm{d}U_\mu}{\mathrm{d}\tau} = q\left(\frac{\partial A_\nu}{\partial x^\mu} - \frac{\partial A_\mu}{\partial x^\nu}\right)U^\nu = qF_{\mu\nu}U^\nu. \tag{A.15}$$

This is the covariant equation of motion for a point charge. The right hand side of this equation is recognized as the Lorentz force in covariant form. The related stress-energy tensor for flat space-time is [72, 138]

$$\mathcal{T}^{\mu\nu} = -\frac{1}{\mu_0}\left(\eta_{\alpha\lambda}F^{\mu\alpha}F^{\lambda\nu} + \frac{1}{4}\eta^{\mu\nu}F_{\alpha\beta}F^{\alpha\beta}\right), \tag{A.16}$$

which is known as Maxwell's stress-energy tensor.

APPENDIX B

Fresnel equations

Applying the boundary conditions from Maxwell's equations to a planar interface between two linear, homogeneous, isotropic, non-magnetic dielectrics, and considering an inciding wave which is locally plane, we are able to obtain the fractions of the fields that are transmitted and reflected in terms of the media parameters. In our case, no free charges or currents are assumed to exist at the interface, and the beam is assumed to propagate from medium 1 to medium 2. In terms of the incidence angle θ, the Fresnel coefficients are given by:

$$r_{\mathrm{s}}(\theta) = \frac{n_1\cos\theta - \sqrt{n_2^2 - n_1^2\sin^2\theta}}{n_1\cos\theta + \sqrt{n_2^2 - n_1^2\sin^2\theta}}, \tag{B.1}$$

$$t_{\mathrm{s}}(\theta) = \frac{2n_1\cos\theta}{n_1\cos\theta + \sqrt{n_2^2 - n_1^2\sin^2\theta}}, \tag{B.2}$$

$$r_{\mathrm{p}}(\theta) = \frac{n_2^2\cos\theta - n_1\sqrt{n_2^2 - n_1^2\sin^2\theta}}{n_2^2\cos\theta + n_1\sqrt{n_2^2 - n_1^2\sin^2\theta}}, \tag{B.3}$$

$$t_{\mathrm{p}}(\theta) = \frac{2n_2^2\cos\theta}{n_2^2\cos\theta + n_1\sqrt{n_2^2 - n_1^2\sin^2\theta}}\frac{n_1}{n_2}, \tag{B.4}$$

where $n_1 = \sqrt{\epsilon_{1r}}$ and $n_2 = \sqrt{\epsilon_{2r}}$ are the dielectric refractive indexes, r_{s} and r_{p} are the reflection coefficients for s and p polarizations and t_{s} and t_{p} are the transmission coefficients of the s and p polarizations. The derivation of these equations can be found in most electromagnetic theory textbooks, and we mention Ref. [120] as a good example.

APPENDIX C

Radiation pressure at oblique incidence

The radiation pressure for oblique incidence in non-magnetic dielectrics is given in literature by Eq. (3.62). This equation is equivalent to [133]

$$\mathcal{P}_{\mathrm{rad}} = -\frac{I}{2c}\frac{n_2^2 - n_1^2}{n_2}\frac{\cos\theta_{\mathrm{i}}}{\cos\theta_{\mathrm{t}}}\left[(\sin^2\theta_{\mathrm{i}} + \cos^2\theta_{\mathrm{t}})T_{\mathrm{p}}\cos^2\alpha + T_{\mathrm{s}}\sin^2\alpha\right], \tag{C.1}$$

where α is the angle between the electric field and the plane of incidence. Thus, for $\alpha = 0$ we have a p polarized beam, while for $\alpha = \pi/2$ we have a s polarized beam. In the former case, we have then

$$\mathcal{P}_{\mathrm{rad}}^{(\mathrm{p})} = -\frac{I}{2c}\frac{n_2^2 - n_1^2}{n_2}\frac{\cos\theta_{\mathrm{i}}}{\cos\theta_{\mathrm{t}}}\left[(\sin^2\theta_{\mathrm{i}} + \cos^2\theta_{\mathrm{t}})T_{\mathrm{p}}\right]. \tag{C.2}$$

We can rewrite this equation by using the relation $T = (n_2\cos\theta_{\mathrm{t}}/n_1\cos\theta_{\mathrm{i}})|t^2|$, which is valid for both polarizations [155], obtaining

$$\mathcal{P}_{\mathrm{rad}}^{(\mathrm{p})} = -\frac{n_1 I}{2c}\frac{n_2^2 - n_1^2}{n_1}\left[(\sin^2\theta_{\mathrm{i}} + \cos^2\theta_{\mathrm{t}})t_{\mathrm{p}}^2\right]. \tag{C.3}$$

Recalling that the (instantaneous) intensity for a plane wave is $I = \varepsilon_0 c n E_0^2$ we have then

$$\mathcal{P}_{\mathrm{rad}}^{(\mathrm{p})} = -\frac{(\varepsilon_2 - \varepsilon_1)}{2}E_0^2\left[(\sin^2\theta_{\mathrm{i}} + \cos^2\theta_{\mathrm{t}})t_{\mathrm{p}}^2\right]. \tag{C.4}$$

This last equation is significantly different from our equation for the radiation pressure for p polarization, Eq. (3.60), even though they both originate from the Abraham-Minkowski force density. Even if we neglect the transmitted part of the normal component in our expression and further apply the relation $t_{\mathrm{p}}^2 = (n_1^2/n_2^2)(1+r_{\mathrm{p}})^2$, the two different forms can not be reconciled. Therefore, we expect that Eq. (3.60) is the correct one for p polarized beams. For s polarization, Eqs. (C.1) and (3.62) remain correct.

APPENDIX D

The paraxial approximation of electromagnetic fields

In many analyses of laser beams propagation it is very common the majority of the beam's energy is transported along the longitudinal direction of propagation. In this situation, the longitudinal component of the wavevector $\mathbf{k}$ of the ASR can be approximated by

$$k_z = k\sqrt{1-(k_x^2+k_y^2)/k^2} \approx k - \frac{k_x^2+k_y^2}{2k}. \tag{D.1}$$

This approximation is known as paraxial approximation and is frequently used for analytical treatments of weakly focused laser beams. In particular, we will consider as example the fundamental mode of a linearly polarized laser beam with a gaussian distribution at the beam waist, namely

$$\mathbf{E}(x,y,z=0) = \mathbf{E}_0\,\mathrm{e}^{-\frac{x^2+y^2}{w_0^2}}, \tag{D.2}$$

where $\mathbf{E}_0$ is constant through the transverse plane xy and w_0 is the beam waist, located at $z=0$. The spatial Fourier spectrum of this beam is given by

$$\begin{aligned}\hat{\mathbf{E}}(k_x,k_y;0) &= \frac{1}{4\pi^2}\iint_{-\infty}^{+\infty} \mathbf{E}_0\,\mathrm{e}^{-\frac{x^2+y^2}{w_0^2}}\,\mathrm{e}^{\mathrm{i}(k_x x+k_y y)}\,\mathrm{d}x\,\mathrm{d}y \\ &= \mathbf{E}_0\frac{w_0^2}{4\pi}\,\mathrm{e}^{-(k_x^2+k_y^2)w_0^2/4}.\end{aligned} \tag{D.3}$$

This expression is then inserted on the ASR, Eq. (4.14), with k_z given by the paraxial approximation, Eq. (D.1), yielding

$$\mathbf{E}(x,y,z) = \mathbf{E}_0 \frac{w_0^2}{4\pi}\,\mathrm{e}^{\mathrm{i}kz} \iint\limits_{-\infty}^{+\infty} \mathrm{e}^{-(k_x^2+k_y^2)\left(\frac{w_0^2}{4}+\mathrm{i}\frac{z}{2k}\right)}\,\mathrm{e}^{\mathrm{i}(k_x x + k_y y)}\,\mathrm{d}k_x\,\mathrm{d}k_y. \tag{D.4}$$

This equation can be analytically integrated, resulting in

$$\mathbf{E}(x,y,z) = \frac{\mathbf{E}_0\,\mathrm{e}^{\mathrm{i}kz}}{1+2\,\mathrm{i}z/(kw_0^2)}\,\mathrm{e}^{-\frac{x^2+y^2}{w_0^2}\frac{1}{1+2\,\mathrm{i}z/(kw_0^2)}}, \tag{D.5}$$

which corresponds to the gaussian beam in the paraxial approximation. Defining a new parameter $z_0 = kw_0^2/2$ (the Rayleigh range) and using the cylindrical coordinate $\rho = \sqrt{x^2+y^2}$ we get a more familiar form

$$\mathbf{E}(\rho,z) = \mathbf{E}_0 \frac{w_0}{w(z)}\,\mathrm{e}^{-\frac{\rho^2}{w^2(z)}}\,\mathrm{e}^{\mathrm{i}(kz+k\rho^2/2R(z)-\eta(z))}, \tag{D.6}$$

where $w(z) = w_0\sqrt{1+z^2/z_0^2}$ is the beam waist, $R(z) = z(1+z_0^2/z^2)$ is the beam curvature radius and $\eta(z) = \tan^{-1}(z/z_0)$ is the phase correction.

It is important to recall that, once the paraxial approximation is introduced, the electric field is not an exact solution of Maxwell's equation anymore. Indeed, the smaller the beam waist w_0, the greater the error in the approximation. When w_0 becomes of the order of the wavelength in the medium – which is the case for tightly focused beams – more terms must be added to Eq. (D.1). In this case, however, the series will converge too slowly [145], so that some other approach, such as the Angular Spectrum Representation, is necessary for an accurate treatment.

APPENDIX E

Magnetic field expressions for x-polarization

Complementing Section 4.2.1, we show here the focused magnetic fields of a x polarized fundamental gaussian beam within the ASR framework:

$$H_{\mathrm{t},x}(\rho,\varphi,z) = \frac{k_1 f E_0 \mathrm{e}^{-\mathrm{i}k_1 f}}{2\,\mathrm{i} Z_2} I_{2\mathrm{t},h}(\rho,z)\sin 2\varphi, \tag{E.1}$$

$$H_{\mathrm{t},y}(\rho,\varphi,z) = \frac{k_1 f E_0 \mathrm{e}^{-\mathrm{i}k_1 f}}{2\,\mathrm{i} Z_2}\left[I_{0\mathrm{t},h}(\rho,z) - I_{2\mathrm{t},h}(\rho,z)\cos 2\varphi\right], \tag{E.2}$$

$$H_{\mathrm{t},z}(\rho,\varphi,z) = \frac{-k_1 f E_0 \mathrm{e}^{-\mathrm{i}k_1 f}}{Z_2} I_{1\mathrm{t},h}(\rho,z)\sin\varphi, \tag{E.3}$$

where $Z_2 = \sqrt{\mu_2/\epsilon_2}$ corresponds to the wave impedance of medium 2. The one-dimensional integrals are given by

$$\begin{aligned} I_{0\mathrm{t},h}(\rho,z) = \int_0^{\theta_{max}} & \mathrm{e}^{\mathrm{i}(k_1\cos\theta - k_2\cos\theta_t)z_0}\mathrm{e}^{-\frac{f^2\sin^2\theta}{w_0^2}}\sqrt{\cos\theta}\,(t_\mathrm{p}(\theta) + t_\mathrm{s}(\theta)\cos\theta_t) \\ & \times\sin\theta\mathrm{e}^{\mathrm{i}k_2 z\cos\theta_t}J_0(\rho k_1\sin\theta)\mathrm{d}\theta, \end{aligned} \tag{E.4}$$

$$\begin{aligned} I_{1\mathrm{t},h}(\rho,z) = \int_0^{\theta_{max}} & \mathrm{e}^{\mathrm{i}(k_1\cos\theta - k_2\cos\theta_t)z_0}\mathrm{e}^{-\frac{f^2\sin^2\theta}{w_0^2}}\sqrt{\cos\theta} \\ & \times\sin\theta\mathrm{e}^{\mathrm{i}k_2 z\cos\theta_t}t_\mathrm{s}(\theta)\sin\theta_t J_1(\rho k_1\sin\theta)\mathrm{d}\theta, \end{aligned} \tag{E.5}$$

$$I_{2\mathrm{t},h}(\rho, z) = \int_0^{\theta_{max}} \mathrm{e}^{\mathrm{i}(k_1 \cos\theta - k_2 \cos\theta_t) z_0} \mathrm{e}^{-\frac{f^2 \sin^2\theta}{w_0^2}} \sqrt{\cos\theta}\,(t_\mathrm{p}(\theta) - t_\mathrm{s}(\theta)\cos\theta_t) \times \sin\theta \mathrm{e}^{\mathrm{i}k_2 z \cos\theta_t} J_2(\rho k_1 \sin\theta) \mathrm{d}\theta. \tag{E.6}$$